NASA CONTRACTOR REPORT

NASA CR-341

NASA CR-341

SPECTRAL ANALYSIS OF NONSTATIONARY SPACECRAFT VIBRATION DATA

by Allan G. Piersol

Prepared under Contract No. NAS 5-4590 *by*
MEASUREMENT ANALYSIS CORPORATION
Los Angeles, Calif.

for Goddard Space Flight Center

NATIONAL AERONAUTICS AND SPACE ADMINISTRATION - WASHINGTON, D. C. - NOVEMBER 1965

NASA CR-341

SPECTRAL ANALYSIS OF NONSTATIONARY SPACECRAFT VIBRATION DATA

By Allan G. Piersol

Prepared under Contract No. NAS 5-4590 by
MEASUREMENT ANALYSIS CORPORATION
Los Angeles, Calif.

for Goddard Space Flight Center

NATIONAL AERONAUTICS AND SPACE ADMINISTRATION

For sale by the Clearinghouse for Federal Scientific and Technical Information
Springfield, Virginia 22151 – Price $4.00

ABSTRACT

This document is concerned with practical procedures for describing and analyzing the frequency composition of spacecraft launch vibration data. Since such data are generally nonstationary, conventional analysis techniques based upon time averaging individual sample records of data can produce misleading results. To help clarify the basic problems, the concept of stationarity is reviewed, and theoretical methods for describing the frequency composition of nonstationary data are summarized. Both ensemble averaging and time averaging procedures are discussed with emphasis on the various errors associated with each approach. Experimental studies of actual spacecraft launch vibration data are then pursued to seek out typical or common trends which can be exploited to improve practical time averaging analysis procedures. Based upon the experimental studies as well as theoretical ideas, a specific procedure is recommended for the spectral analysis of nonstationary spacecraft vibration data, based upon time averaging short selected sample records of data.

TABLE OF CONTENTS

LIST OF FIGURES

LIST OF TABLES

1. INTRODUCTION

The spectral analysis of flight vehicle vibration data is relatively well defined and straightforward, at least in theory, so long as the vibration data are "stationary" in nature. In practical terms, stationary vibrations are those whose average characteristics do not change with time. For example, the vibration environment in a jet airplane during a continuous cruise at a fixed altitude with constant airspeed and invariant atmosphere conditions would probably be stationary for the duration of the cruise. The measurement and interpretation of power spectral density functions for stationary vibration data is discussed in Reference 1 and elsewhere.

Unfortunately, not all flight vehicle vibration environments are stationary during pertinent flight phases. For example, the vibration environment in a spacecraft during launch is generally nonstationary, i.e., the characteristics of the vibration change continuously throughout the launch phase. The measurement and analysis techniques outlined in Reference 1 are not strictly applicable to such data (although they are widely used), because those techniques are based upon time averaging procedures which inherently assume stationarity.

From a theoretical viewpoint, nonstationary data should be analyzed by ensemble averaging procedures; i.e., by averaging over a collection of sample records at specific instances of time. However, as will be illustrated later, ensemble averaging requires data from a large number of repeated experiments. Although ensemble averaging is the most straightforward approach to the problem, it is often difficult in actual practice to acquire data from a sufficiently large number of repeated experiments. This is particularly true for spacecraft applications where only a

few or perhaps just one experiment (test launch) may be performed due to the high cost of such experiments. Hence, for practical reasons, it is usually necessary to employ some sort of time averaging procedure for the analysis of spacecraft vibration data, regardless of the fact that such data are generally nonstationary.

The most common procedure currently used to analyze spacecraft launch vibration data is to compute individual time averaged power spectra for short time intervals covering significant launch events, such as lift-off, transonic flight and maximum dynamic pressure flight. Another approach is to compute a "time varying spectrum" over the entire launch phase. This is accomplished by continuous averaging (usually with a lowpass RC smoothing filter) at each frequency of interest, where the averaging time used is short relative to the length of pertinent events during launch. For this case, a parallel filter type instrument is desirable, although the same results can be obtained by repeated playback through a single filter instrument where the filter is shifted in frequency by one bandwidth for each playback. This general approach is suggested in References 2 and 3.

The above procedure produces "usable" information in the sense that the resulting "time varying spectrum" can be readily translated into a vibration test specification. The usual procedure is to form a "maximum spectrum" based upon the highest level observed at each frequency of the "time varying spectrum." A stationary vibration test is then performed using the "maximum spectrum." This approach to the problem may be completely acceptable. However, certain theoretical and practical questions do arise. For example, how do the above "time varying spectra" and the resulting "maximum spectra" relate to theoretical spectral representations for nonstationary data? How long should sample records be and where should they be selected during the launch phase? How long should the averaging time be? How can statistical errors be minimized in practical terms? The purpose of this document is to help answer these important questions.

2. CLASSES OF NONSTATIONARITY

2.1 REVIEW OF BASIC DEFINITIONS

Any sample time history record of a random physical phenomenom will represent a unique set of circumstances that are not likely to be repeated. In other words, a given sample time history record is merely a special example out of a large set of possible records that might have occurred. The collection of all possible records that might have occurred is called an ensemble which forms a random process. Hence, a given sample record of a random physical phenomenom may be thought of as a single physical realization of a random process. Hypothetically, for continuous phenomena such as mechanical vibrations, the number of possible physical realizations (sample records forming the random process) would be infinitely large.

Let $\{y(t)\}$ denote the ensemble of sample records forming a random process, and let $y_k(t)$ be the kth sample record from the ensemble. The properties of the random process may be computed by taking averages over the ensemble at any instant of time t_1, as illustrated in Figure 1. For example, the mean value at time t_1 and the autocorrelation function at times t_1 and $t_1 + \tau$ for the random process $\{y(t)\}$ would be given by

$$\mu_y(t_1) = \lim_{N\to\infty} \frac{1}{N} \sum_{k=1}^{N} y_k(t_1) \tag{1a}$$

$$R_y(t_1, t_1+\tau) = \lim_{N\to\infty} \frac{1}{N} \sum_{k=1}^{N} y_k(t_1)\, y_k(t_1+\tau) \tag{1b}$$

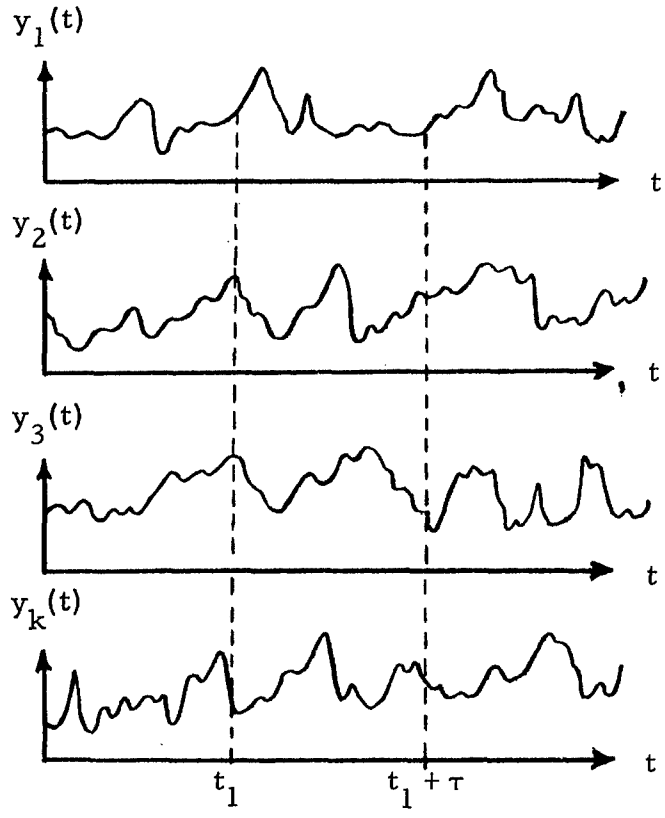

Figure 1. Ensemble of Sample Records

For the general case where the properties defined in Eq. (1) vary with time t_1, the random process is said to be nonstationary. For the special case where the properties defined in Eq. (1) do not vary with time, the random process is said to be weakly stationary. That is, if

$$\mu_y(t_1) = \mu_y(t_2) = \mu_y$$

$$R_y(t_1, t_1 + \tau) = R_y(t_2, t_2 + \tau) = R_y(\tau)$$

then $\{y(t)\}$ is weakly stationary. If all higher order moments of the random process determined by ensemble averaging are also time invariant, the random process is said to be strongly stationary. In most cases, verification of weak stationarity is sufficient to justify an assumption of strong stationarity.

If a random process is stationary, then with few exceptions in practice, the ensemble averages in Eq. (1) can be replaced by time averages over any one sample record from the ensemble. That is, if $\{y(t)\}$ is stationary,

$$\mu_y = \lim_{T\to\infty} \frac{1}{T} \int_0^T y(t)\, dt \tag{2a}$$

$$R_y(\tau) = \lim_{T\to\infty} \frac{1}{T} \int_0^T y(t)\, y(t+\tau)\, dt \tag{2b}$$

The justification for the above relationships evolves from the "ergodic theorem," which effectively states that time averages can replace ensemble averages for a wide class of stationary random processes. Note that the ergodic theorem does not apply to nonstationary random processes.

2.2 PRACTICAL INTERPRETATIONS

When flight vehicle vibration data are gathered and analyzed, the ultimate objective is to obtain information concerning the vibration environment to be expected during future missions for that and all similar vehicles. However, the measurements obtained from data for a single flight of one vehicle will strictly describe only the vibration environment in that vehicle for that interval of time in the past when the data were obtained. If such data are to be used as predictors for the vibration environment during future missions for that and other similar vehicles, it is necessary to make certain assumptions involving stationarity and ergodicity.

In order to place the concepts of stationarity and ergodicity into a meaningful physical context, consider the specific case of a vibration response at some point on the structure of a flight vehicle. Assume a continuous time history record of that vibration response is obtained for a given mission of the flight vehicle. That time history record is actually a sample record from a random process which represents the vibration

response at that point. The other sample records needed to completely define the random process can be visualized as the time history records for the vibration responses at that same point during identical missions performed by an infinitely large collection of identical flight vehicles.

The hypothetical ensemble of sample records described above cannot, of course, be physically realized. However, such a collection of sample records could be simulated by collecting data from repeated flights of one or more flight vehicles of the same type and performing similar missions. All sample records would be assigned a common time base where the start of the flight would be t_0. The result would be a physical approximation to an ensemble forming a random process. In this context, stationarity and ergodicity are interpreted as follows. The mean value and autocorrelation function for the vibration at any instant of time measured from the start of the flight could be estimated by averaging over the collection of sample records. If these estimated properties did not vary significantly from one instant of time to another, at least during some specific phase of the flight, then the vibration during that flight phase would be considered stationary. An ergodic assumption means that the vibration during that flight phase for one mission of one flight vehicle may be considered representative of the vibration which will occur during that flight phase for all similar missions of all flight vehicles of the same type.

Now consider the case of nonstationary vibration data such as would occur in a spacecraft during launch. In classical terms, an ergodic hypothesis is not valid here since the data is not stationary, even for limited time intervals. At first glance, this would seem to imply that the vibration recorded during one launch cannot be considered representative of the vibration during any other launch. However, it is known intuitively as well as from experience that this implication is not necessarily true. For example, assume the rms value for the vibration response at some point

on a spacecraft structure is measured over each of a contiguous series of one second long time intervals covering the entire launch phase. The result would be a sequence of rms values which describe an "rms value time history" for the vibration. Further assume that similar rms value time histories are obtained at the same location for several different launches of spacecraft of the same type under the same conditions. One would intuitively expect these rms value time histories to be similar from launch to launch, and indeed they will be as indicated in Figure 2. This figure presents three broadband rms value time histories for the vibration response measured at the same location on three different ATLAS-AGENA vehicles during launch.

The results in Figure 2 clearly illustrate that the nonstationary vibration data for one spacecraft launch is at least somewhat representative of the data for other launches of similar spacecraft. Obviously, something similar to an ergodic hypothesis appears justified. This is true because a special type of nonstationary random process is involved, where each sample record has a common underlying time varying characteristic. In other words, there is clearly a deterministic factor in the nonstationary random process which describes the vibration in a spacecraft during launch. It appears reasonable that this nonstationary random process might be represented by a stationary random process with deterministic time varying parameters. Assuming the time varying parameters can be identified and separated out, the data from one launch can be used to determine the properties of the vibration for all other launches.

2.3 SPECIAL NONSTATIONARY MODELS

Various types of nonstationary random processes have been considered in the past as models for specific physical phenomena. For example, a simple model for a nonstationary random process with a time varying mean

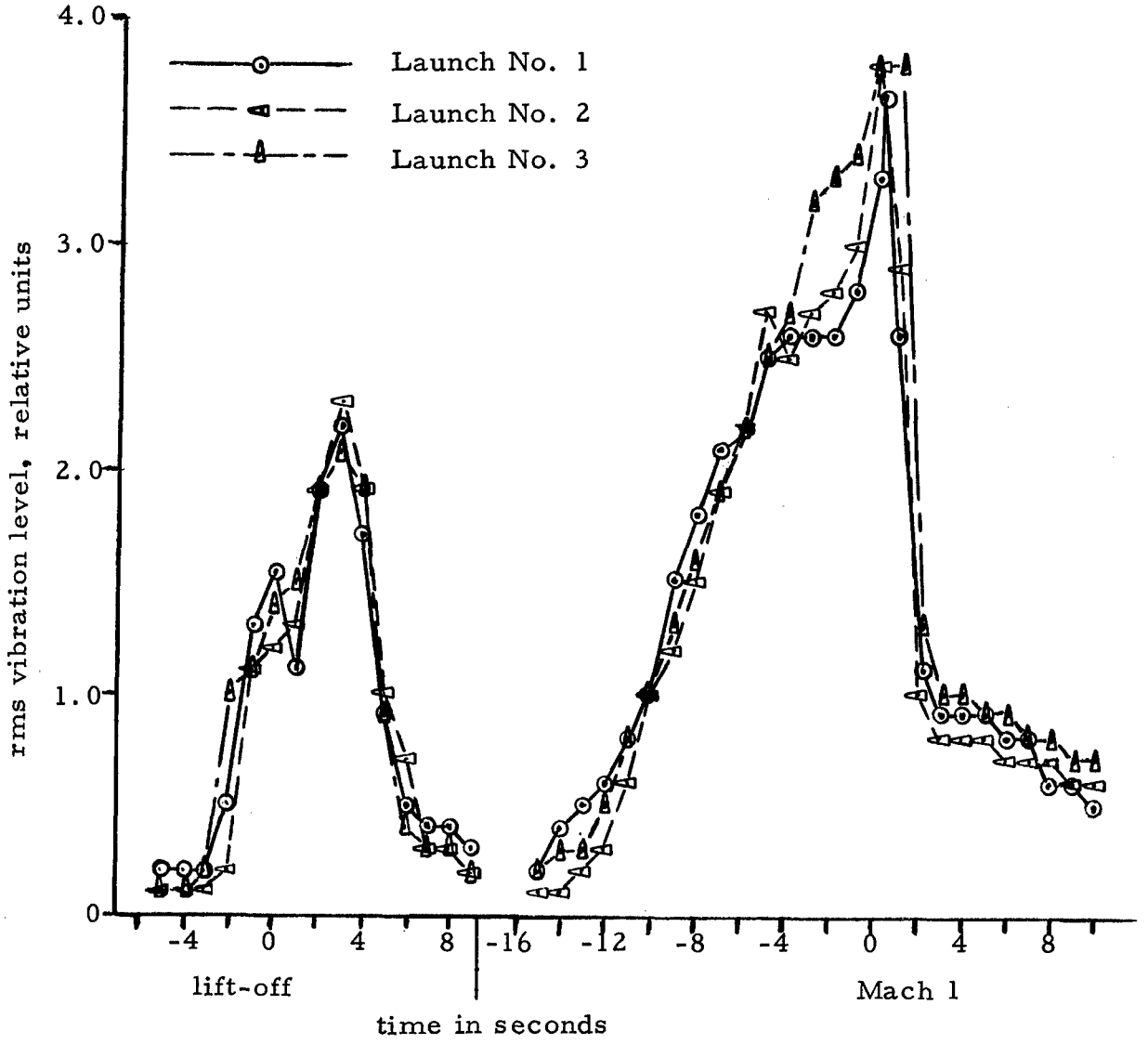

Figure 2. RMS Vibration Time Histories for Three Launches of the Same Type of Spacecraft

value is given by a process $\{y(t)\}$ where each sample record is of the form

$$y(t) = A(t) + x(t) \tag{3}$$

Here, $A(t)$ is a deterministic function and $x(t)$ is a sample record from a stationary random process $\{x(t)\}$. Illustrations of interest in this model are presented in References 4 and 5.

As a second example, a common model used to describe a nonstationary random process with a time varying mean square value is given by the process $\{y(t)\}$ where each sample record is of the form

$$y(t) = A(t)\ x(t) \tag{4}$$

Again, $A(t)$ is deterministic and $x(t)$ is a sample record from a stationary random process $\{x(t)\}$. Studies of this model are presented in References 6 and 7. As will be shown later, the model of Eq. (4) leads to an important special case. Specifically, if the fluctuations of $A(t)$ are very slow relative to the fluctuations of $\{x(t)\}$, then the spectral characteristics of $\{y(t)\}$ can be described by a time varying power spectrum approximated by

$$G_y(t, f) \approx A^2(t)\ G_x(f) \tag{5}$$

Assuming $\{x(t)\}$ has a mean square value of unity, the function $A(t)$ is the time varying root mean square (rms) value of the nonstationary process $\{y(t)\}$. Nonstationary random processes of this form are referred to in Reference 8 as being "locally stationary." A locally stationary random process can be visualized as one whose power spectrum varies with time such that the mean square value (area under the power spectrum) changes while the general shape of the power spectrum remains unchanged.

For the case of spacecraft vibration data, the mean value of the data can usually be considered time invariant. It is the mean square value of the vibration which is the significant time varying parameter. Furthermore, the variations in the mean square value are usually very slow relative to the instantaneous fluctuations of the vibration. Hence, a model similar to Eq. (5) might be a suitable representation for spacecraft vibration data, at least for certain time intervals during the launch phase. If so, the measurement and description of spacecraft vibration environments would be greatly simplified, as will be discussed later. These possibilities are pursued in this document.

3. THEORETICAL BACKGROUND

3.1 SPECTRAL REPRESENTATIONS FOR NONSTATIONARY DATA

From the viewpoint of both engineering interpretation and physical simulation, the single most valuable descriptive property for stationary vibration data is a power spectrum, or some similar measure of frequency composition. It follows that some type of spectral representation would also be valuable for nonstationary vibration data. Several such spectral representations have been suggested over the years, including the following.

3.1.1 Instantaneous Power Spectrum

One of the earlier methods for describing the spectral composition of nonstationary data is in terms of a Fourier transform of a time varying autocorrelation function. From Eq. (1b), the autocorrelation function for a nonstationary random process, $\{y(t)\}$, may be defined by

$$R_y(t_1, t_2) = \lim_{N\to\infty} \frac{1}{N} \sum_{k=1}^{N} y_k(t_1)\, y_k(t_2) \tag{6}$$

By making the change of variables, $\tau = t_2 - t_1$ and $t = (t_1 + t_2)/2$, Eq. (6) reduces to

$$R_y(t, \tau) = \lim_{N\to\infty} \frac{1}{N} \sum_{k=1}^{N} y_k\left(t - \frac{\tau}{2}\right) y_k\left(t + \frac{\tau}{2}\right) \tag{7}$$

An expression which is a function of time and frequency can then be obtained by taking the Fourier transform of $R_y(t, \tau)$, as follows.

$$s_y(t, f) = \int_{-\infty}^{\infty} R_y(t, \tau) \cos 2\pi f\tau \, d\tau \tag{8}$$

Note that $s_y(t, f)$ is defined for both positive and negative values of f. The quantity $s_y(t, f)$ in Eq. (8) is called the instantaneous power spectral density function for the process $\{y(t)\}$. This spectral function can take on negative values for certain cases. However, an integral of the function over either time or frequency will always yield nonnegative results which are physically meaningful.

The instantaneous power spectral density function is not directly measurable in the frequency domain. An experimental estimate for the function can be obtained only by, 1) computing the time varying correlation function $R_y(t, \tau)$ from an ensemble average at each value of t and τ of interest and, 2) computing the Fourier transform for each value of t of interest. See References 9, 10, and 11 for more extensive developments and discussions.

3.1.2 Generalized Power Spectrum

A second method for describing the spectral composition of nonstationary data is in terms of a double Fourier transform of the time varying autocorrelation function defined in Eq. (6). The result is a double frequency expression as follows.

$$\mathcal{S}_y(f_1, f_2) = \int_{-\infty}^{\infty} \cdot \int_{-\infty}^{\infty} R_y(t_1, t_2)\, e^{j2\pi(f_1 t_1 - f_2 t_2)}\, dt_1\, dt_2 \qquad (9)$$

Note that $\mathcal{S}_y(f_1, f_2)$ is defined for both positive and negative values of f_1 and f_2. The quantity $\mathcal{S}_y(f_1, f_2)$ in Eq. (9) is called the generalized power spectral density function for the process $\{y(t)\}$. This spectral description for nonstationary data is of great value for analytical treatments of nonstationary problems. However, like the instantaneous power spectral density function, it cannot be directly measured in the frequency domain. See Reference 7, pages 2-7, for more detailed discussions.

3.1.3 Time Varying Power Spectrum

A third method for describing the spectral composition of non-stationary data is in terms of an expression given by

$$G_y(t, f) = \frac{1}{B} \psi_y^2(t, f, B) \tag{10}$$

where $\psi_y^2(t, f, B)$ is the instantaneous mean square value of that part of $\{y(t)\}$ which is passed by a narrow bandpass filter with a bandwidth of B and a center frequency of f. Note that $\psi_y^2(t, f, B)$ is defined only for positive values of f. The value of $\psi_y^2(t, f, B)$ is given theoretically by

$$\psi_y^2(t, f, B) = 2 \int_{-\infty}^{\infty} \int_{-\infty}^{\infty} H(f_1) H^*(f_2) \mathcal{S}_y(f_1, f_2) e^{j2\pi(f_1 - f_2)t} \, df_1 \, df_2 \tag{11}$$

where H(f) is the frequency response function of the narrow bandpass filter, $H^*(f)$ is the complex conjugate of H(f), and $\mathcal{S}_y(f_1, f_2)$ is the generalized power spectral density function for $\{y(t)\}$. The quantity $G_y(t, f)$ in Eq. (10) is called the time varying power spectral density function for the process $\{y(t)\}$. This function will always be nonnegative.

The time varying power spectral density function is directly measurable in the frequency domain by ensemble averaging procedures. Specifically, the bandwidth limited mean square value is given in terms of an ensemble average by

$$\psi_y^2(t, f, B) = \lim_{N \to \infty} \frac{1}{N} \sum_{k=1}^{N} y_k^2(t, f, B) \tag{12}$$

where $y_k(t, f, B)$ is the value of the kth sample record after narrow bandpass filtering with a bandwidth of B and a center frequency of f. Hence, a time varying spectrum can be experimentally estimated by computing ensemble averages at specific times for a finite collection of records. See Reference 7, pages 7-10, for more detailed discussions.

The concept of the time varying power spectrum involves one serious restriction. This concerns the specification of the bandwidth B in Eq. (10). On the one hand, B should be very narrow so that $G_y(t, f)$ will present properly resolved spectral information for all values of f. On the other hand, B should be sufficiently wide to permit proper response to nonstationary time trends in the data. That is, if B is too narrow, time trends in the data will be smoothed out since the narrow bandpass filtering operation is equivalent to taking a weighted time average. In more practical terms, if $G_y(t, f)$ is to properly describe the time trends in the nonstationary data, the narrow bandpass filter must have a rise time which is very rapid compared to such time trends. The rise time for an ideal rectangular bandpass filter with a bandwidth of B cps is approximated by

$$T_f \approx 1/B \tag{13}$$

3.1.4 Short Time Averaged Power Spectrum

A final method for describing nonstationary spectra involves the computation of a time varying power spectrum as defined in Eqs. (10) and (12), except the ensemble average is replaced by a short time average. The result is a short time averaged power spectral density function given by

$$\overline{G_y}(t, f, T) = \frac{1}{B} \overline{y^2}(t, f, B, T) \tag{14}$$

where

$$\overline{y^2}(t, f, B, T) = \frac{1}{T} \int_{t-T}^{t} y^2(\xi, f, B)\, d\xi$$

The term $y(\xi, f, B)$ is the value of the sample record being investigated after narrow bandpass filtering with a bandwidth of B and a center frequency of f. The operations in Eq. (14) define the currently used procedure to analyze nonstationary data, as discussed in References 2 and 3, and here in Section 1.

A short time average power spectrum is clearly much easier to measure in practice than the time varying power spectrum discussed in Section 3.1.3. Only one sample record of the nonstationary process of interest is required (there is no ensemble averaging). Furthermore, the smoothing effect introduced by the narrow bandpass filter is less of a problem since time averaging is desired. On the other hand, the nonstationary process in question must be such that all time trends are deterministic and, hence, represented in every sample record which might be obtained. Also, the time averaging operation introduces a bias error which can be reduced only at the expense of increased variability errors. These matters are discussed further in the next section.

As the averaging time T in Eq. (14) is increased, the time varying spectral characteristics of the data are blurred such that $\overline{G}_y(t, f, T)$ is no longer a function of time t. In the limit where the averaging time includes the entire record length, a time averaged power spectral density function is obtained. In terms of the three previously defined spectra, the time averaged power spectral density function for the process $\{y(t)\}$ is given by

$$\overline{G}_y(f) = \lim_{T\to\infty} \frac{2}{T} \int_0^T s_y(t, f)\, dt \tag{15}$$

$$\overline{G}_y(f) = 2\, \mathcal{S}_y(f, f) \quad ; \quad (f_1 = f_2 = f) \tag{16}$$

$$\overline{G}_y(f) = \lim_{T\to\infty} \frac{1}{T} \int_0^T G_y(t, f)\, dt \tag{17}$$

Equations (15), (16) and (17) will yield identical results. Note that the quantity $\overline{G}_y(f)$ is physically realizable (defined for positive frequencies only). This is accomplished in Eqs. (15) and (16) by folding over the negative frequencies to obtain the following relationships.

$$\overline{G}_y(f) = \overline{g}_y(t, f) = 2\,\overline{s}_y(t, f) \quad ; \quad f \geq 0 \tag{18}$$

$$\overline{G}_y(f) = \mathcal{J}_y(f, f) = 2\,\mathcal{L}_y(f, f) \quad ; \quad f \geq 0 \tag{19}$$

One final point should be noted here. The computation of a time varying power spectrum could also be accomplished by curve fitting procedures instead of either ensemble or short time averaging procedures. Specifically, the bandwidth limited mean square value in Eq. (10) could be estimated at each frequency by making a "best" fit over the record length with a set of orthogonal polynomial functions. This approach is suggested and studied theoretically in References 5 and 6.

3.1.5 Experimental Illustration

For purposes of illustration, consider a nonstationary random process $\{y(t)\}$ where each sample record is given by

$$y(t) = A \cos 2\pi f_0 t\, x(t) \tag{20}$$

Here, $x(t)$ is a sample record from a stationary process $\{x(t)\}$. A time dependent autocorrelation function for $\{y(t)\}$ is obtained by substituting Eq. (20) into Eq. (7) as follows.

$$R_y(t, \tau) = A^2 \cos 2\pi f_0 \left(t - \frac{\tau}{2}\right) \cos 2\pi f_0 \left(t + \frac{\tau}{2}\right) R_x(\tau) \tag{21}$$

Here, $R_x(\tau)$ is the autocorrelation function for the stationary random process, $\{x(t)\}$. Noting the identity, $\cos(a - b)\cos(a + b) = \frac{1}{2}(\cos 2a + \cos 2b)$, Eq. (21) reduces to

$$R_y(t, \tau) = \frac{A^2}{2} (\cos 2\pi f_0 \tau + \cos 4\pi f_0 t)\, R_x(\tau) \tag{22}$$

The instantaneous power spectral density function for $\{y(t)\}$ is obtained by substituting Eq. (22) into Eq. (8) as follows.

$$s_y(t, f) = \frac{A^2}{2} \int_{-\infty}^{\infty} (\cos 2\pi f_0 \tau + \cos 4\pi f_0 t) \cos 2\pi f \tau \, R_x(\tau) \, d\tau \tag{23}$$

$$= \frac{A^2}{4} \int_{-\infty}^{\infty} \left[\cos 2\pi(f-f_0)\tau + \cos 2\pi(f+f_0)\tau + 2 \cos 2\pi f\tau \cos 4\pi f_0 t\right] R_x(\tau) \, d\tau$$

Since $R_x(\tau)$ is an even function of τ, the integral of $\cos\left[2\pi(f \pm f_0)\tau\right] R_x(\tau)$ is simply a Fourier transform of $R_x(\tau)$ which equals $S_x(f \pm f_0)$. Hence, Eq. (23) reduces to

$$s_y(t, f) = \frac{A^2}{4}\left[S_x(f - f_0) + S_x(f + f_0)\right] + \frac{A^2}{2}\left[S_x(f) \cos 4\pi f_0 t\right] \tag{24}$$

where $S_x(f)$ is the power spectral density function (defined for both positive and negative frequencies) for the stationary random process $\{x(t)\}$. From Eqs. (16) and (19), the physically realizable time averaged power spectrum is given by

$$\overline{G}_y(f) = \frac{A^2}{4}\left[G_x(f - f_0) + G_x(f + f_0)\right] \tag{25}$$

In words, Eq. (25) states that the time averaged power spectrum for $\{y(t)\}$ consists of two sidebands, each offset in frequency by $\pm f_0$, and each having the same power spectrum (excluding a gain factor) as $\{x(t)\}$. This well-known result is the basis for the heterodyning principle employed by most analog spectrum analyzers to translate an applied signal in frequency past a single fixed bandpass filter. Note that the same result could have been obtained from either the generalized power spectrum or the time varying power spectrum using Eqs. (17) or (18).

The theoretical result in Eq. (25) is illustrated for actual experimental data in Figure 3. Here, $\{x(t)\}$ is narrow bandwidth Gaussian noise with an approximately rectangular bandpass characteristic having a bandwidth of $B = 20$ cps and a center frequency of $f = 100$ cps. For convenience, a constant of $A = \sqrt{2}$ is used so that the mean square value of $\{x(t)\}$ and $\{y(t)\}$ are equal. The time averaged power spectrum for a sample record $y(t)$ is computed using an averaging time which is very much longer than each nonstationary cycle. A detailed discussion of the test set-up and measurement parameters is presented in Appendix A.

In Figure 3(a), the modulating frequency is zero; i.e., a DC voltage was used for $A(t)$. Hence, this case constitutes the spectrum of the underlying stationary process $\{x(t)\}$, since each sample record $y(t) = x(t)$. In Figure 3(b), the modulating frequency is $f_0 = 1$ cps. In this case, the spectrum for $\{y(t)\}$ is not significantly different from the spectrum for $\{x(t)\}$ because the two sidebands are offset by only $\pm$ 1 cps. As the modulating frequency increases, the power spectrum for $\{y(t)\}$ gradually changes, as seen in Figures 3(c) through 3(e), and finally breaks into two distinct sidebands, as seen in Figure 3(f).

The illustration presented in Figure 3 constitute only one case. However, the frequency shifting or heterodyning displayed in Figure 3 will occur for any desired spectral characteristics of $\{x(t)\}$, although the results may not always be so obvious. For example, assume $\{x(t)\}$ is white noise; i.e., a random process with a uniform power spectral density function over all frequencies. In this case, by definition, $G(f - f_0) = G(f)$ for all f_0. Hence, from Eq. (25),

$$\overline{G}_y(f) = \frac{A^2}{2} \quad G_x(f) \tag{26}$$

In words, the time average power spectrum for $\{y(t)\}$ will be identical (excluding a gain factor) to the power spectrum for $\{x(t)\}$, independent of f_0.

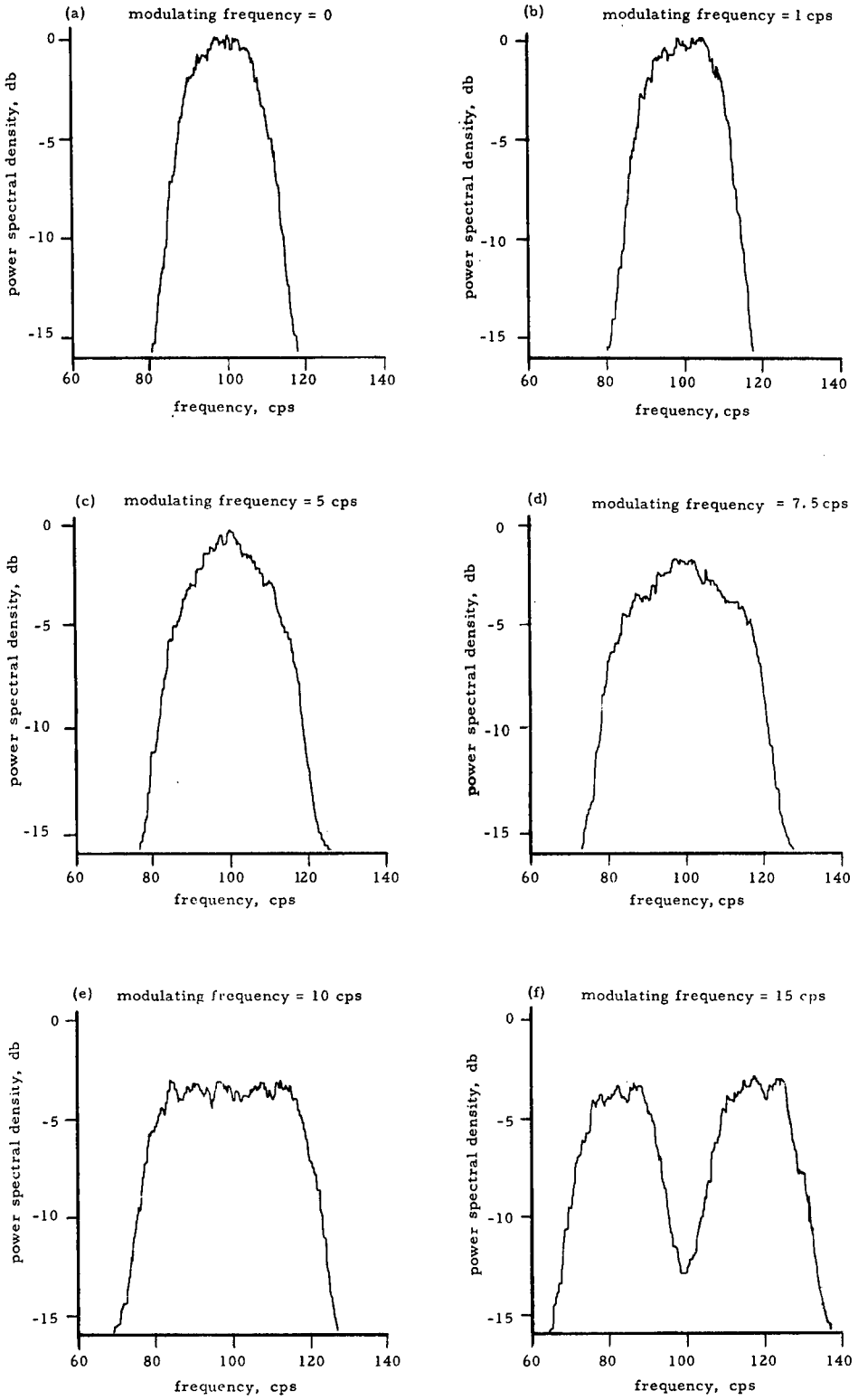

Figure 3. Relative Power Spectra for Cosine Modulated Noise

3.2 ERRORS IN NONSTATIONARY SPECTRA MEASUREMENTS

3.2.1 Stationary Power Spectrum

Before discussing errors in nonstationary spectra measurements, it is desirable to review the errors associated with stationary power spectra measurements. The power spectral density function for a stationary random process $\{x(t)\}$ may be defined by

$$G_x(f) = \lim_{B \to 0} \frac{1}{B} \psi_x^2(f, B) \tag{27}$$

where

$$\psi_x^2(f, B) = \lim_{T \to \infty} \frac{1}{T} \int_0^T x^2(t, f, B)\, dt$$

The term $x(t, f, B)$ is the value of the sample record being investigated after narrow bandpass filtering with a bandwidth of B and a center frequency of f.

The limiting operations in Eq. (27) cannot, of course, be achieved in practice. Hence, the power spectral density function can only be estimated based upon a finite bandwidth and averaging time, as follows.

$$\hat{G}_x(f) = \frac{1}{BT} \int_0^T x^2(t, f, B)\, dt \tag{28}$$

The resulting estimate will include two types of errors. The use of a finite bandwidth for the filtering operation introduces a systematic or bias error in the estimate. The use of a finite time interval for the averaging operation introduces a variability or random error in the estimate. These two errors are now discussed.

Assume a stationary random process, $\{x(t)\}$, has a true power spectral density function of $G_x(f)$. Further assume an estimate $\hat{G}_x(f_1)$ is computed at frequency f_1 using a finite bandwidth B. Although the resulting estimate applies only to a frequency interval, it is usually associated with some specific frequency for convenience of presentation. The specific frequency used is often the center of the bandwidth B. The result is a bandwidth bias error μ_b, as illustrated in Figure 4.

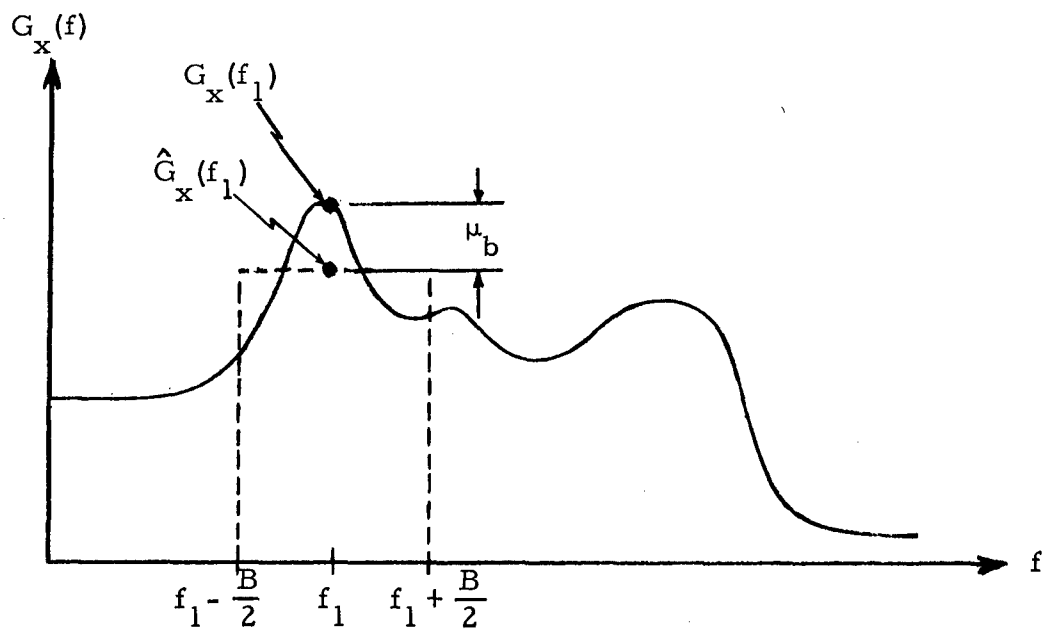

Figure 4. Illustration of Bandwidth Bias Error

From Reference 12, Chapter 5, the bandwidth bias error described in Figure 4 is approximated by

$$\mu_b = \frac{B^2}{24} G_x''(f) \tag{29}$$

where $G_x''(f)$ is the second derivative of $G_x(f)$ with respect to f. Hence, the bandwidth bias error is a function of the shape of the spectrum as well as the bandwidth B. For a fixed bandwidth, μ_b becomes small as $G_x(f)$ becomes more smooth. In the limit where $G_x'(f)$ is a constant, $\mu_b = 0$ independent of B. For a given power spectrum, μ_b becomes small as B becomes small. In the limit where B is zero, $\mu_b = 0$ independent of $G_x(f)$.

Now consider the case where a stationary random process $\{x(t)\}$ is repeatedly sampled to obtain M number of independent sample records, $x_k(t)$; k = 1, 2, 3, . . ., M. Assume an estimate of the power spectral density function at frequency f_1 is computed from each of the sample records using the same bandwidth and averaging time. Since each sample record represents a unique set of circumstances, the estimates will vary from one sample record to another, as illustrated in Figure 5.

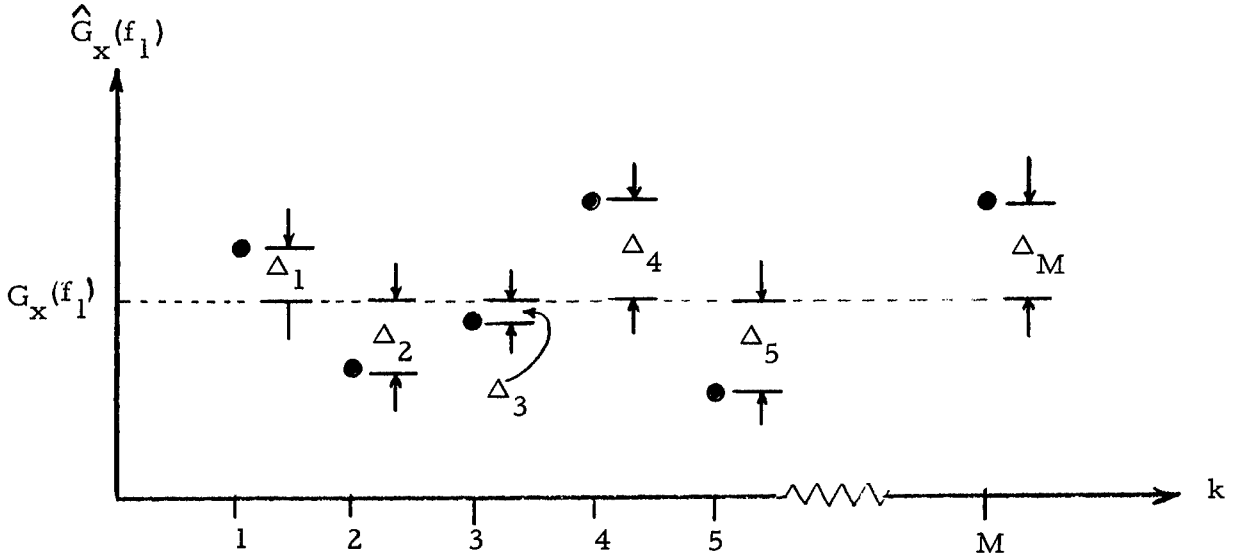

Figure 5. Illustration of Random Error

The variation in the sample estimates illustrated in Figure 5 constitutes a random error. The magnitude of this random error may be described by the standard deviation of the sample estimates, which by definition is

$$\sigma = \lim_{M \to \infty} \sqrt{\frac{1}{M-1} \sum_{k=1}^{M} \Delta_k^2} \tag{30}$$

where Δ_k is the deviation of the kth estimate from the true value at frequency f_1. From Reference 12, Ch. 5, this standard deviation is approximated by

$$\sigma = \frac{G(f)}{\sqrt{BT}} \tag{31}$$

where B is the bandwidth of the narrow bandpass filter in cps and T is the averaging time in seconds. Hence, the random error is a function of both the bandwidth and the averaging time.

A comparison of Eqs. (29) and (31) immediately reveals the conflicting requirements on the selection of a proper bandwidth B for a power spectral density analysis of stationary random data. Specifically, the bandwidth bias error becomes large as B becomes large while the random error becomes large as B becomes small. Assuming the available sample record length T is limited, the selection of an analysis bandwidth B is always a compromise between these two errors. Of course, if the available sample record length is unlimited, both errors can be made as small as desired by increasing T while reducing B to obtain a large value of the product BT with a small value of B.

3.2.2 Time Varying Power Spectrum

Now consider the time varying power spectral density function, $G_y(t, f)$, defined by Eq. (10). Assume $G_y(t, f)$ is estimated using a finite bandwidth B which is sufficiently wide to avoid any significant smoothing of nonstationary time trends in the data. Further assume the ensemble average is performed over a finite number of sample records, N. That is

$$\hat{G}_y(t, f) = \frac{1}{BN} \sum_{k=1}^{N} y_k^2(t, f, B) \tag{32}$$

The resulting estimate will again include two types of errors. The use of a finite bandwidth for the filtering operation introduces a bandwidth bias error μ_b, and the use of a finite number of records for the averaging operation introduces a random error σ. These two effects are analogous to the results for estimating power spectra of stationary data, as discussed in Section 3.2.1. In fact, the nature of the errors at any instant of time will be as illustrated in Figures 4 and 5. An exact expression for the bandwidth bias error has not been established, although Eq. (29) should provide a reasonable approximation in most cases. Noting that the time varying power spectrum is effectively a collection of ensemble averaged mean square values, the random error at any instant of time is given from Reference 6, pp. 15-18, as

$$\sigma = \sqrt{\frac{2}{N}}\, G_y(t, f) \tag{33}$$

It is important to note here that the random error σ and the bias error μ_b are independent. Hence, the bias error can be controlled by reducing the bandwidth of the filtering operation without adversely effecting the random error. On the other hand, the random error can be reduced only by increasing the number of sample records. The acquisition of a sufficient number of sample records may be difficult to accomplish in practice. For example, if the estimate is to have a standard deviation equal to 10% of the quantity being measured, then $\sigma/G(t, f) = 0.10$, and the number of sample records required is $N = 200$.

3.2.3 Short Time Averaged Power Spectrum

Finally, consider the short time averaged power spectral density function, $\bar{G}_y(t, f, T)$, defined by Eq. (14). Assume $\bar{G}_y(t, f, T)$ is estimated using a finite bandwidth B which is sufficiently wide to have an effective averaging time less than the finite averaging time T ($T > 1/B$). It follows that

$$\hat{\bar{G}}_y(t, f, T) = \frac{1}{BT} \int_{t-T}^{t} y^2(\xi, f, B) \tag{34}$$

The resulting estimate will include, as before, a bandwidth bias error introduced by the use of a finite bandwidth for the filtering operation, and a random error introduced by the use of a finite time interval for the averaging operation. These two effects are again analogous to the results for estimating power spectra for stationary data, as discussed in Section 3.2.1. However, there is another source of bias in the short time averaged power spectrum introduced by the averaging operation. This additional bias error is illustrated in Figure 6.

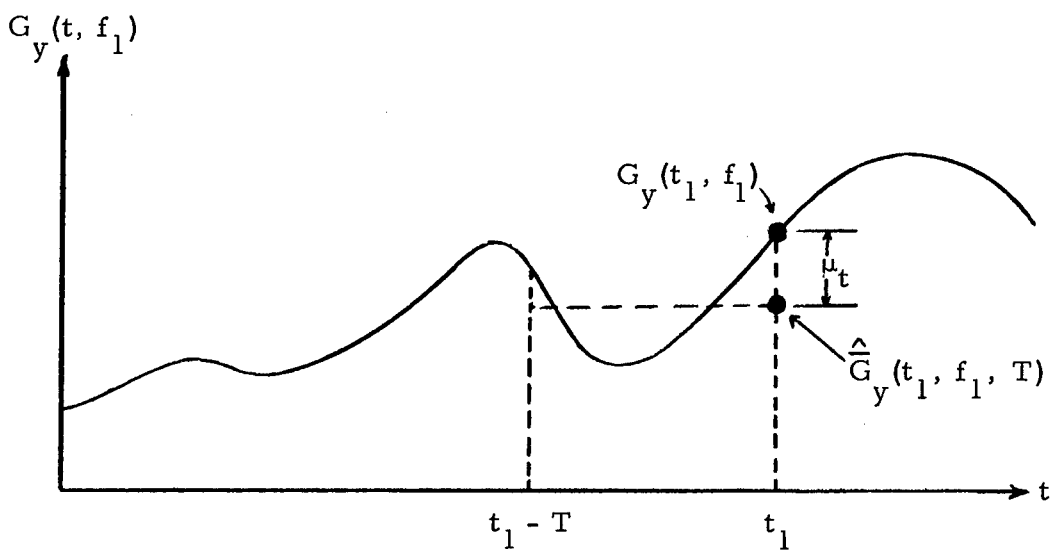

Figure 6. Illustration of Time Interval Bias Error

Assume a nonstationary random process, $\{y(t)\}$, has a true time varying power spectral density function at any frequency f_1, as illustrated in Figure 6. Further assume a short time averaged power spectral density estimate $\hat{\hat{G}}_y(t_1, f_1, T)$, is computed over a time interval from $t_1 - T$ to t_1. Although the resulting estimate applies only to a time interval, it is usually associated with some specific instant of time for convenience of presentation. The specific time used is often the end of the interval T, as noted in Figure 6. Of course, any other instant of time such as the center of the interval or the beginning of the interval could also be used. In any case, the result is a time interval bias error, μ_t.

It is clear that the time interval bias error is a function of the time trend in the data as well as the averaging time T. For a fixed averaging time, μ_t becomes small as $\{y(t)\}$ becomes more stationary. In the limit where $\{y(t)\}$ is stationary, $\mu_t = 0$ independent of T. For a given time trend, μ_t becomes small as T becomes small. In the limit where T is zero, $\mu_t = 0$ independent of $\{y(t)\}$.

From the above discussion, it is desirable to make the averaging time T short to minimize the bias error μ_t. However, as T becomes short, the random error σ becomes large. An exact expression for the random error has not been established, although the general form of the error is similar to the error expression for stationary data given by Eq. (31). That is, in most cases, the random error of the estimate can be reduced by increasing either the bandwidth B or the averaging time T. On the other hand, increasing B will increase the bandwidth bias error μ_b, and increasing T will increase the time interval bias error μ_t. Hence, the selection of a bandwidth B and an averaging time T for a short time averaged power spectral density measurement is always a compromise between a random error and a bias error. The same situation exists for

power spectra measurements of stationary data, as discussed in Section 3.2.1. For the stationary case, however, both the bias and random errors can be reduced to any desired level by increasing the averaging time T, since $\mu_t = 0$ for stationary data measurements. This is not true for nonstationary data measurements.

3.3 SPECIAL APPLICATIONS

Consider the product type nonstationary random process defined in Eq. (4). The autocorrelation function for this process at any two times, t_1 and t_2, is given by

$$R_y(t_1, t_2) = \lim_{N\to\infty} \sum_{k=1}^{N} A(t_1)\, A(t_2)\, x_k(t_1)\, x_k(t_2) \tag{35}$$

Letting $t_1 = t - \tau/2$ and $t_2 = t + \tau/2$, Eq. (35) reduces to

$$R_y(t, \tau) = A(t - \frac{\tau}{2})\, A(t + \frac{\tau}{2})\, R_x(\tau) \tag{36}$$

where $R_x(\tau)$ is a stationary autocorrelation function. If the fluctuations of $A(t)$ are relatively slow compared to the fluctuations of $\{x(t)\}$, then $A(t + \frac{\tau}{2}) \approx A(t - \frac{\tau}{2})$ for all values of τ where $R_x(\tau)$ is significantly different from zero. Thus, for this case,

$$R_y(t, \tau) = A^2(t)\, R_x(\tau) \tag{37}$$

which is a time varying autocorrelation function of a form referred to as being "locally stationary." A time varying power spectral density function for this case is given by the Fourier transform of $R_y(t, \tau)$, as follows.

$$G_y(t, f) = A^2(t)\, G_x(f) \tag{38}$$

For example, consider the cosine product type nonstationary random process defined in Eq. (20). For this case, $A(t) = A \cos 2\pi f t$. By a rather lengthy development presented in Reference 12, Chapter 9, which assumes the bandwidth of the data is wide compared to f_0, the time varying power spectrum for this model is given by

$$G_y(t, f) = \frac{A^2}{4} \int_{f-(B/2)}^{f+(B/2)} \left[G_x(f - f_0) + G_x(f + f_0) \right] df + G_x(f) \frac{A^2}{2} \cos 4\pi f_0 t \quad (39)$$

Assume the modulating frequency is very low compared to the lowest data frequency of interest ($f_0 \ll f$), and that the spectral density measurements are highly resolved (B much narrower than any spectral peaks in the data). The time varying power spectrum is then given approximately by

$$G_y(t, f) \approx \frac{A^2}{2} \left[1 + \cos 4\pi f_0 t \right] G_x(f) = \left[A^2 \cos^2 2\pi f_0 t \right] G_x(f) = A^2(t) G_x(f) \quad (40)$$

The same result can be arrived at directly using the instantaneous power spectrum given by Eq. (24). For $f_0 \ll f$, Eq. (24) reduces to

$$s_y(t, f) \approx \frac{A^2}{2} \left[1 + \cos 4\pi f_0 t \right] S_x(f) \quad (41)$$

Hence, the cosine product nonstationary random process reduces to the locally stationary form defined in Eq. (38) as f_0 becomes small compared to f.

The important point to be observed here is as follows. Assuming a nonstationary random process defined by Eq. (4) is locally stationary, a short time averaged power spectrum for a sample record will yield from Eq. (40)

$$\overline{G}_y(t, f, T) = A_0^2(t, T)\, G_x(f) \quad (42)$$

where

$$A_0^2(t, T) = \int_{t-T}^{t} A^2(\xi)\, d\xi$$

Thus, the power spectrum computed by a time average will be the same (except for a gain factor) as the time varying power spectrum, independent of the averaging time.

The above result can often be applied to improve the quality of non-stationary vibration data analysis as follows. If the nonstationary vibration data of interest fits a locally stationary model, at least over some defined time interval, then a time varying power spectrum for the data during that time interval can be established by two simple steps. The first step is to measure an over-all rms value (or mean square value) time history for the data during the locally stationary time interval. The second step is to measure a power spectrum by time averaging over the entire locally stationary time interval. The result will be as indicated in Figure 7.

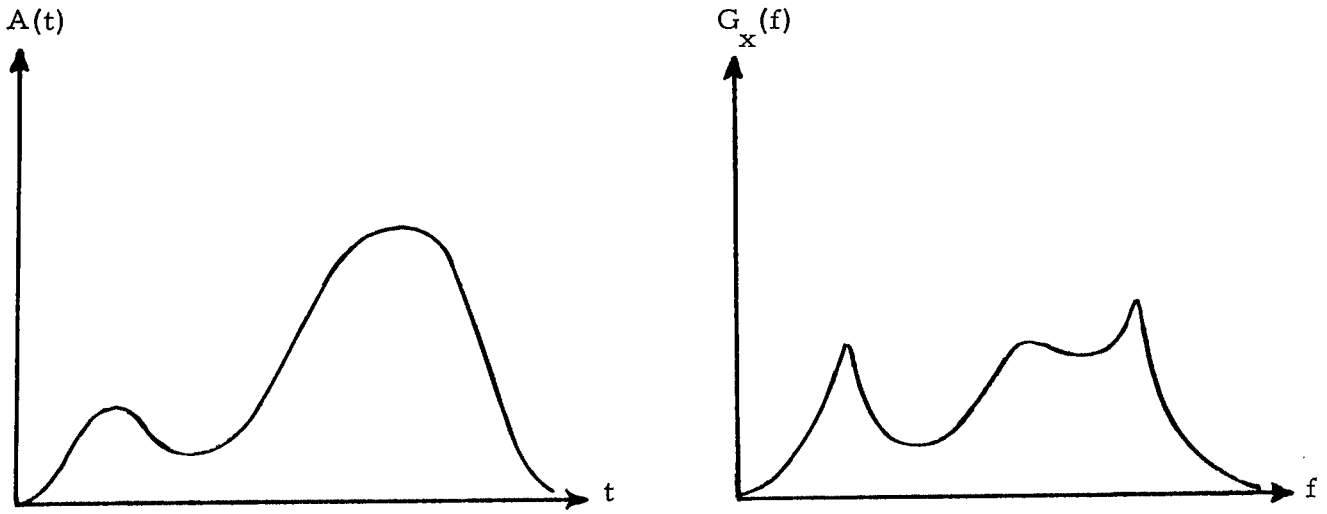

(a) rms value time history

(b) time averaged power spectrum

Figure 7. Illustration of Description for Locally Stationary Spectrum

From Figure 7, the area under the power spectrum is established by plot (a) while the shape of the power spectrum is established by plot (b).

The advantage of the above analysis procedure over the measurement of a conventional short time averaged power spectrum is that, for a given frequency bandwidth bias error and time interval bias error, the random error in the measurement at any time and frequency will be very much less. This is true because the random error is minimized for a given time interval bias error by using the entire bandwidth of the data to determine the time varying characteristics in plot (a), and minimized for a given bandwidth bias error by using the entire length of the data to determine the spectral characteristics in plot (b).

4. EXPERIMENTAL STUDIES

4.1 GENERAL APPROACH

The theoretical discussions in Section 3 indicate that analysis of nonstationary data can be greatly simplified if a locally stationary assumption is applicable to the data. Hence, it is desirable to establish whether or not this assumption is applicable to spacecraft vibration data during any portion of the launch phase. Because of the complexities and uncertainties of available analytical models for spacecraft vibration, a direct experimental investigation is considered to be the most practical way to approach the problem.

Typical launch vibration environments for spacecraft (or missile payloads) may be broadly attributed to three principal sources, as follows.

1. Acoustic excitation generated by the rocket engine. This source is most pronounced at lift-off.
2. Transonic excitation generated by combined shock wave and boundary layer activity at Mach 1.
3. Aerodynamic excitation generated by boundary layer turbulence. This source is most pronounced at maximum dynamic pressure (max "q") flight.

There are, of course, other sources of excitation which might contribute significantly to spacecraft vibration environments. For example, self-excited oscillations such as resonant burning and "pogo" may produce intense periodic vibrations which are more damaging than the vibration produced by all of the above listed sources combined. Self-excited oscillations, however, are easy to detect and can generally be analyzed by conventional periodic data reduction procedures, as outlined in Reference 1. A more common although less severe problem is the transient modal response of the launch vehicle to lift-off and control system loads. Nonstationary data of this type is sometimes quite pronounced during lift-off, as will be seen later.

There are also some very short duration transients which contribute to spacecraft dynamic environments. Included are ignition shocks, staging shocks, and explosive device operations. These short duration transients are not considered in this study.

Because of the widely different nature of the sources producing vibration during lift-off, transonic flight, and max "q" flight, it is unlikely that a locally stationary assumption would apply to all three of these launch phase events together. On the other hand, it is feasible that the assumption might apply to one or more of the events individually. It is on this basis that an experimental investigation is approached. Specifically, if the spacecraft launch vibration data is locally stationary over the time interval for one of these events, then the power spectra measured over short contiguous time intervals covering the event should differ only by a constant gain factor. Hence, a procedure to determine whether or not actual data is locally stationary is as follows:

a) Measure the short time averaged power spectrum for each of a series of contiguous time intervals which together cover the launch event of interest.

b) Normalize the area under each measured spectrum by dividing the spectral level at each frequency by the mean square value of the data for that time interval.

c) If the data is locally stationary, the resulting normalized spectra should not differ, except for variations due to statistical sampling considerations.

4.2 VEHICLES AND MEASUREMENTS

The procedure of Section 4.1 is applied here to seven individual vibration time history records collected during the launch of five different launch vehicle-spacecraft configurations. The specific vehicles and measurement locations for the vibration data were as follows.

Spacecraft	Launch Vehicle	Location	Measurement Designation
NIMBUS-1	THOR-AGENA	1. Engine mount at station 409 longitudinal direction.	NIMBUS, Location 1
		2. Forward interface of AGENA-spacecraft adaptor at station 220, lateral direction.	NIMBUS, Location 2
Orbiting Geophysical Observatory (OGO - 1)	ATLAS-AGENA	1. Base of spacecraft, lateral direction	OGO, Location 1
		2. Base of spacecraft, longitudinal direction	OGO, Location 2
Orbiting Solar Observatory (OSO - B2)	THOR-DELTA	Interface between forward motor shoulder and payload attach fitting, longitudinal direction.	OSO
ECHO A-12 (AVT - 2)	THOR	Base of spacecraft adapter, longitudinal direction.	AVT
Re-entry Vehicle	MINUTE-MAN	Base flange of A and F shelf, longitudinal direction	MINUTE-MAN

Table 1. Vehicles and Locations for Vibration Measurements

The NIMBUS, OGO, OSO, and AVT measurements represent typical spacecraft launch vibration environments. Note that both lateral and

longitudinal data are included. The MINUTEMAN Re-entry Vehicle measurement provides an example of launch vibration where the effects of transonic excitation and maximum dynamic pressure excitation are clearly separated. This situation did not occur so distinctly in the other available measurements.

Power spectra for each of the seven vibration measurements were computed over short contiguous time intervals covering those portions of the launch phase where lift-off, transonic, and/or max "q" vibrations were pronounced. The approximate times after lift-off when Mach 1 and max "q" occurred for each vehicle were as follows.

Measurement	Approximate Time After Lift-Off, Seconds (t_0 = time at lift-off)	
	Mach 1	max "q"
NIMBUS	$t_0 + 52$	$t_0 + 70$
OGO	$t_0 + 55$	$t_0 + 75$
OSO	$t_0 + 40$	$t_0 + 60$
AVT	$t_0 + 39$	$t_0 + 50$
MINUTEMAN	$t_0 + 18$	$t_0 + 37$

Table 2. Approximate Times to Mach 1 and Max "q"

The actual measurements of power spectra were accomplished using a one-third octave band filter set with a true rms value detector, an RC type lowpass filter averager, and a logarithmic readout. All vibration records were analyzed by obtaining continuous rms time history plots of the data in each of the one-third octaves where pertinent data existed. The averaging time constant used for the analysis was selected to be as long as possible without introducing observable time interval bias errors. Details are presented in Appendix B.

The continuous rms time histories were converted into discrete values at specific times by recording the instantaneous rms values noted at equally spaced time intervals. The interval between readings was selected to be at least 5 RC averaging time constants (5K) to assure that each rms value was reasonably independent of the preceding or following value. The discrete rms values were then converted into mean square values in decibels relative to the over-all mean square value by dividing the one-third octave values at each time by the over-all value at that time. Since the data were recorded in terms of a logarithmic ordinate (decibels), the division was actually accomplished by subtracting the over-all value in db from the one-third octave values in db at each time (there is no difference between mean square and rms values on a db scale). The resulting relative mean square values in the one-third octave bands were finally converted into normalized power spectra (when desired) by subtracting off the frequency bandwidth for each third octave expressed in db. Instrumentation and data reduction details are presented in Appendix B.

Note that all vibration time history records were retrieved by use of radio telemetry where lowpass filtering operations were involved. The lowpass cut-off frequencies varied from 750 to 2000 cps depending upon the telemetry channel used. This fact, however, is not pertinent to the experimental studies of interest here.

4.3 RESULTS

The over-all rms time history and the relative mean square value time histories for the pertinent one-third octave levels are presented in Appendix C. Note that the data measured during lift-off are presented on separate plots from the data measured during transonic and max "q" flight so that the time scale for lift-off can be expanded. Data are presented only for those cases where the indicated vibration levels exceeded the background noise by at least 5 db, which explains why data are omitted in certain octaves. A summary of the location of data in Appendix C is presented in Table 3 below.

Measurement	Figure Numbers in Appendix C			
	Lift-Off Data		Transonic and Max "q" Data	
	Over-all RMS Time History	One-Third Octave Band Levels Relative to Over-all	Over-all RMS Time History	One-Third Octave Band Levels Relative to Over-all
NIMBUS, Location 1	C-1	C-2	C-9	C-10
NIMBUS, Location 2	C-1	C-3	C-9	C-11
OGO, Location 1	C-4	C-5	C-12	C-13
OGO, Location 2	C-4	C-6	C-12	C-14
OSO	C-7	C-8	None*	None*
AVT	None*	None*	C-15	C-16
MINUTEMAN	None*	None*	C-17	C-18

* not included because date were of poor quality or repetitious of other available data.

Table 3. Summary of Reduced Data

To translate the data in Appendix C from relative mean square values to normalized power spectra, the bandwidth in db for each one-third octave must be subtracted from the relative mean square value for that one-third octave. A list of bandwidths in db for one-third octaves is presented in Table 4.

Center Frequency cps	Bandwidth		Center Frequency cps	Bandwidth	
	cps	db		cps	db
12.5	2.9	4.6	125	29	14.6
16.0	3.7	5.6	160	37	15.6
20.0	4.6	6.6	200	46	16.6
25.0	5.8	7.6	250	58	17.6
31.5	7.3	8.6	315	73	18.6
40.0	9.2	9.6	400	92	19.6
50.0	11.6	10.6	500	116	20.6
63.0	14.5	11.6	630	145	21.6
80.0	18.0	12.6	800	180	22.6
100.0	23.0	13.6	1000	230	23.6
			1250	290	24.6
			1600	370	25.6
			2000	460	26.6

Table 4. One-Third Octave Bandwidths

5. DISCUSSION OF EXPERIMENTAL RESULTS

5.1 STATISTICAL EVALUATION TECHNIQUES

If the vibration data summarized in Appendix C are locally stationary, then the relative mean square value time histories for the one-third octave band levels should not differ "significantly" from one time to another. Because the basic data are random in nature, the relative mean square measurements are also random variables. Hence, variations due to statistical sampling considerations (random errors) should be expected in the results. The problem is to establish a criterion for deciding whether or not observed variations among a collection of measurements are significant, or simply the result of random error.

There are several types of tests for significant differences which could be applied here. The simplest of these is the F_{max} test, which is now described. Consider N sample records of vibration data, each of which has a mean value of zero and a mean square value of ψ_i^2 $(i = 1, 2, \ldots, N)$. Assume a sample mean square value, s_i^2 $(i = 1, 2, \ldots, N)$, is measured for each of the N sample records, where a similar averaging time is used for each measurement. Let s_{max}^2 be the largest of the sample mean square values and s_{min}^2 be the smallest. If the sample records are obtained from the same random data (that is, if $\psi_1 = \psi_2 = \ldots = \psi_N$), then the sampling distribution for the maximum to minimum mean square value ratio is given by the F_{max} distribution. That is,

$$\frac{s_{max}^2}{s_{min}^2} = F_{max} \tag{43}$$

The distribution for F_{max} is a function of N, the number of sample mean square values, and n, the number of degrees-of-freedom for each sample value.

The F_{max} distribution may be applied as a test for significant differences among a collection of N mean square values as follows. Determine the maximum and minimum of the N mean square values. A $100\ (1 - \alpha)$ % confidence interval for this ratio is given by the $100\ (1 - \alpha)$

percentile point (or 100α percentage point) of the F_{max} distribution, denoted by $F_{max;\,(1-\alpha)}$. Now, if the ratio of s^2_{max} to s^2_{min} is greater than $F_{max;\,(1-\alpha)}$, the differences among the N mean square values would be considered significant at the α level of significance. If the ratio of s^2_{max} to s^2_{min} is less than $F_{max;\,(1-\alpha)}$, the differences among the N mean square values would not be considered significant.

A table of $100\,(1-\alpha) = 99$ percentile values ($\alpha = 0.01$) for F_{max} is presented in decibels for various values of N and n in Table 5. For example, assume $N = 8$ mean square values are measured where each has $n = 12$ degrees-of-freedom. Further assume that the ratio of the maximum to minimum value is 8.7. Does this constitute a significant difference? From Table 5, the difference is not significant at the $\alpha = 0.01$ level of significance since $F_{max;\,0.99} = 9.6$. Hence, there is no reason to believe that the measurements were obtained from different random processes.

99 Percentile Values for F_{max}, in Decibels*

n \ N	2	3	4	5	6	7	8	9	10	11	12
3	16.8	19.3	20.8	21.8	22.6	23.3	24.0	24.5	24.9	25.3	25.6
4	13.7	15.7	16.9	17.7	18.4	19.0	19.5	19.9	20.3	20.5	20.8
6	10.4	11.9	12.8	13.4	14.0	14.3	14.8	15.1	15.3	15.6	15.7
8	8.8	10.0	10.7	11.2	11.6	12.0	12.3	12.5	12.8	13.0	13.2
10	7.7	8.7	9.3	9.8	10.2	10.5	10.7	10.9	11.1	11.3	11.4
12	6.9	7.9	8.4	8.8	9.1	9.4	9.6	9.8	10.0	10.1	10.3
15	6.1	6.9	7.4	7.8	8.1	8.3	8.5	8.6	8.8	8.9	9.0
20	5.2	5.8	6.3	6.6	6.9	7.1	7.2	7.4	7.5	7.6	7.7
30	4.2	4.8	5.2	5.4	5.6	5.7	5.8	5.9	6.0	6.1	6.2
60	2.9	3.4	3.6	3.8	3.9	4.0	4.1	4.2	4.3	4.3	4.3

* The data in this table are obtained from Reference 13, pages 468, 469.

Table 5. 99 Percentile Values for F_{max} Distribution

For the experimental data of interest here, the F_{max} distribution can be applied as a test for significant differences among N relative mean square values in one-third octaves if two assumptions are permitted. The first assumption is that the statistical variability or random error in relative mean square value measurements for locally stationary data is the same as for stationary data. The second assumption is that the power spectral density function for the vibration data within one-third octaves is reasonably uniform. Neither assumption is rigorously valid, but the lack of validity of either assumption should tend to produce greater variability than predicted by the F_{max} distribution. Hence, the F_{max} test should yield conservative results.

With the above assumptions, the degrees-of-freedom for a relative mean square value measurement in a one-third octave bandwidth is given from Reference 1, Appendix A, as

$$n = 4BK \tag{44}$$

where B is the one-third octave bandwidth and K is the equivalent RC averaging time constant. Equation (44) assumes K is very much less than the available record length.

5.2 LIFT-OFF VIBRATION DATA

Referring to Figures C-1 through C-6 in Appendix C, it is seen that the lift-off vibration levels for the NIMBUS and OGO measurements display definite common characteristics. Specifically, the over-all rms vibration levels are constant (within one db) for the first few seconds after t_0, and then fall off gradually as the lift-off is accomplished. The relative mean square values in one-third octaves tend to remain constant during the time intervals that the over-alls are constant (about the first two seconds after t_0 for NIMBUS and the first four seconds after t_0 for OGO). Hence, during the few seconds after t_0, the data is not just locally stationary, but completely stationary in terms of absolute values as well.

To further illustrate these results, consider the summary of power spectra for the OGO measurements presented in Figure 8. These plots represent the range of eight power spectra for the vibration levels at 1/2 second intervals from t_0 to $t_0 + 3.5$ seconds. Note that the data in Figure 8 is for absolute power spectra values, and not for normalized power spectra values. A 99 percentile interval for the expected statistical scatter among the measurements at any frequency (based upon an F_{max} distribution) is also included to help indicate the significance of apparent differences among the eight power spectra in each plot. If the vibration is stationary during the interval in question, there should be no significant differences among the power spectra computed during that interval.

It is clear from the data in Figure 8 that an assumption of stationarity is acceptable for the OGO vibration measurements during the first three and one-half seconds of lift-off. Similar results are obtained for the NIMBUS vibration measurement during the first two seconds of lift-off.

Referring to Figures C-7 and C-8, the lift-off vibration levels for the OSO measurement present a completely different situation from the NIMBUS and OGO data. The over-all level during lift-off peaks and then falls off immediately. There is no significant time interval over which the lift-off vibration is stationary. Furthermore, the predominant vibration energy is in the low frequencies (below 100 cps) rather than in the high frequencies. In fact, most of the vibration energy is in the one-third octave centered at 16 cps. This result is due to a strong transient response of the launch vehicle in a longitudinal normal mode which is excited by the lift-off shock. Such longitudinal response is common for certain types of launch vehicles (the AVT measurement displayed similar characteristics during lift-off). High frequency vibration is probably present as it is for the NIMBUS and OGO measurements, but this data is completely masked by the intense low frequency vibration and lost in the background instrument noise.

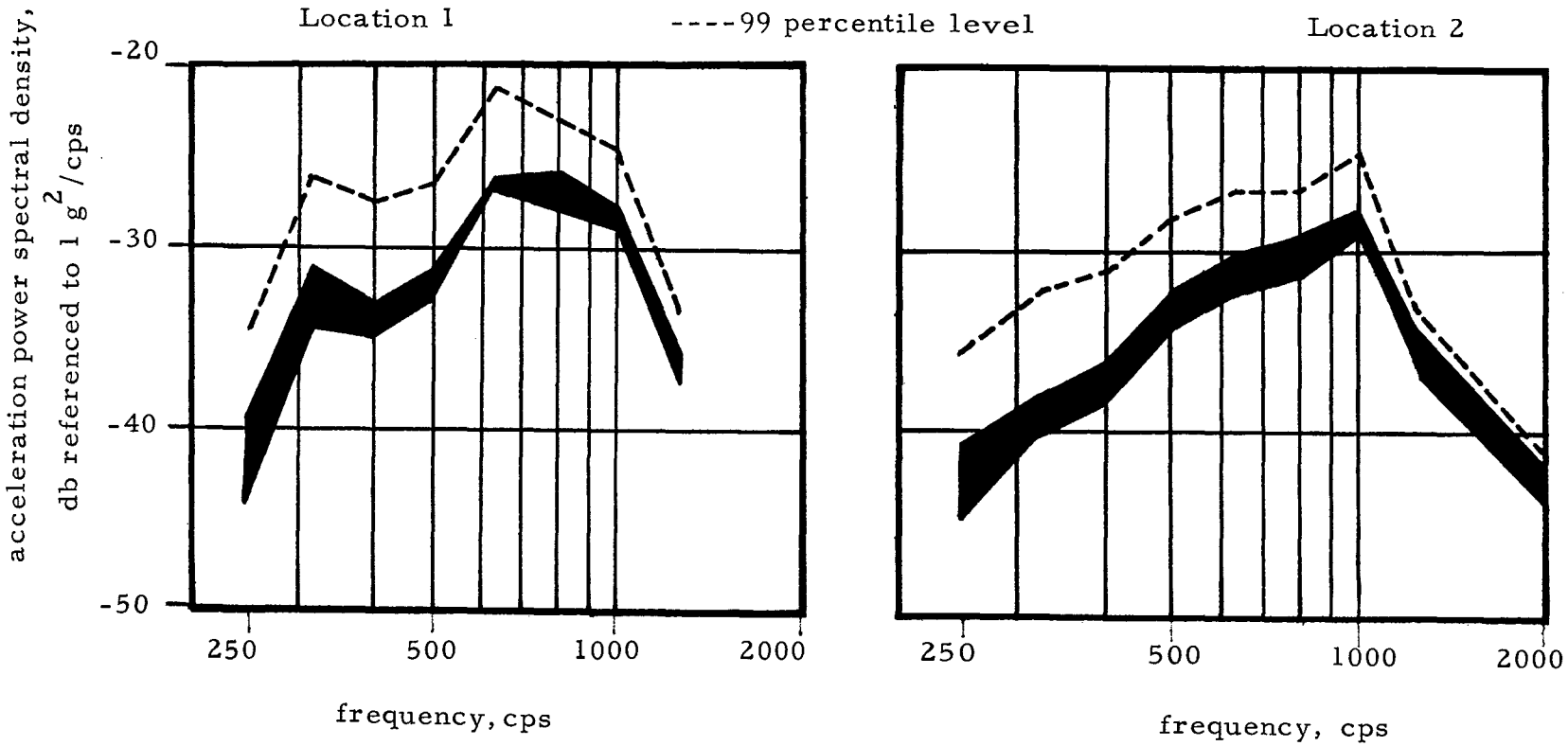

time interval - lift-off region from t_0 to $t_0 + 3.5$ seconds

Figure 8. Range of Power Spectra for OGO Lift-off Vibration

From Figure C-8, it is seen that the relative mean square values in the one-third octaves display considerable variation. However, because the data is concentrated at low frequencies where the one-third octave bandwidths are narrow, and because the averaging time constant was relatively short (K = 0.03), the variations do not constitute significant differences. For example, consider the 63 cps one-third octave where the variation is 14 db among only four measurements. The bandwidth is B = 14.5 cps and the averaging time constant is K = 0.03, which gives $n < 2$. From Table 5, a 99 percentile level for this case is over 20 db. Hence, a 14 db variation is not significant. Similar results are obtained for the other one-third octaves. On this basis, there is no reason to believe the data are not locally stationary over the first two seconds of lift-off. However, the power of this decision is very weak because of the small sample size. For various practical reasons, it is believed that the data would probably fail a locally stationary test under more stringent conditions. This means that a power spectrum computed by time averaging over such transient data could produce misleading results.

There is another problem posed by the use of conventional power spectra techniques for the analysis of such data. Because the data is heavily concentrated in a narrow frequency interval, the bandwidth of the bandpass filter used for a power spectral density analysis would have to be very narrow to avoid large bandwidth bias errors, as discussed in Section 3.2.1. In practice, it perhaps would be better to describe such data in terms of an rms value time history for some defined bandwidth (rather than normalizing the measurement to a mean square value per cps). Another suitable approach is to simply define the data in terms of an instantaneous value time history for some defined bandwidth. Since the data is concentrated in the lower frequencies, this can be accomplished easily using standard galvonometer type oscillographs. Such information can be used to establish an "equivalent" sinusoidal simulation of the transient if one is prepared to accept a peak criterion for equivalent.

5.3 TRANSONIC VIBRATION DATA

Referring to Figures C-9 through C-18 in Appendix C, it is seen that vibration levels for all measurements are neither stationary nor locally stationary through the transonic region. There is a common trend in all data for the over-all vibration to peak near Mach 1 and to shift in frequency composition with energy moving from lower to higher frequencies. These effects are most obvious for the AVT and MINUTEMAN measurements.

To further illustrate these general results, consider the summary of normalized power spectra for the AVT measurements presented in Figure 9. Plot (b) represents the range of seven normalized power spectra for the vibration levels in a 10-second interval covering Mach 1, which occurs at t_0 + 39 seconds. Plot (a) gives the range of seven normalized power spectra for the vibration levels in the preceding 10-second subsonic interval, and Plot (c) gives the range of seven normalized power spectra for the vibration levels in the following 10-second supersonic interval. A 99 percentile interval for the expected scatter among the measurements at any frequency (based upon an F_{max} distribution) is included to help indicate the significance of apparent differences among each group of seven normalized power spectra.

Three principle trends are indicated by the data in Figure 9. First, the range of normalized power spectra values is greatest for the 10-second interval covering Mach 1. In this interval, the range of values constitutes a significant difference at nearly all frequencies, meaning the vibration is not locally stationary in the transonic region. Second, the range of values in the 10-second subsonic interval and the 10-second supersonic interval do not constitute a significant difference at any frequencies, meaning a locally stationary assumption is acceptable for the vibration measurements during these time intervals. Third, the vibration energy shifts sharply up in frequency from the subsonic interval to the supersonic interval. Similar results occur for all the vibration measurements in Appendix C.

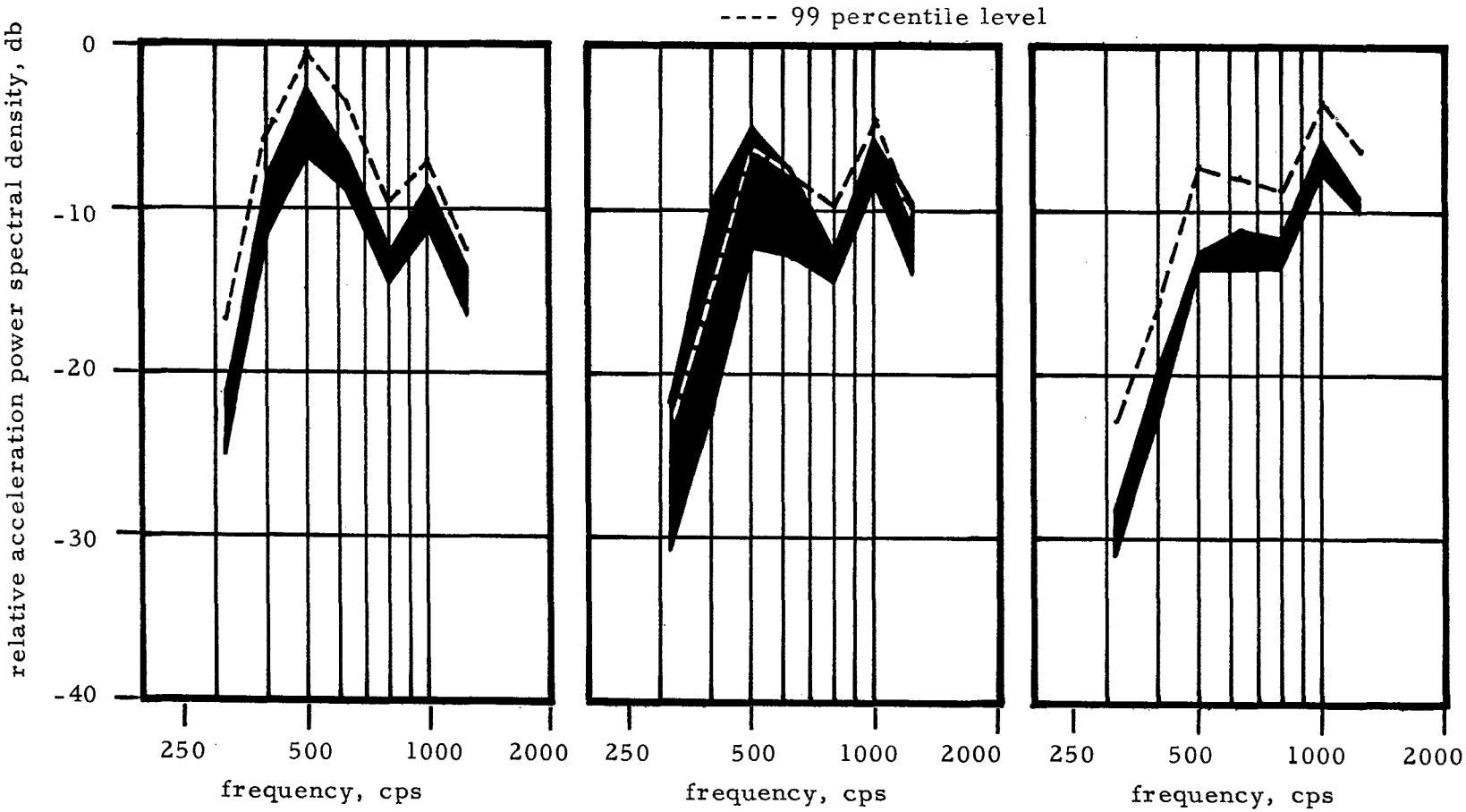

(a) Subsonic Region from $t_0 + 24$ to $t_0 + 34$ secs.

(b) Transonic Region from $t_0 + 34$ to $t_0 + 44$ secs.

(c) Supersonic Region from $t_0 + 44$ to $t_0 + 54$ secs.

Figure 9. Range of Normalized Power Spectra for AVT Transonic Vibration

The above results are particularly significant because the transonic vibration levels are often the most severe which occur during the launch phase. For such cases, a sample record which straddles the maximum vibration level is usually selected for analysis. It is effectively assumed that the data is reasonably stationary during this interval. However, this assumption is not valid, as illustrated by the AVT vibration data summary in Figure 9. Because of the sharp shift in the frequency composition of the vibration data as the vehicle passes through Mach 1, a power spectrum computed from a sample record covering Mach 1 may mask important results.

It should be emphasized that the above conclusions apply even when the over-all rms value for the data is reasonably constant through the transonic interval. For example, consider the over-all rms time history for the NIMBUS , Location 1, vibration data presented in Figure C-9 of Appendix C. It is seen that there is about a 15-second time interval around Mach 1 where the over-all vibration level is constant within 1.5 db. A first impulse would be to consider the vibration data stationary during this interval, meaning a sample record selected for any segment of this time interval will represent the entire interval. This is not true, as is illustrated in Figure 10.

Figure 10 includes three highly resolved (narrow bandwidth) power spectral density measurements for NIMBUS, Location 1, vibration data. All three power spectra were measured from 4-second long sample records covering intervals with similar over-all rms values near Mach 1, which occurs at about $t_0 + 52$ seconds.

The first power spectrum, Plot (a) was measured over the time interval from $t_0 + 48$ to $t_0 + 52$ seconds, which is at the start of the transonic peak

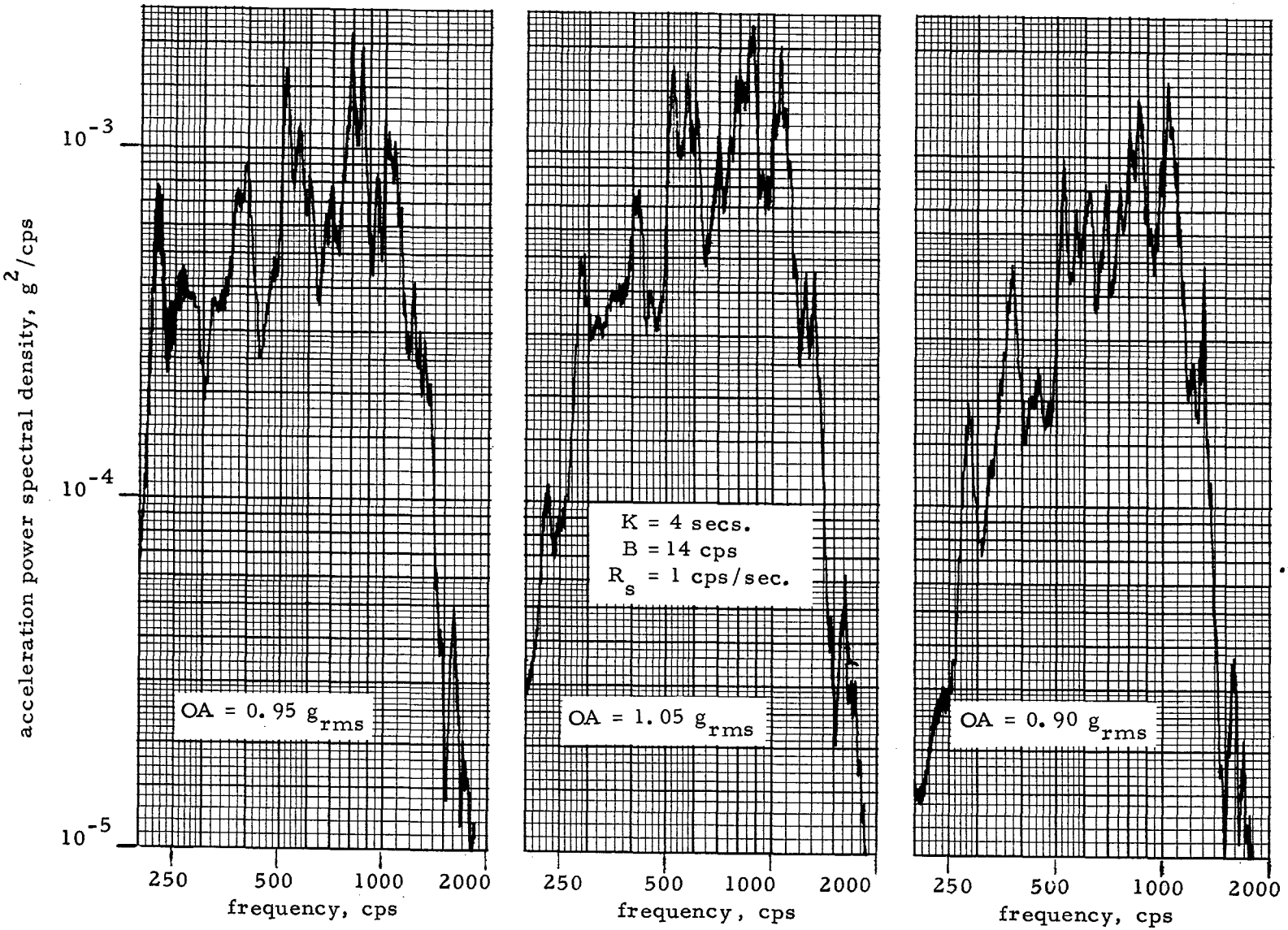

Figure 10. Power Spectra for NIMBUS, Location 1, Transonic Vibration

where the vehicle is still subsonic. The second power spectrum, Plot (b), was measured over the time interval from $t_0 + 54$ to $t_0 + 58$ seconds, which is at the center of the transonic peak just past Mach 1. The third power spectrum, Plot (c), was measured over the time interval from $t_0 + 62$ to $t_0 + 66$ seconds, which is at the end of the transonic peak where the vehicle is supersonic.

From Figure 10, the shift in the spectral composition of the data is apparent, particularly at the low frequencies. For example, Plot (a) includes a relatively intense spectral peak at about 225 cps with a density of 0.0008 g^2/cps. In Plot (b), the peak appears with a density of 0.0001 g^2/cps, or 9 db less than in Plot (a). In Plot (c), the peak is no longer significant. Hence, although the over-all rms vibration level did not change appreciably during the interval from $t_0 + 50$ to $t_0 + 65$ seconds, the spectral composition of the data did.

5.4 MAX "Q" VIBRATION DATA

Referring again to Figures C-9 through C-18 in Appendix C, the over-all vibration levels for all measurements, except MINUTEMAN, fall off rather smoothly through the region of max "q". One might expect to see a distinct peak at max "q" since dynamic pressure is a key parameter in the vibration produced by aerodynamic boundary turbulence. However, for the NIMBUS, OGO, and AVT data, the rise into a max "q" vibration peak is masked by the after effects of transonic excitation, which is much more intense than the max "q" excitation for these cases. In the MINUTEMAN data where max "q" effects are more pronounced, the expected rise to a distinct max "q" vibration peak is present, as seen in Figure C-17.

Now consider the relative mean square values in one-third octaves for the time interval around max "q". In all cases, the relative mean square values are seen to remain reasonably constant over time intervals of 10 to 20 seconds, in spite of the fact that the over-all vibration levels have dropped over 10 db in some cases during this interval. This point is illustrated by the summary of normalized power spectra for the supersonic AVT measurements presented previously in Plot (c) of Figure 9. The range of normalized power spectra values in Plot (c) represents seven power spectra measurements over a 10-second time interval which includes max "q" at t_0 + 50 seconds. As concluded in Section 5.3, the range of normalized power spectra values does not constitute a significant difference, meaning a locally stationary assumption is acceptable for this time interval.

To further illustrate this point, consider the summary of normalized power spectra for the NIMBUS measurements presented in Figure 11. The range of normalized power spectra values in Figure 11 represents eleven power spectra measurements over a 20-second time interval from 10 seconds before max "q" to 10 seconds after max "q". This range of values

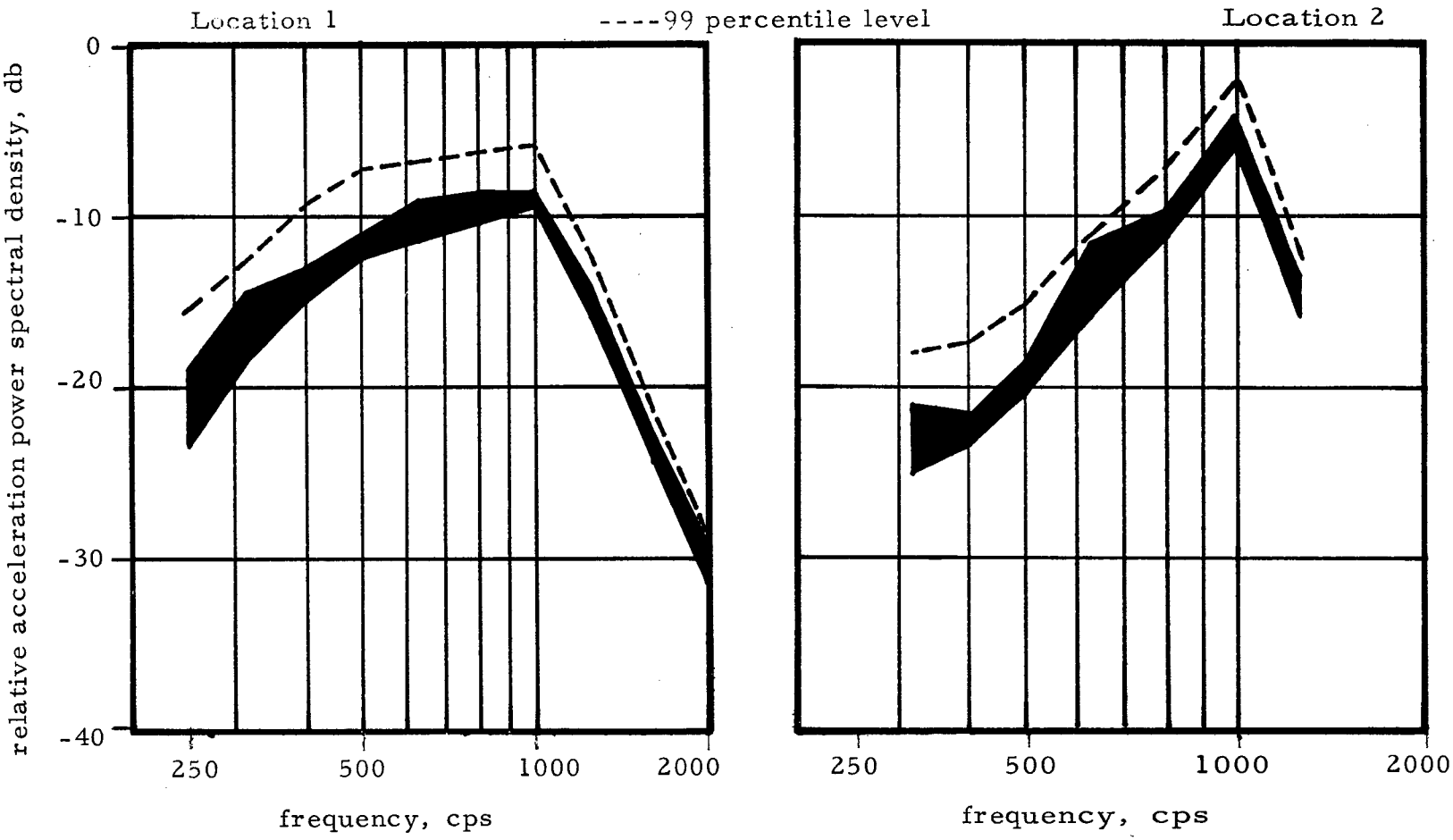

Figure 11. Range of Normalized Power Spectra for NIMBUS Max "Q" Vibration

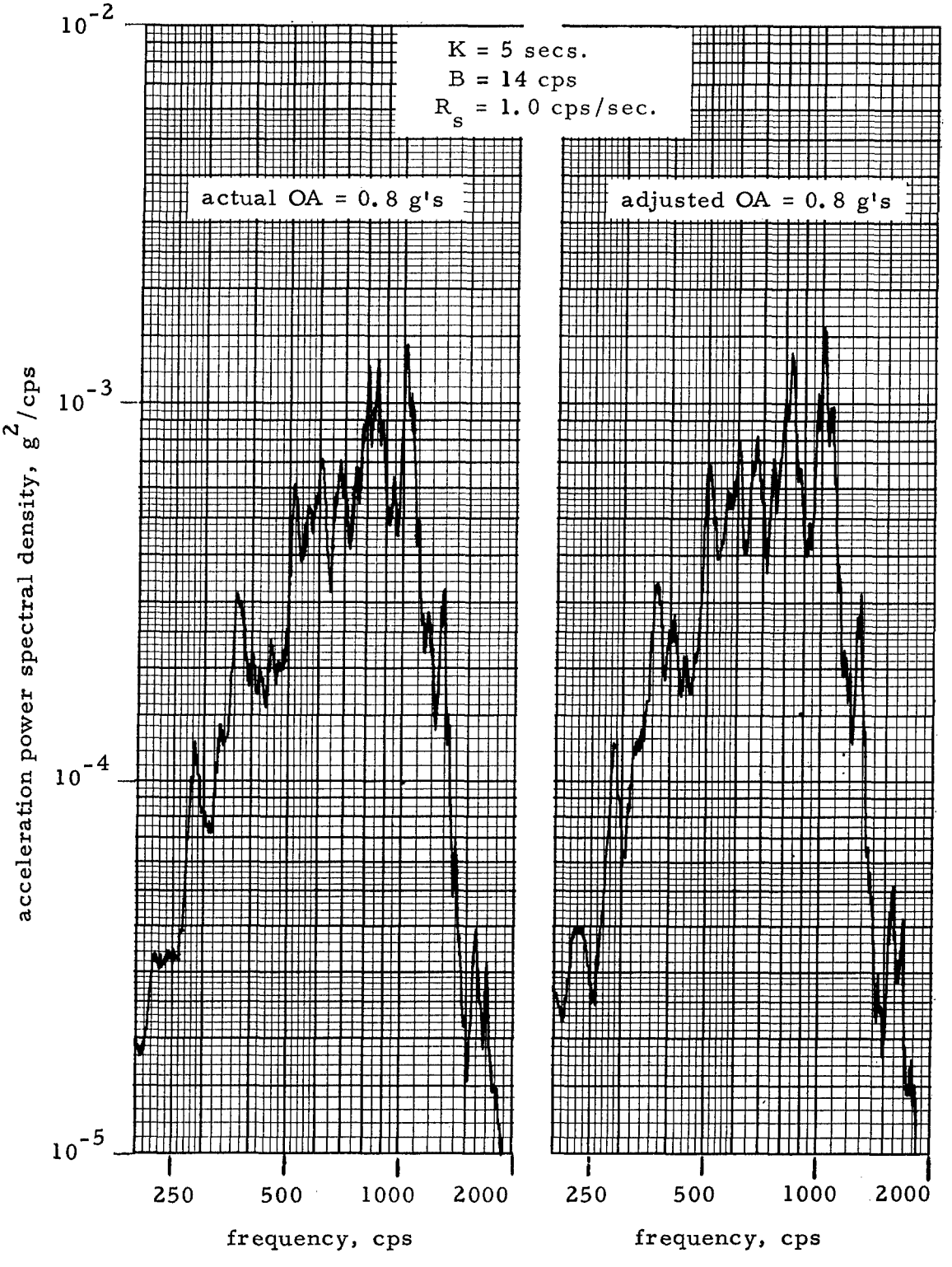

(a) t_0 +65 to t_0 +70 seconds (b) t_0 +70 to t_0 +75 seconds

Figure 12a. Power Spectra for NIMBUS, Location 1, Max "Q" Vibration

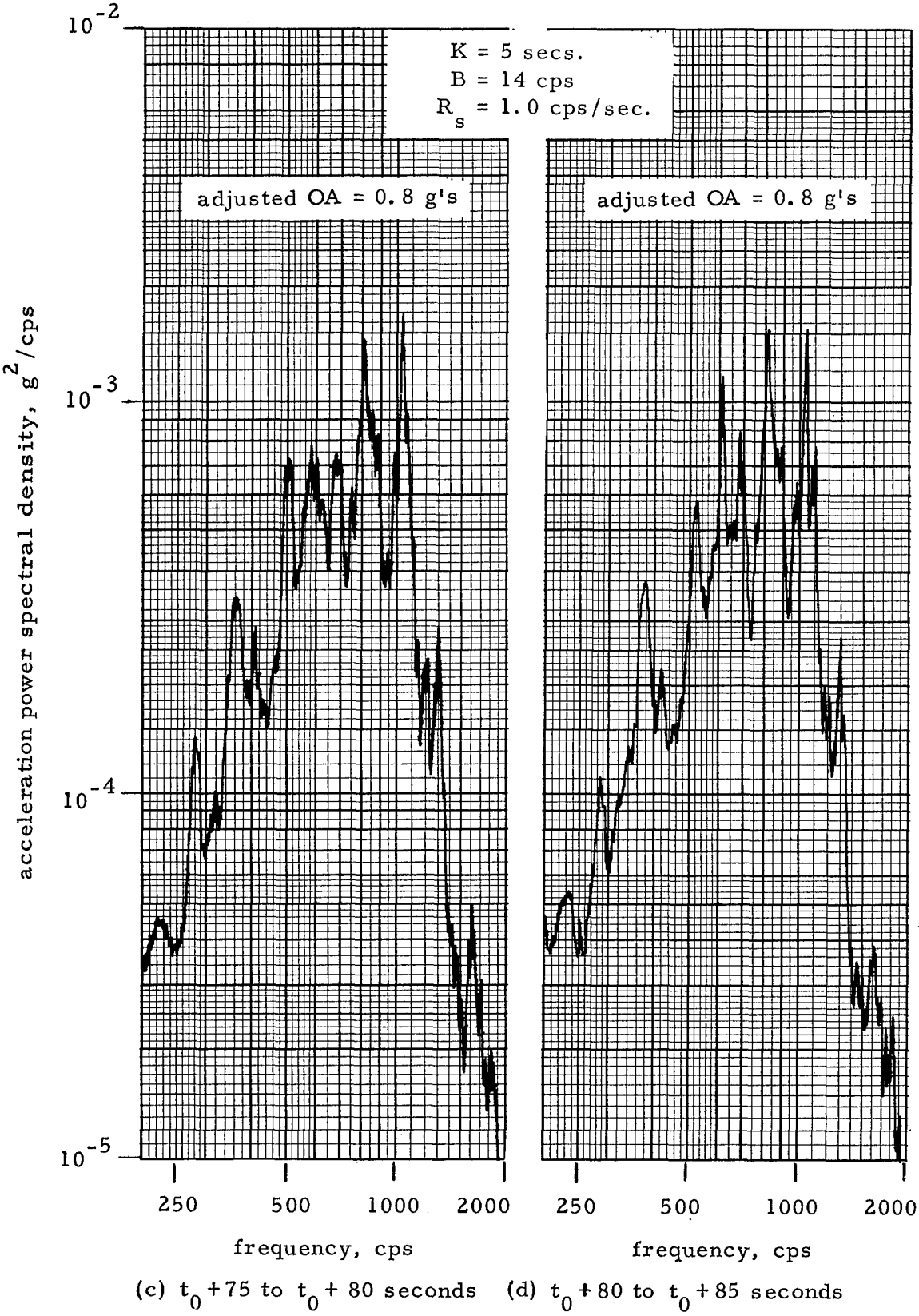

(c) t_0 + 75 to t_0 + 80 seconds (d) t_0 + 80 to t_0 + 85 seconds

Figure 12b. Power Spectra for NIMBUS, Location 1, Max "Q" Vibration

does not constitute a significant difference at any frequency. Similar results occur for all other measurements in Appendix C. Hence, a locally stationary assumption appears to be acceptable for the nonstationary vibration data in the region of max "q" for time intervals of as long as 20 seconds.

The above results indicate that the vibration data in the region of max "q" may be defined by the procedure outlined in Section 3. 3. Specifically, the power spectrum shape can be computed from a long sample record covering the max "q" region, and the area under the power spectrum at any instant of time can be determined from an over-all rms value time history (area = rms^2).

To illustrate this fact, consider Figure 12 which includes four highly resolved power spectra computed for NIMBUS, Location 1, max "q" vibration. The four power spectra are computed over four contiguous intervals, each of five seconds duration, which together cover the period from t_0 + 65 to t_0 + 85 seconds (max "q" occurs at about t_0 + 70 seconds). Now, the data is definitely nonstationary during this total period with an over-all rms level that falls from about 0. 8 g's average for the first interval to about 0. 35 g's average for the fourth interval. However, based upon the over-all rms time history, the ordinate of all four power spectra is set up as if the over-all rms level was 0. 8 g's in all cases. Note that the power spectral density at each frequency represents a mean square value measurement with $n = 2BT_r = 140$ degrees-of-freedom. A 99 percentile level for the scatter among the four measurements at any frequency is estimated from Table 5 to be about 2. 5 db (a ratio of 1. 8 to 1). With this in mind, it is clear that there are no significant differences among the four plots.

6. CONCLUSIONS AND RECOMMENDATIONS

Experimental studies in this document indicate that the nonstationary vibration data associated with spacecraft launch vibration environments display certain important typical characteristics. These typical characteristics may be summarized as follows.

1. For those cases where lift-off vibration is due principally to to acoustic excitation generated by rocket engine noise, the vibration data during lift-off can be considered stationary for time intervals of two seconds or longer. For those cases where the lift-off vibration is due principally to a longitudinal modal response of the launch vehicle to lift-off shock, the vibration data during lift-off will be nonstationary with the energy concentrated around the frequency of the responding normal mode.

2. The vibration data during transonic flight is highly nonstationary. A pronounced shift in the vibratory energy from lower to higher frequencies occurs as the spacecraft passes through Mach 1. A locally stationary assumption, however, appears to be acceptable for the vibration data which occurs before and after Mach 1.

3. The vibration data during max "q" flight is nonstationary, but a locally stationary assumption is generally applicable to the data for time intervals of up to 20 seconds.

Based upon the above conclusions, specific procedures are now suggested for the analysis and description of spacecraft launch vibration data. The suggested procedures are intended to produce the most accurate and representative measurements practical for the pertinent characteristics of the data. Emphasis is placed upon the proper selection and detailed analysis of individual sample records covering critical time intervals, rather than a general analysis of the entire launch phase vibration. The selected sample records can be analyzed either by one pass through a

multiple filter type power spectral density analyzer, or by recirculation through a single filter type power spectral density analyzer. Of course, the sample records could be analyzed on a digital computer as well.

1. Compute an over-all rms (or mean square) value time history record for each vibration measurement over the entire launch phase interval. Compute the rms value time history using an averaging time which is just short enough to make time interval bias errors negligible. See Appendix B-2 for details and illustrations.

2. If there is an interval of one second or more during lift-off when the over-all rms vibration level is reasonably uniform, compute the power spectrum by averaging over this entire stationary interval. If there is no significant time interval during lift-off when the over-all rms vibration level is reasonably uniform, then the data is probably narrow in bandwidth and concentrated around the frequency of a launch vehicle normal mode. See Section 5.2 for a discussion of possible analysis procedures.

3. If significant transonic vibration occurs, as it usually will, compute a power spectrum from a sample record which terminates just prior to Mach 1. The sample record should be two to five seconds long, depending upon the flight profile. Note that the time at which any measurement point on the spacecraft passes through Mach 1 can usually be identified by listening to an audio playback of the vibration signal recorded at that point. The typical sharp shift in the composition of the vibration data at Mach 1 is clearly detectable by ear.

4. If significant max "q" vibration occurs, compute a power spectrum for the max "q" vibration data from a sample record which covers the max "q" region. The length of the sample record should be reasonably long, at least five seconds, to minimize statistical errors. The length may be as long as 10 to 20 seconds depending upon the flight profile. In many cases, transonic vibration will be completely dominant over max "q" vibration to the point where no distinct max "q" peak is visible in the over-all rms time history. If this occurs, a post-Mach 1 sample record which covers the time of max "q" should still be analyzed.

5. All short duration transients such as ignition shocks, staging shocks, etc., must be detected from a plot of either the instantaneous vibration time history or the rms value time history, and analyzed separately by appropriate techniques. The same is true for self-excited oscillations such as resonant burning or "pogo," when they occur. The analysis procedures presented above do not apply to these cases.

The data obtained in Steps 1 through 4 above can be used to describe the time varying spectral characteristics of the pertinent launch vibration environment, as illustrated in Figure 13.

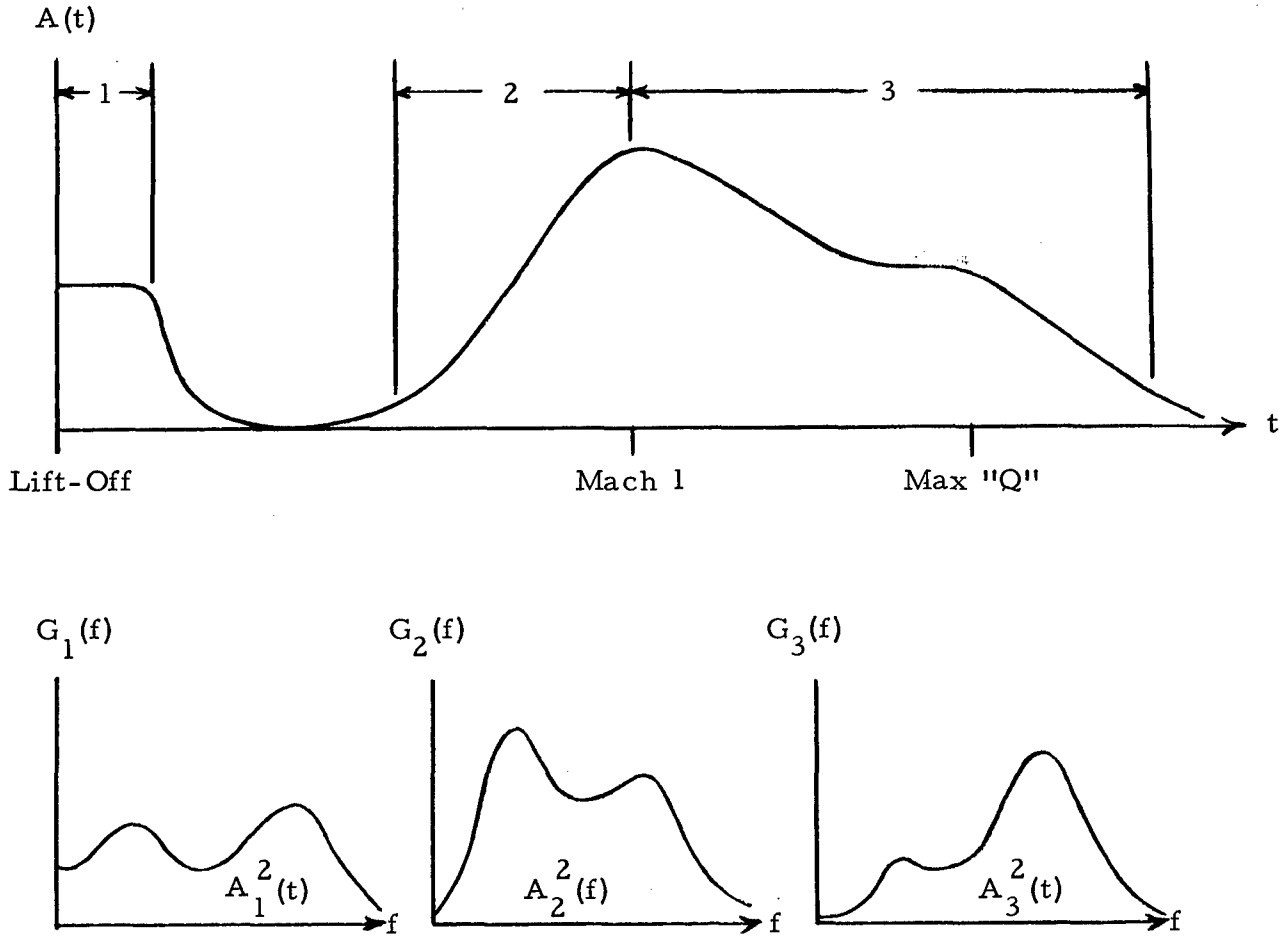

Figure 13. Spectral Representation for Spacecraft Launch Vibration Data

In words, the pertinent vibration during the launch phase can be described by three relative power spectra representing lift-off, pre-Mach 1, and post-Mach 1 (max "q") time intervals. The area under each power spectrum at any instant during the appropriate time interval is equal to the mean square value at that time from the over-all rms value time history plot.

If it is desired to reduce the launch vibration data to a single "maximum spectrum" as defined in Section 1, this can be accomplished as follows. Compute the highest level power spectra for the lift-off, pre-Mach 1, and post-Mach 1 (max "q") time intervals by adjusting the area under the relative power spectrum for each interval to equal the highest mean square value which occurred during that interval. For the pre-Mach 1 interval, the highest mean square value will usually be at Mach 1. For the post-Mach 1 interval, the highest mean square value may occur at either Mach 1 or max "q". In any case, superimpose the three spectra and record a single over-all power spectrum which covers the highest levels of all three. The result is a "maximum spectrum" which can be used as a conservative environmental specification for either vibration tests or design requirements.

One final point should be mentioned. Laboratory vibration tests are usually performed by applying a stationary vibration input to the test article of interest. This is true even for spacecraft components where the actual environment is nonstationary in nature. For this case, the "maximum spectrum" would normally be used to specify the test levels. Nonstationary vibration testing procedures have rarely been used to date. However, the studies herein indicate that nonstationary vibration tests could easily be implemented to simulated spacecraft vibration environments. Specifically, the nonstationary vibration for each launch event of interest could be simulated as illustrated in Figure 14.

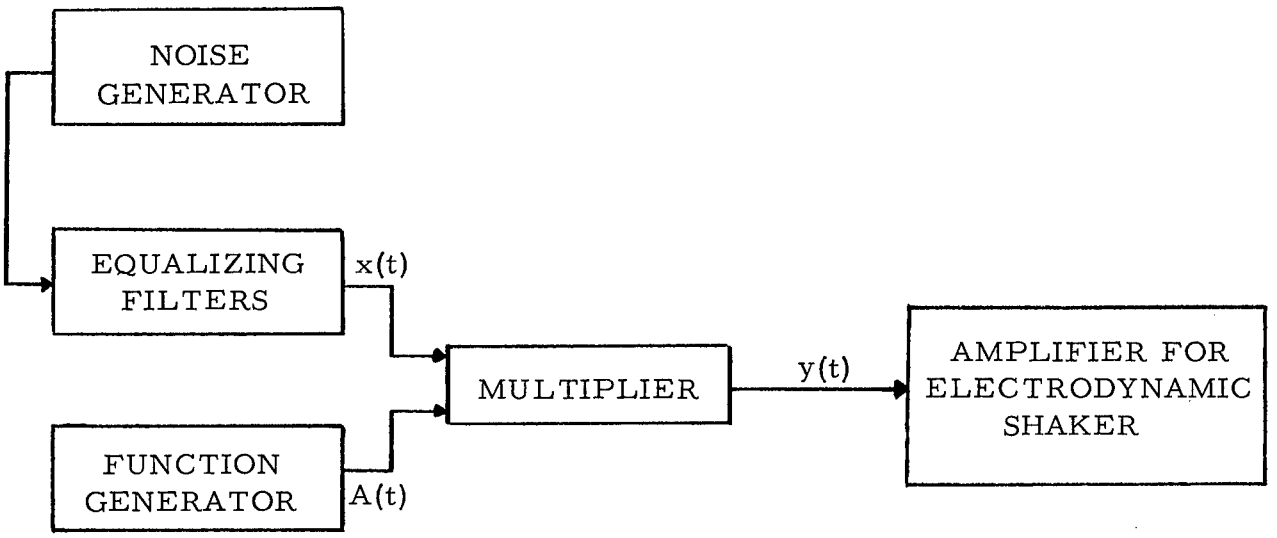

Figure 14. Block Diagram for Nonstationary Testing Machine

The function generator in Figure 14 would produce a signal proportional to the rms value time history during one of the locally stationary time intervals. The equalizing filters would be used to shape noise to have the relative power spectrum associated with that time interval. The multiplier would produce the desired nonstationary vibration signal to be delivered to the shaker.

REFERENCES

1. Piersol, A. G., "The Measurement and Interpretation of Ordinary Power Spectra for Vibration Problems," NASA CR-90(N64-30830), National Aeronautics and Space Administration, Washington, D. C., September 1964.

2. Kelly, R. D., "A Method for the Analysis of Short Duration Nonstationary Random Vibration," Shock, Vibration and Associated Environments Bulletin No. 29, Part IV, pp. 126-137, Department of Defense, Washington, D. C., June 1961.

3. Schoenemann, P. T., "Techniques for Analyzing Nonstationary Vibration Data," Shock, Vibration and Associated Environments Bulletin No. 33, Part II, pp. 259-263, Department of Defense, Washington, D. C., February 1964.

4. McCarty, R. C. and G. W. Evans II, "On Some Theorems for a Nonstationary Stochastic Process with a Continuous, Non-Random, Time Dependent Component," SRI Technical Report No. 4, Contract SD-103, Stanford Research Institute, Menlo Park, California, September 1962.

5. Zimmerman, J., "Correlation and Spectral Analysis of Time Varying Data," Shock, Vibration and Associated Environments Bulletin No. 26, Part II, pp 237-258, Department of Defense, Washington, D. C., December 1958.

6. Thrall, G. P. and J. S. Bendat, "Mean and Mean Square Measurements of Nonstationary Random Processes," CR-226, National Aeronautic and Space Administration, Washington, D. C., May 1965.

7. Bendat, J. S., and G. P. Thrall, "Spectra of Nonstationary Random Processes," AFFDL TR-64-198, Research and Technology Division, AFSC, USAF, Wright-Patterson AFB, Ohio, November 1964.

8. Silverman, R. A., "Locally Stationary Random Processes," IRE Transactions on Information Theory, Vol. IT-3, No. 1, pp. 182-187, March 1957.

9. Page, C. G., "Instantaneous Power Spectra," Journal of Applied Physics, Vol. 23, No. 1, January 1952.

10. Turner, C. H. M., "On the Concept of an Instantaneous Power Spectrum, and its Relationship to the Autocorrelation Function," Journal of Applied Physics, Vol. 25, No. 11, November 1954.

11. Kharkevich, A. A., Spectra and Analysis, (translated from Russian), Chapter III, Consultants Bureau, New York, 1960.

12. Bendat, J. S., and A. G. Piersol, Measurement and Analysis of Random Data, John Wiley and Sons, Inc., New York, 1966 (to be published).

13. Walker, H. M. and J. Lev, Statistical Inference, Henry Holt and Company, New York, 1953.

APPENDIX A

EXPERIMENTAL STUDIES OF THEORETICAL MODELS

The experimental studies of the cosine product model for nonstationary random data were performed in the Dynamics Section Data Reduction Laboratory of the Norair Division, Northrop Corporation. The test set-up used to study the cosine product model of Eq. (20) is illustrated schematically in Figure A-1.

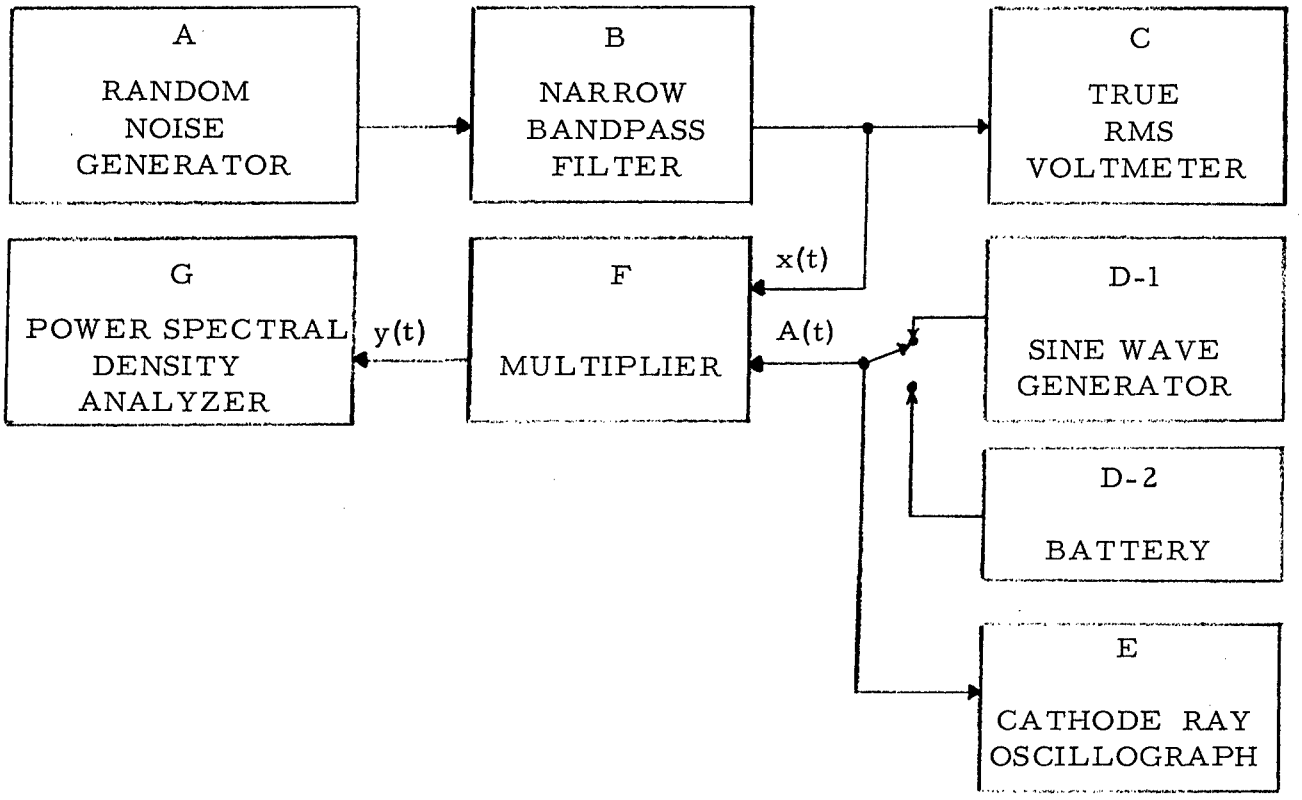

Figure A-1. Block Diagram for Studies of Cosine Product Model

The random noise generator (Item A) was used as a source of a sample record from a stationary random process. The bandpass filter (Item B) was used to shape the power spectrum of the sample record to a sharply defined

narrow bandwidth of 20 cps. The voltmeter (Item C) was used to establish the narrow band random signal level. The sine wave generator (Item D-1) was used to supply the cosine function for the model, while the battery (Item D-2) was inserted when a zero frequency product was required. The cathode ray oscillograph (Item E) was used to establish the sine wave or DC signal level. The multiplier (Item F) was used to form the product $A(t)\,x(t)$ which gave the desired nonstationary signal. The power spectral density analyzer (Item G) was used to obtain a conventional time averaged power spectrum.

The instruments employed for the experiments are summarized in Table A-1.

Item	Description	Manufacturer	Model Number
A	Random Noise Generator	General Radio Co.	1390A
B	Narrow Bandpass Filter	Spectral Dynamics Corp.	101A
C	True RMS Voltmeter	Bruel & Kjaer Instruments	2409R
D-1	Sine Wave Generator	Hewlett Packard	200AB
D-2	Battery	Fabricated	------
E	Cathode Ray Oscilloscope	Tektronix, Inc.	531
F	Multiplier	Technical Products Co.	645
G	Power Spectral Density Analyzer	Technical Products Co.	626 633 627

Table A-1. Instruments Used for Experiments.

The time averaged power spectra for $y(t) = A(t)\,x(t)$ presented in Figure 3 were computed using an analyzer filter bandwidth of $B = 6$ cps and an RC averaging time constant of $K = 8$ seconds. This produced an estimate with a standard deviation at any frequency of $\sigma = G_y(f)/\sqrt{2BK} \approx 0.1\,G_y(f)$ or 10% of the true value. The scan rate used was $R_s = B/(4K) \approx 0.2$ cps/second.

APPENDIX B

DATA REDUCTION PROCEDURES

B. 1 INSTRUMENTS AND BASIC SET-UP

The experimental studies of actual launch vibration data were performed in the Dynamics Section Data Reduction Laboratory of the Norair Division, Northrop Corporation. The data reduction set-up is illustrated schematically in Figure B-1.

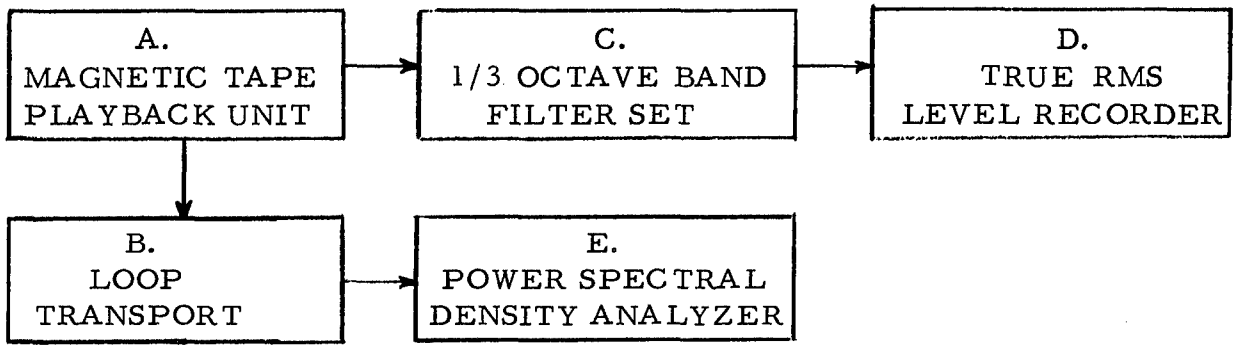

Figure B-1. Block Diagram for Studies of Launch Vibration Data

The magnetic tape playback unit (Item A) was used to recreate the vibration data signals. When using the 1/3 octave band equipment, each record of the launch phase vibration was played back repeatedly from start to finish. When using the power spectral density analyzer, selected intervals of each record were removed and spliced into a loop for continuous playback by recirculation with a loop transport (Item B). The 1/3 octave band filter set (Item C) and the true rms level record (Item D) were used to measure and record rms time histories in 1/3 octave bands. The power spectral density analyzer was used to measure finely resolved (narrow bandwidth) power spectra for the data.

The instruments employed for the data reduction are summarized in Table B-1.

Item	Description	Manufacturer	Model Number
A	Magnetic Tape Playback Unit	Honeywell	LAR-7300
B	Loop Transport	Ampex Corp.	LR-100
C	1/3 Octave Band Filter Set	Bruel& Kjaer Instruments	2112
D	True rms Level Recorder	Bruel& Kjaer Instruments	2305
E	Power Spectral Density Analyzer	Technical Products Co.	626 627 645

Table B-1. Instruments Used for Data Reduction

B. 2 BANDWIDTH AND AVERAGING TIME SELECTIONS

As discussed in Section 3. 2. 1, the measurement of a short time averaged power spectrum will include a random error σ, a bandwidth bias error μ_b, and a time interval bias error μ_t. The selection of a bandwidth and averaging time for the measurement involves a compromise between these various errors. For the experiments outlined in Section 4, a highly resolved power spectrum (small μ_b) is not considered necessary to arrive at the desired conclusions. Hence, 1/3 octave bandwidths ($B = 0.22f$) are used rather than narrower bandwidths which would make μ_b smaller, but also make σ larger for a given averaging time.

The selection of an averaging time now reduces to a compromise between the random error σ and the time interval bias error μ_t. The bias error μ_t is considered to be more detrimental to the desired conclusions since this error tends to mask the time trends in the data which are of principal interest here. Hence, the selection of an averaging time is based upon making the bias error μ_t negligible. For the special case of nonstationary data where the time trend is slow relative to the instantaneous fluctuations of the data (as in general true for spacecraft vibration data), this desired averaging time selection may be accomplished as follows.

Determine the rms value time history for the data using a very short averaging time. Repeat the rms value time history measurement using a longer averaging time. The result should be two rms value time history plots with similar trends but with less uncertainty fluctuation for the longer averaging time, as indicated in Figure B-2. This procedure can be repeated with increasing averaging time until it is clear that the basic time trend in the data is being altered or smoothed, as again indicated in Figure B-2. That averaging time which is just short enough to avoid noticeable smoothing of the under-lying time trend constitutes the maximum averaging time which can be used without introducing a significant time interval bias error. The critical

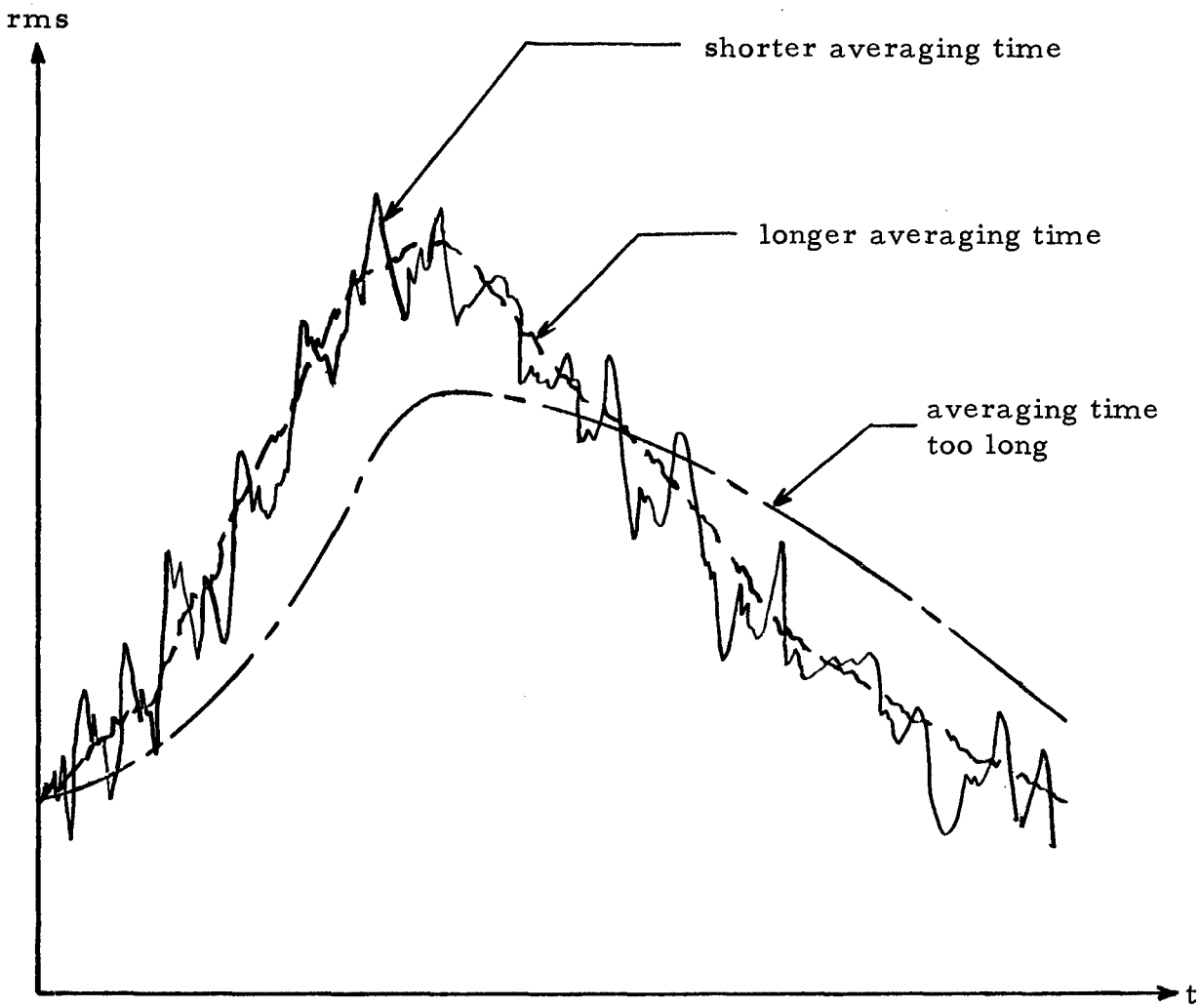

Figure B-2. RMS Value Time Histories for Different Averaging Times

requirement, of course, is to be able to distinguish between actual time trends in the data and inherent statistical uncertainty fluctuations (random errors).

The above procedure was employed here to select averaging times for the power spectra measurements summarized in Appendix C. An illustration of the actual selection procedure for a NIMBUS measurement is presented in Figure B-3. The first rms value time history in Figure B-3 was obtained using a very short averaging time (K=0.005 second). The extreme uncertainty

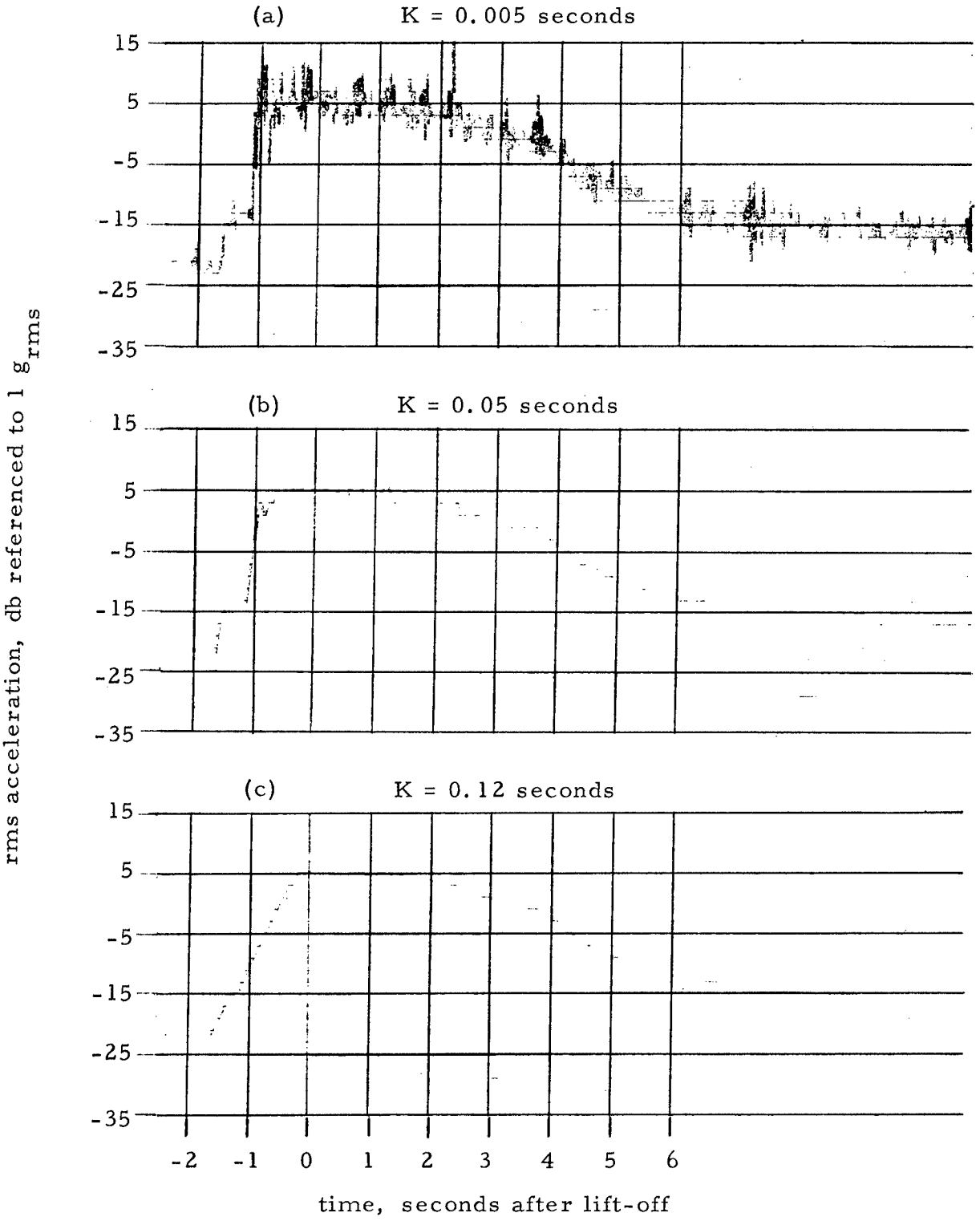

Figure B-3. Averaging Time Constant Selection for NIMBUS, Location 1, Measurement

fluctuations about a basic underlying trend are clearly seen, The second rms value time history was obtained using a ten-fold larger averaging time (K = 0. 05 second). The uncertainty fluctuations have been strongly suppressed while the basic underlying trend has not been significantly altered. The third rms value time history was obtained using a still larger averaging time (K = 0. 12 second). It is now obvious that the averaging time is too long. The basic underlying trend has been significantly altered producing a large time interval bias error in the rms value time history data.

The averaging time selections used for all measurements are summarized in Table B-2. Note that longer averaging times could have been used in some cases for the transonic and max "q" data. However, the averaging time required for proper measurements of the lift-off data was employed throughout the launch phase for convenience.

Measurement	Approximate Averaging Time Constants, Seconds			
	Lift-Off Data		Transonic and Max "Q" Data	
	Over-all	1/3 Octave Bands	Over-all	1/3 Octave Bands
NIMBUS Location 1	0. 05	0. 08	0. 05	0. 08
NIMBUS Location 2	0. 05	0. 08	0. 05	0. 08
OGO Location 1	0. 05	0. 08	0. 05	0. 08
OGO Location 2	0. 05	0. 08	0. 05	0. 08
OSO	0. 03	0. 03	----	----
AVT	----	----	0. 05	0. 05
MINUTEMAN	----	----	0. 05	0. 05 to 0. 08

Table B-2 Averaging Time Constant Selections

APPENDIX C

MEAN SQUARE VALUE TIME HISTORY DATA

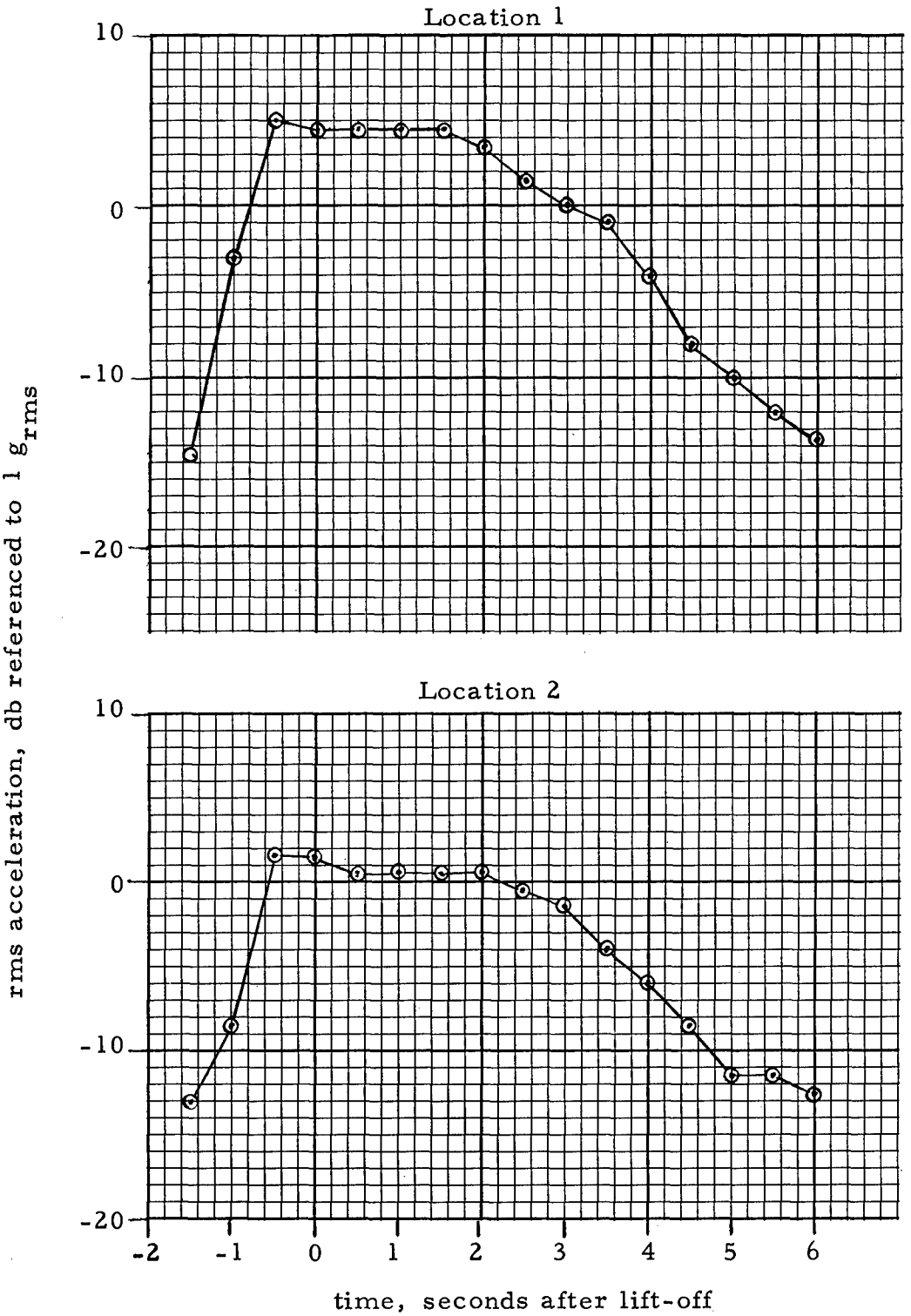

Figure C-1. Over-all RMS Time History for NIMBUS Lift-off Vibration

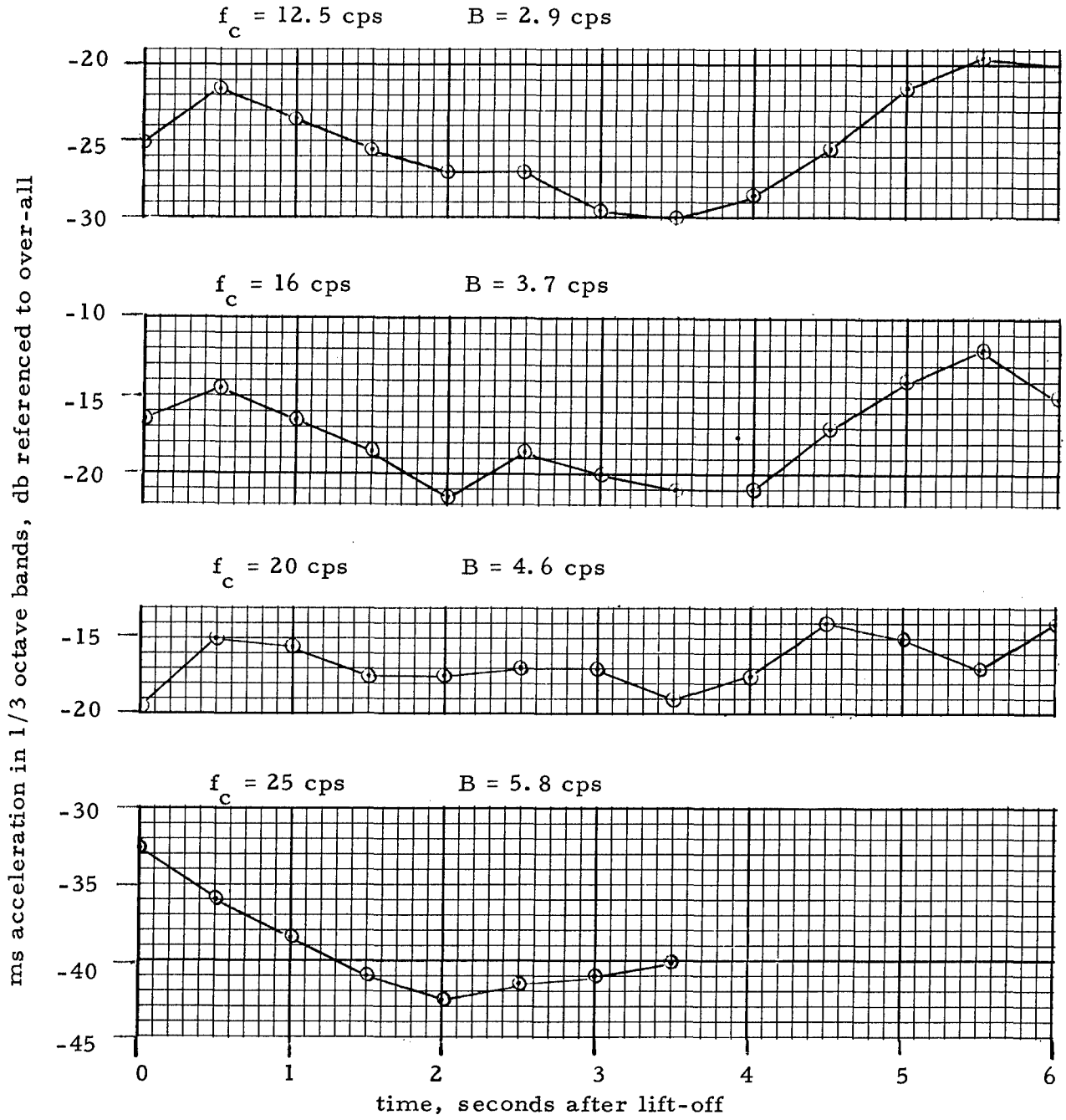

Figure C-2a. Relative Mean Square Values in 1/3 Octave Bands for NIMBUS, Location 1, Lift-off Vibration

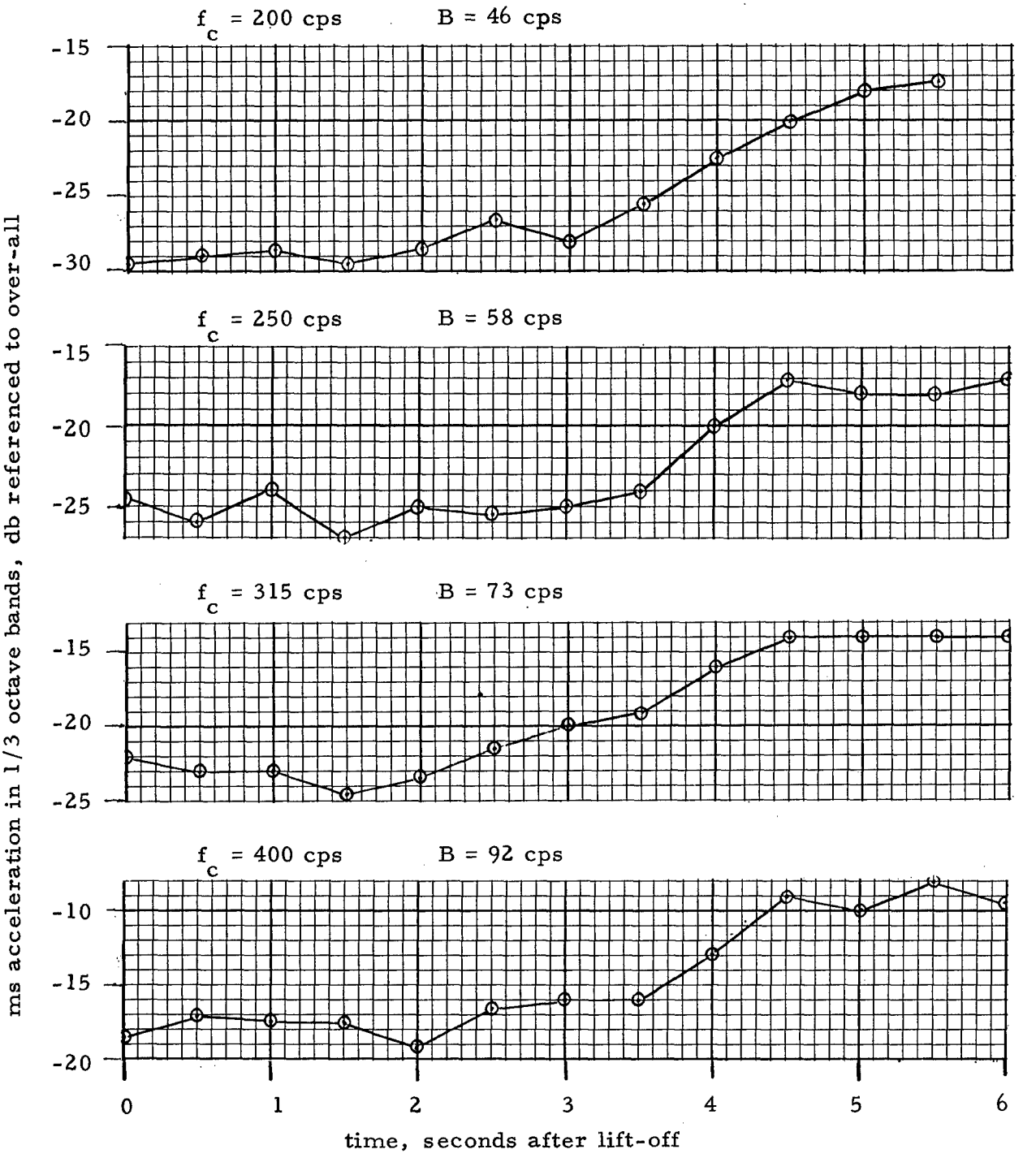

Figure C-2b. Relative Mean Square Values in 1/3 Octave Bands for NIMBUS, Location 1, Lift-off Vibration

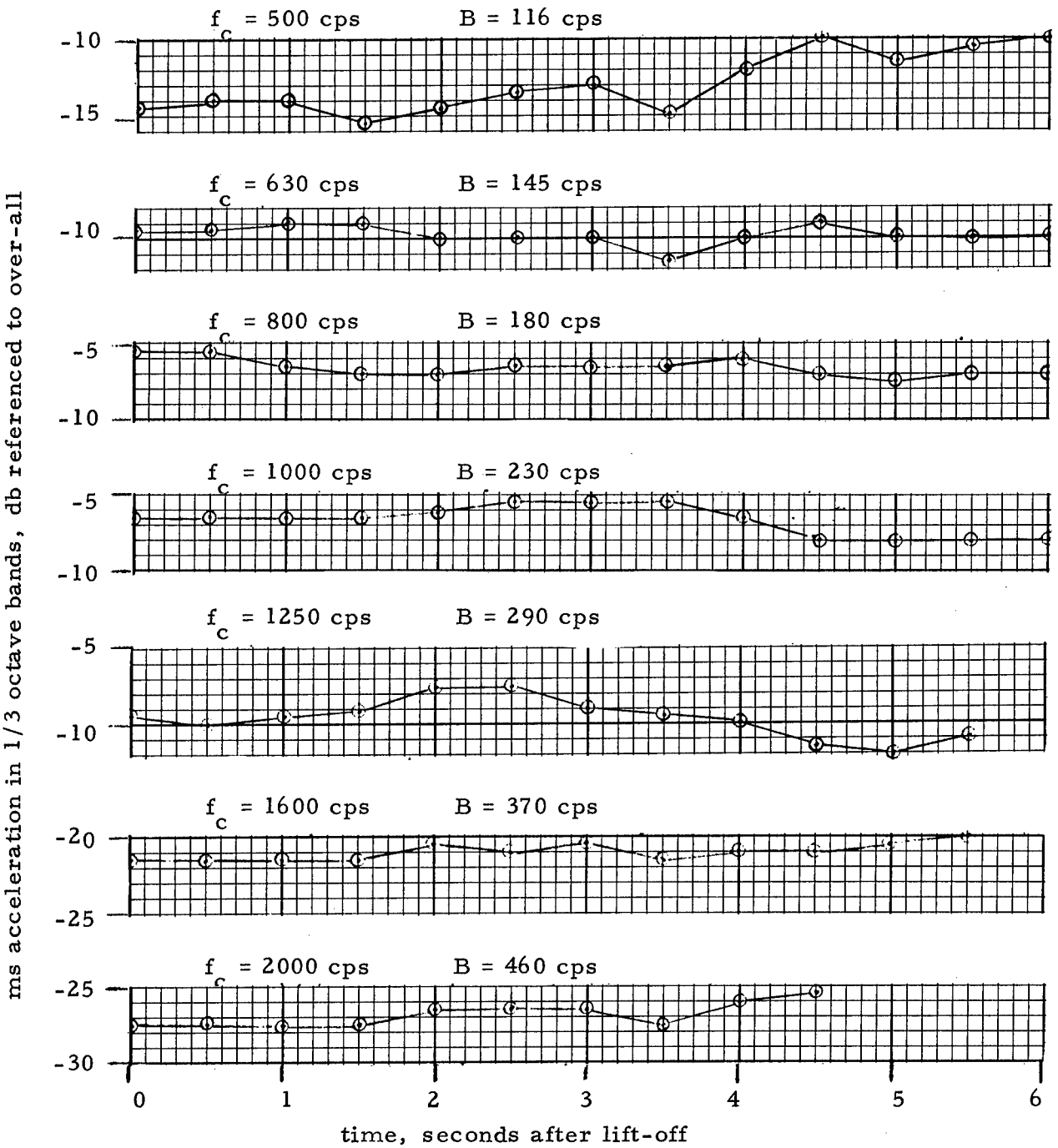

Figure C-2c. Relative Mean Square Values in 1/3 Octave Bands for NIMBUS Location 1, Lift-off Vibration

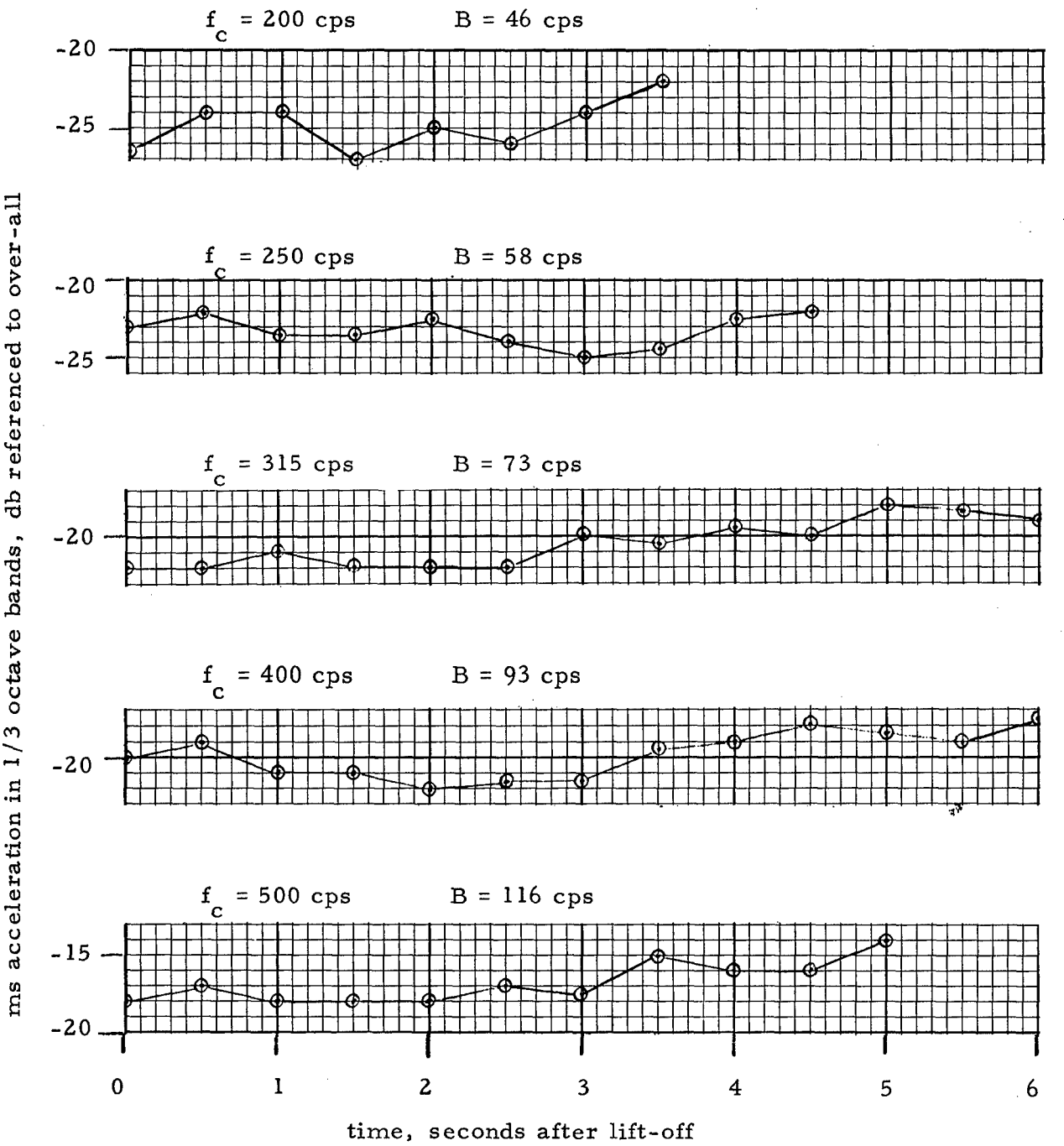

Figure C-3a. Relative Mean Square Values in 1/3 Octave Bands for NIMBUS, Location 2, Lift-off Vibration

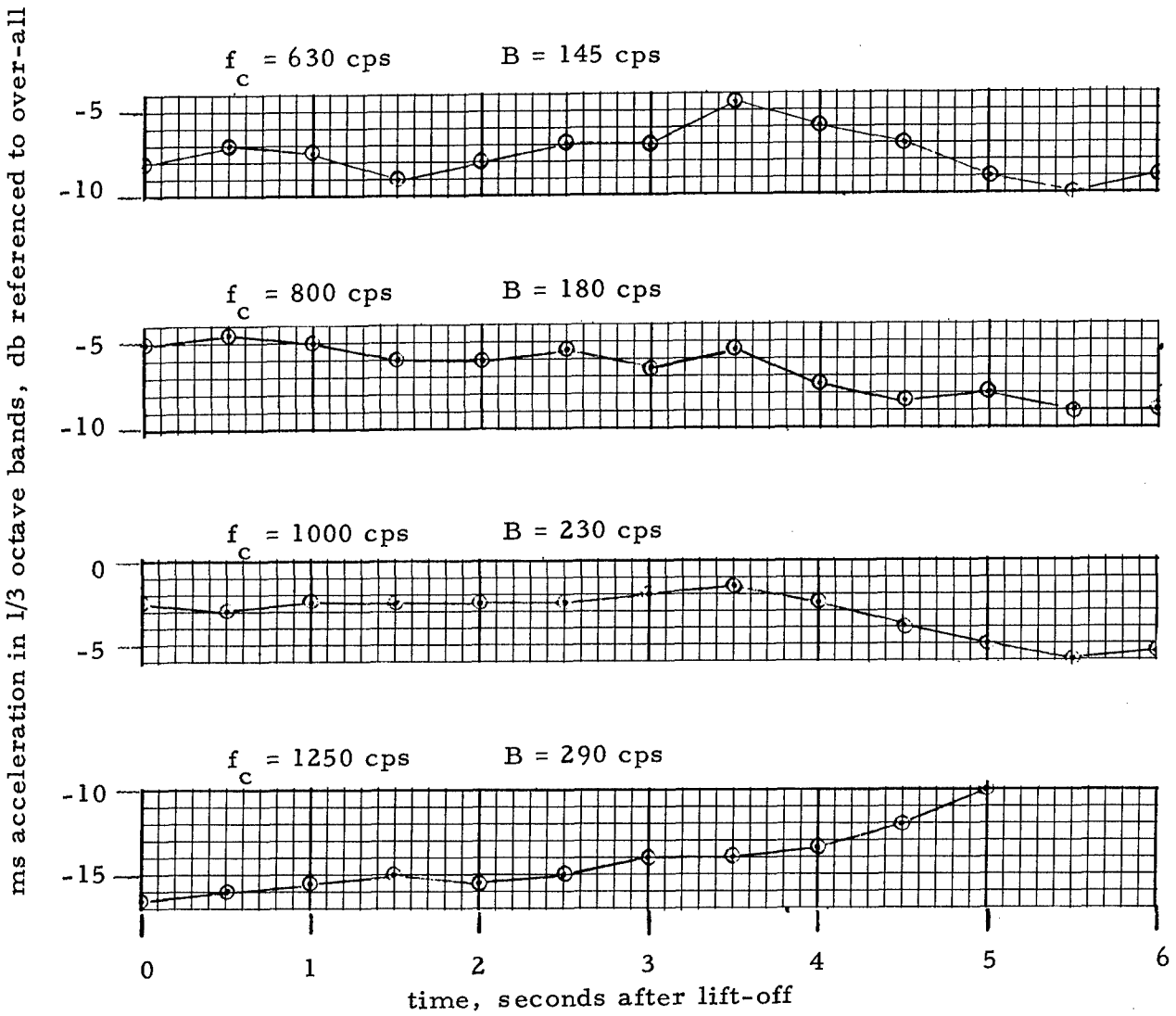

Figure C-3b. Relative Mean Square Values in 1/3 Octave Bands for NIMBUS, Location 2, Lift-off Vibration

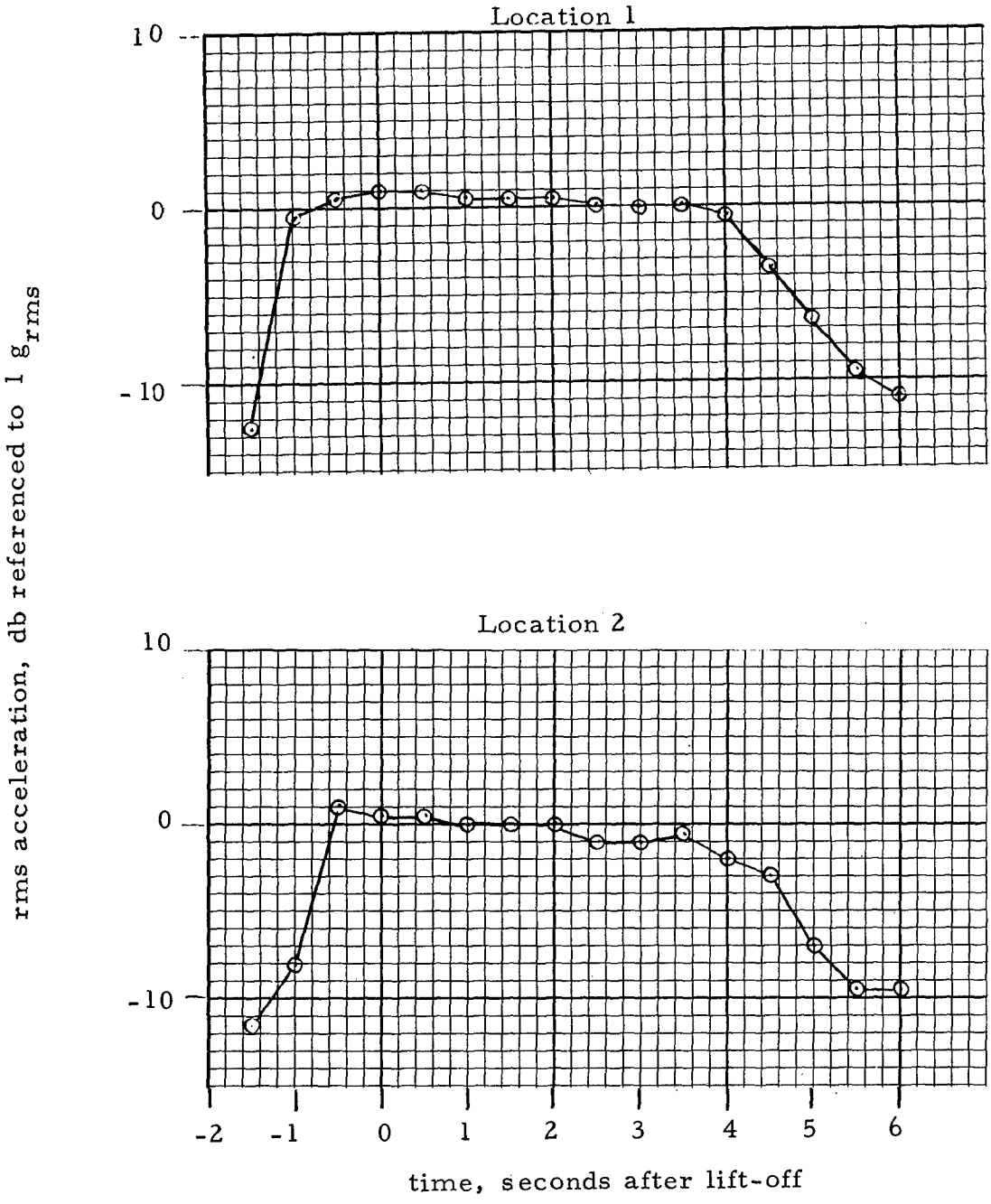

Figure C-4. Over-all RMS Time History for OGO Lift-off Vibration

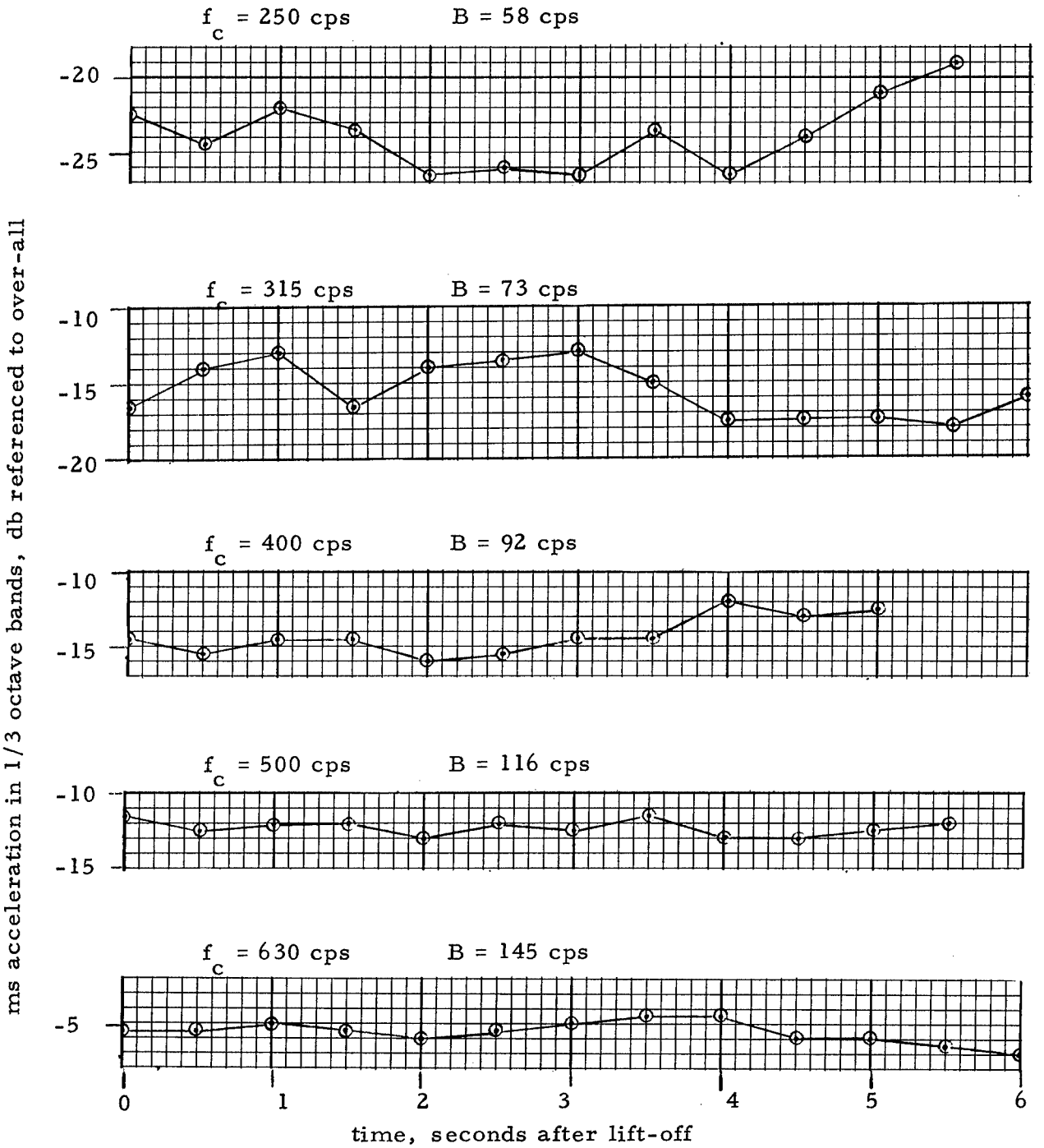

Figure C-5a. Relative Mean Square Values in 1/3 Octave Bands for OGO, Location 1, Lift-off Vibration

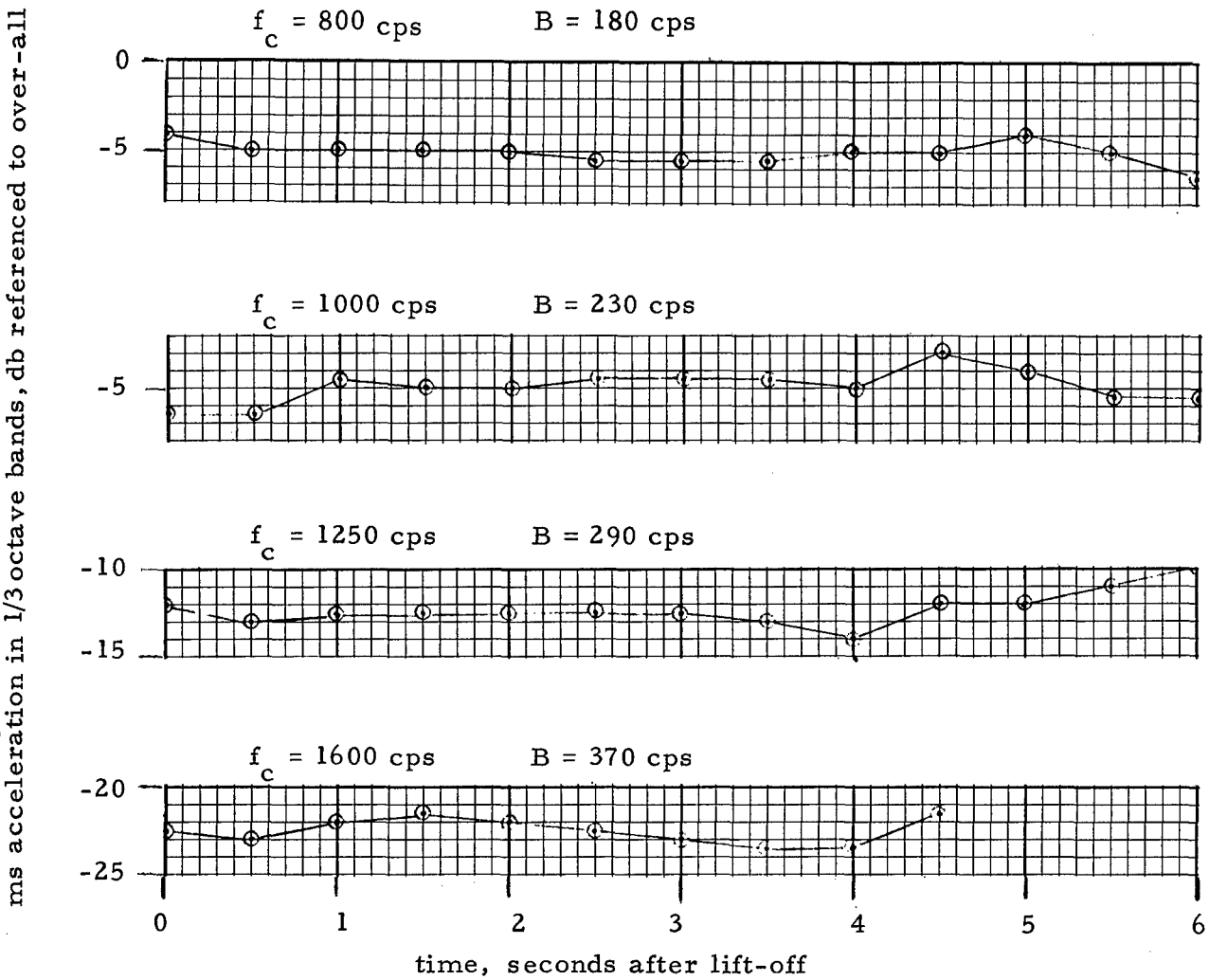

Figure C-5b. Relative Mean Square Values in 1/3 Octave Bands for OGO, Location 1, Lift-off Vibration

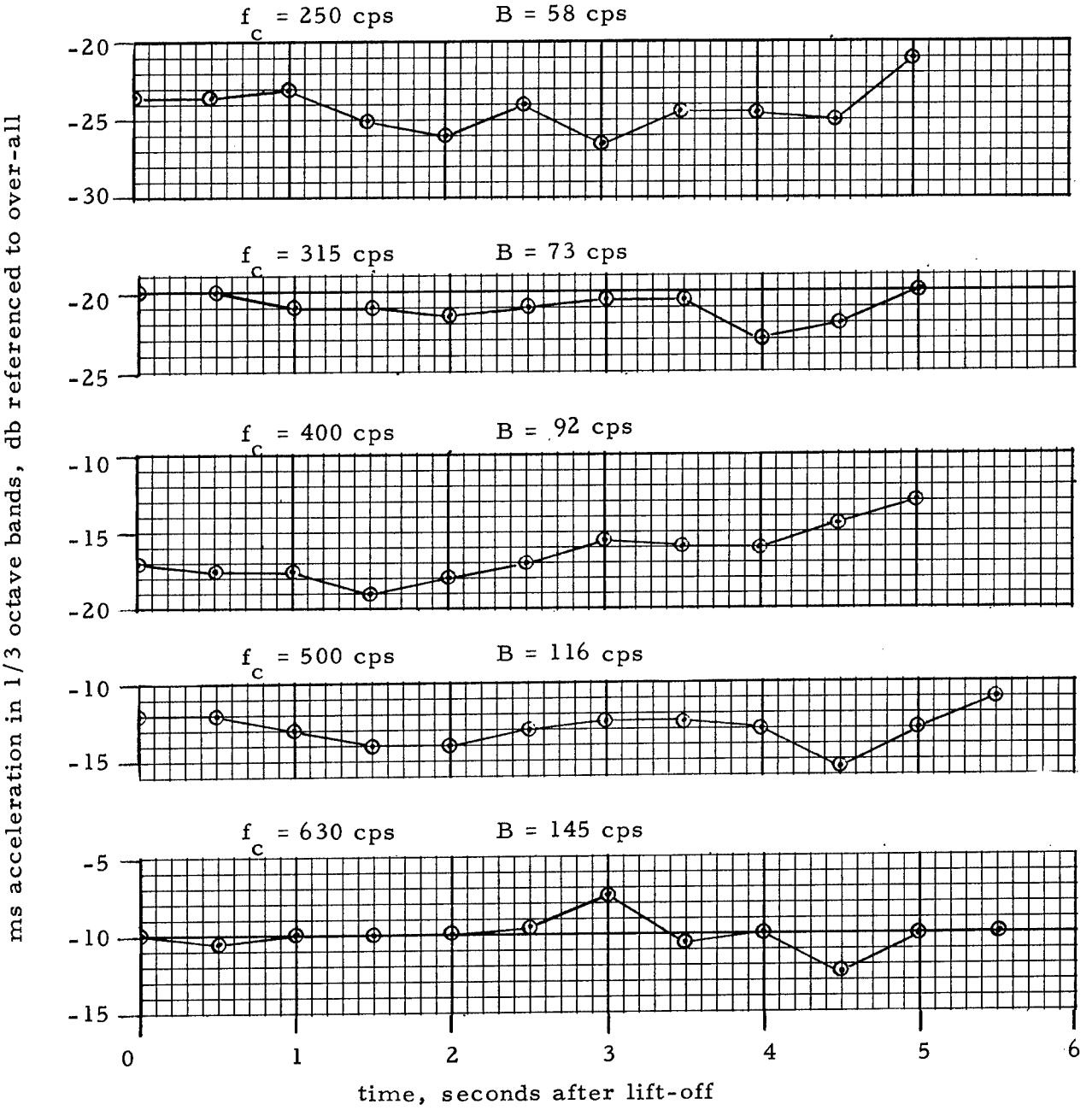

Figure C-6a. Relative Mean Square Values in 1/3 Octave Bands for OGO, Location 2, Lift-off Vibration

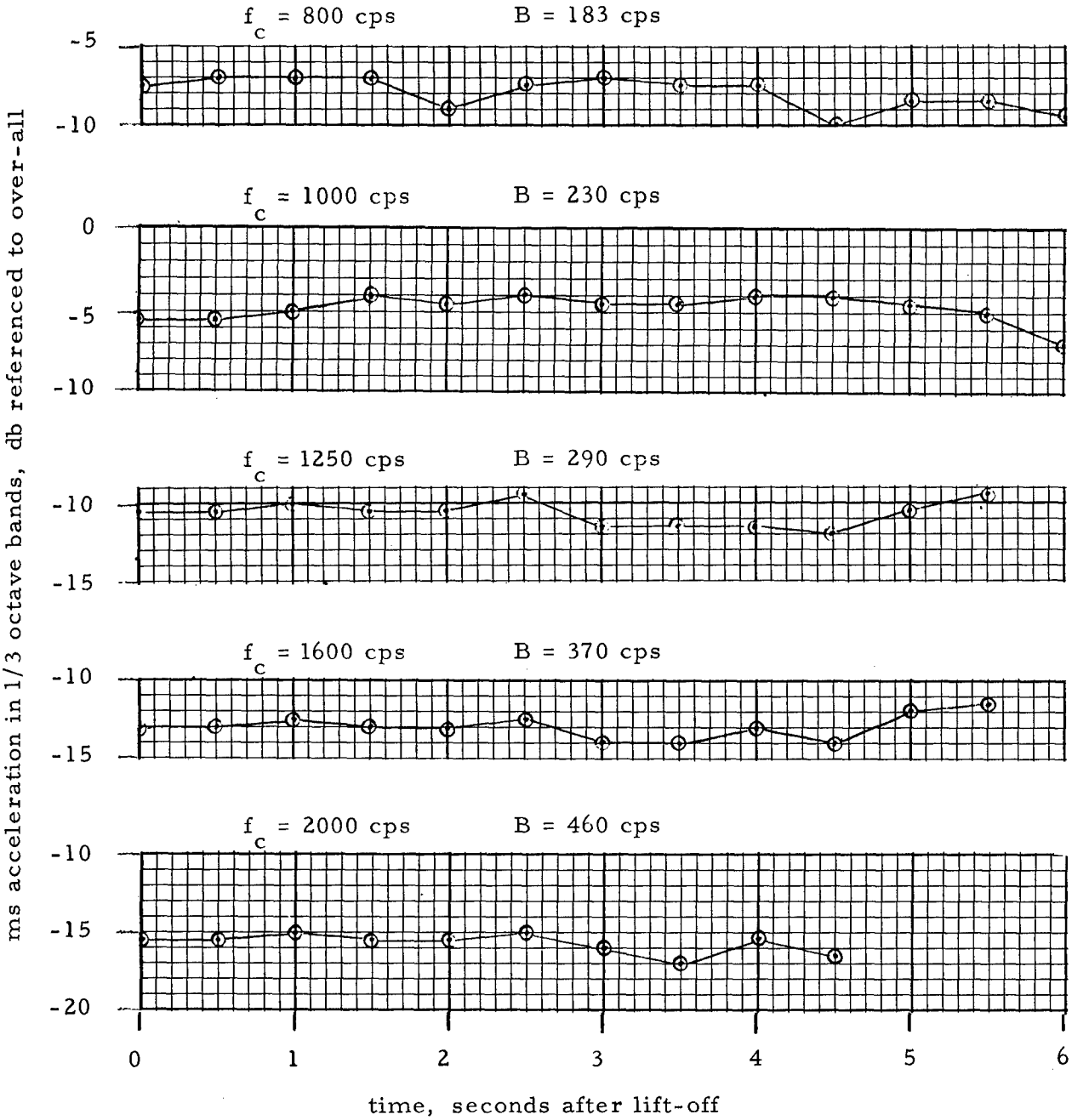

Figure C-6b. Relative Mean Square Values in 1/3 Octave Bands for OGO, Location 2, Lift-off Vibration

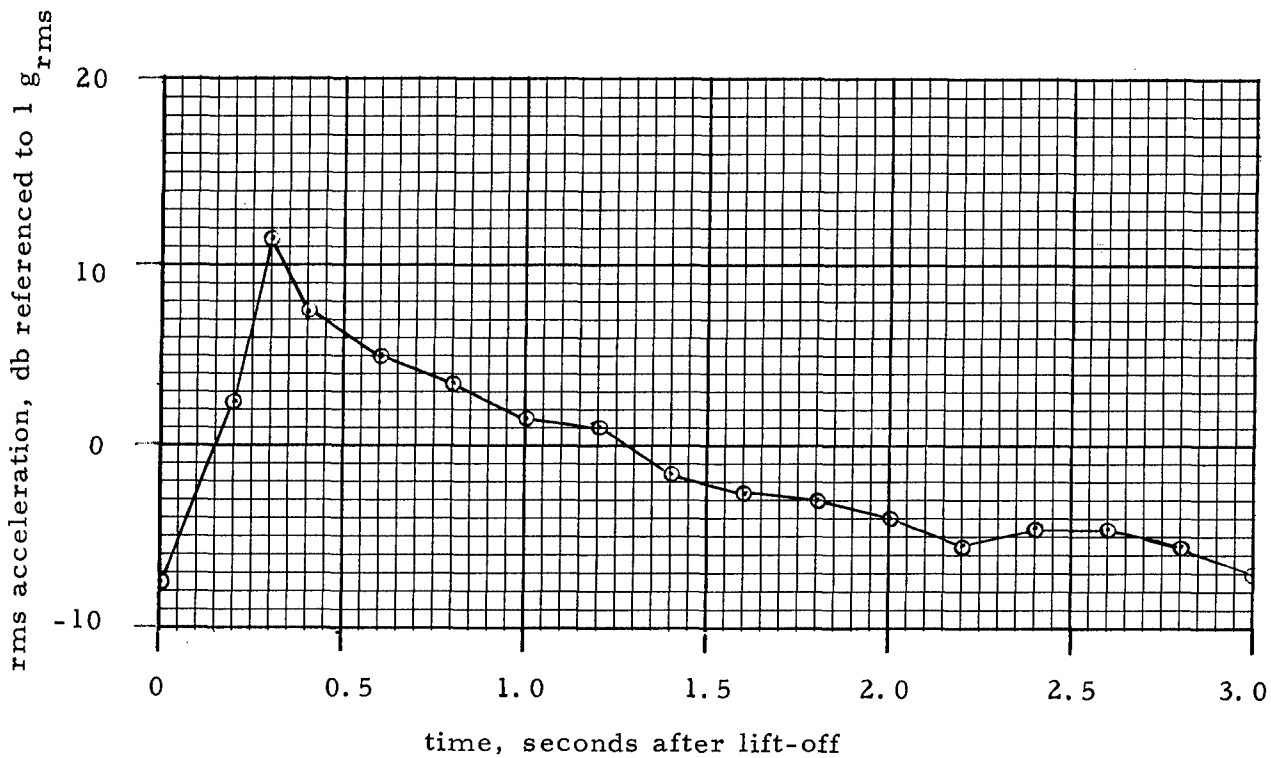

Figure C-7. Over-all RMS Time History for OSO Lift-off Vibration

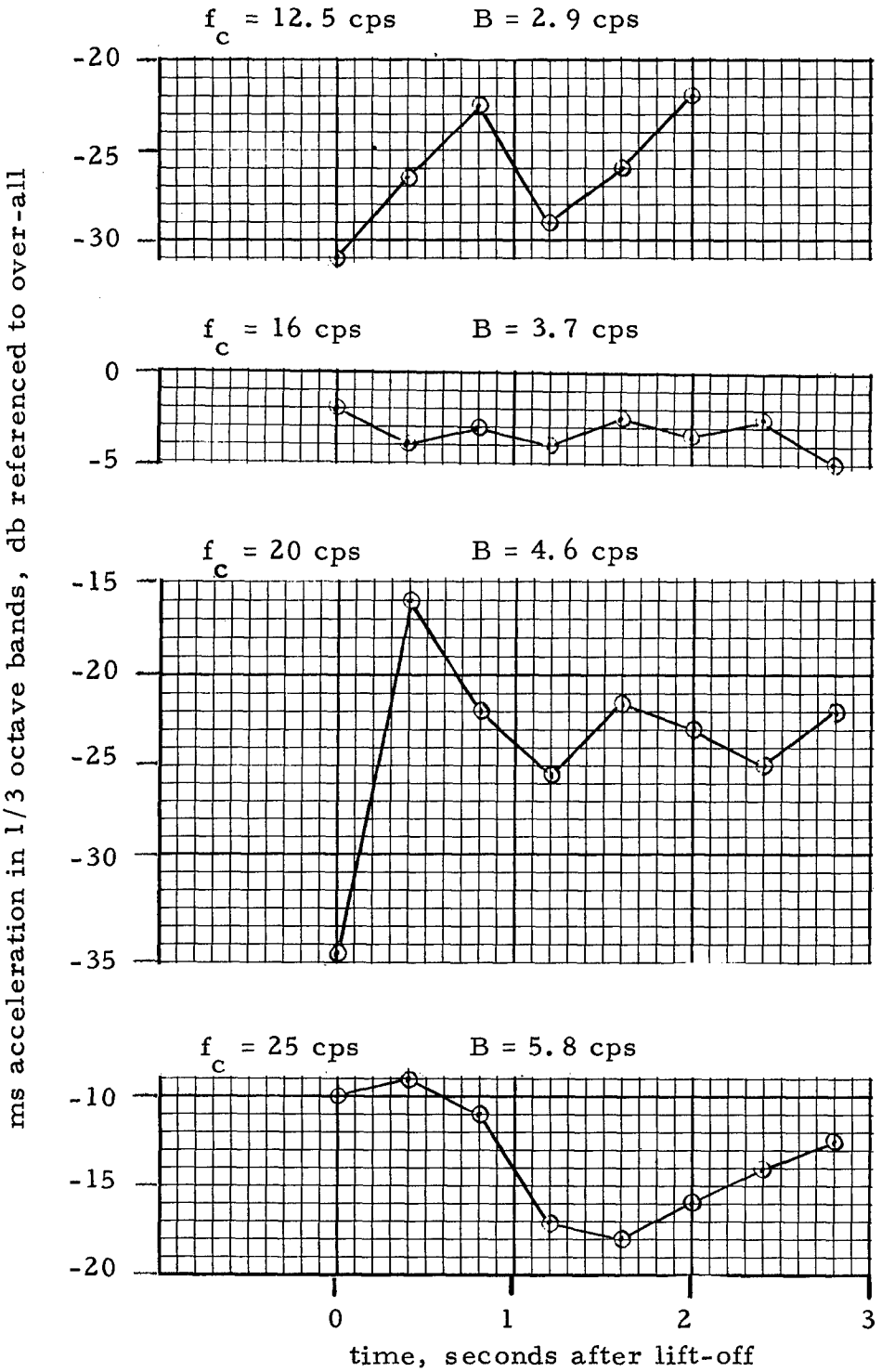

Figure C-8a. Relative Mean Square Values in 1/3 Octave Bands for OSO Lift-Off Vibration

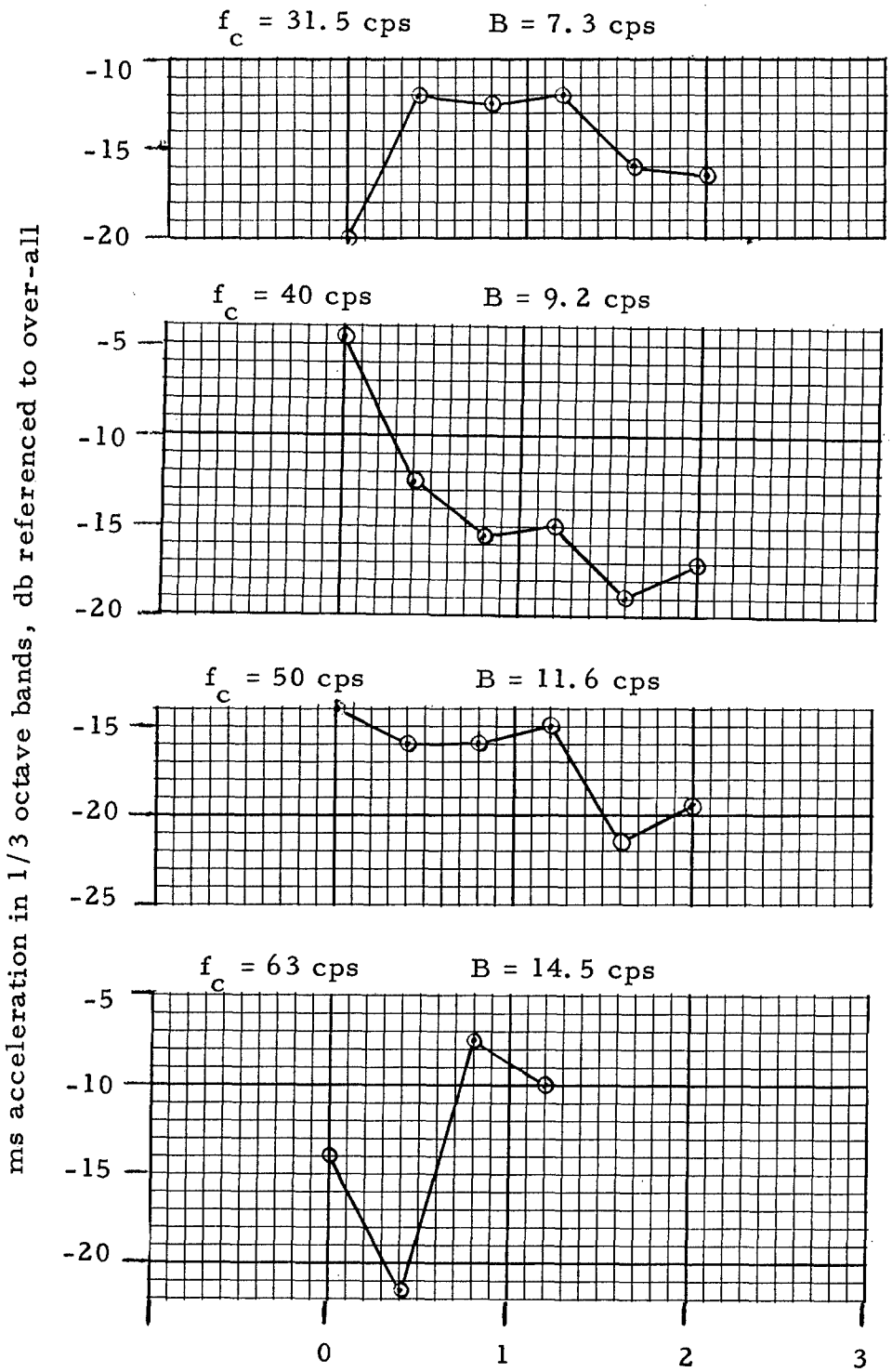

Figure C-8b. Relative Mean Square Values in 1/3 Octave Bands for OSO Lift-Off Vibration

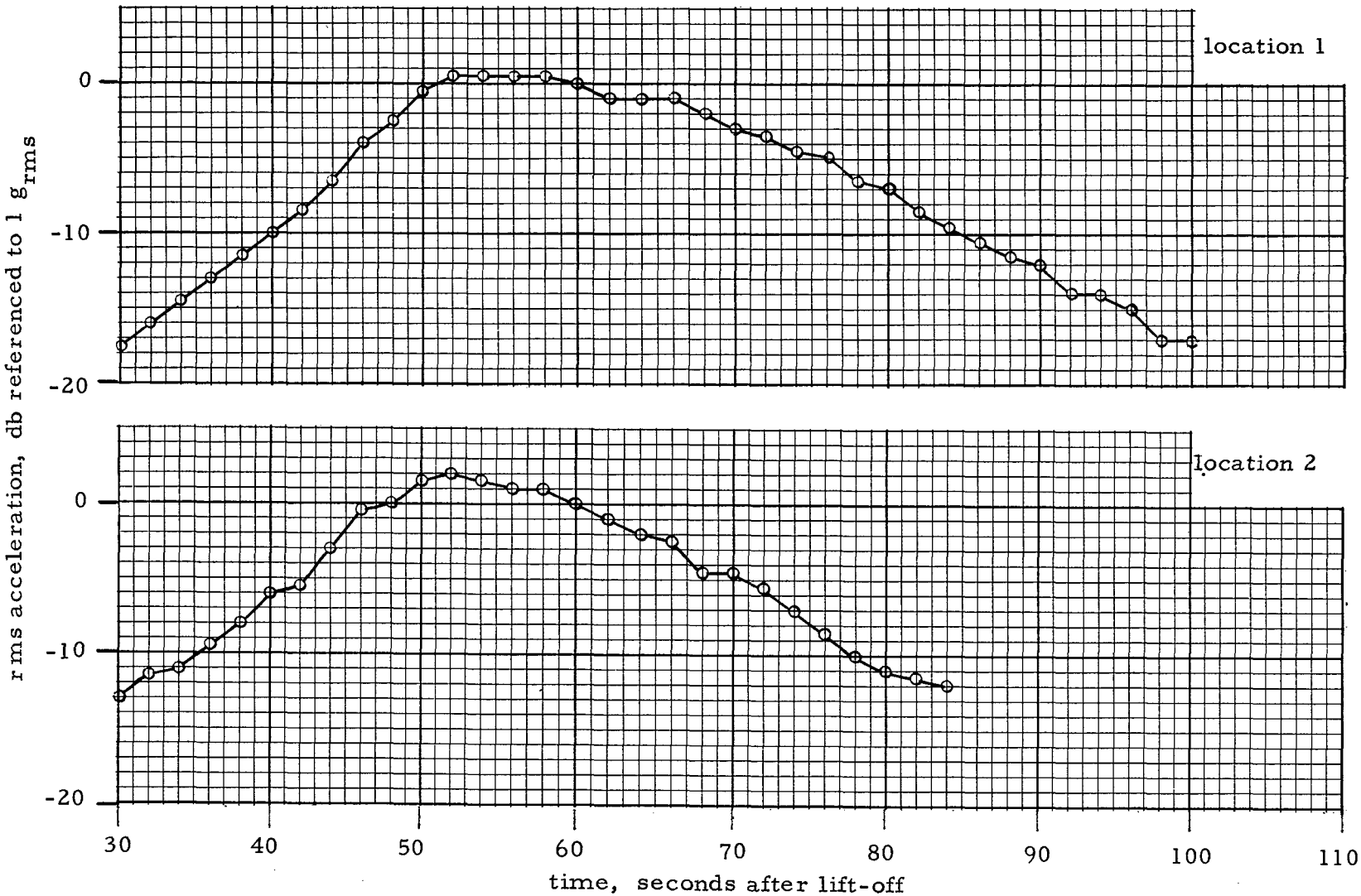

Figure C-9. Over-all RMS Time History for NIMBUS Flight Vibration

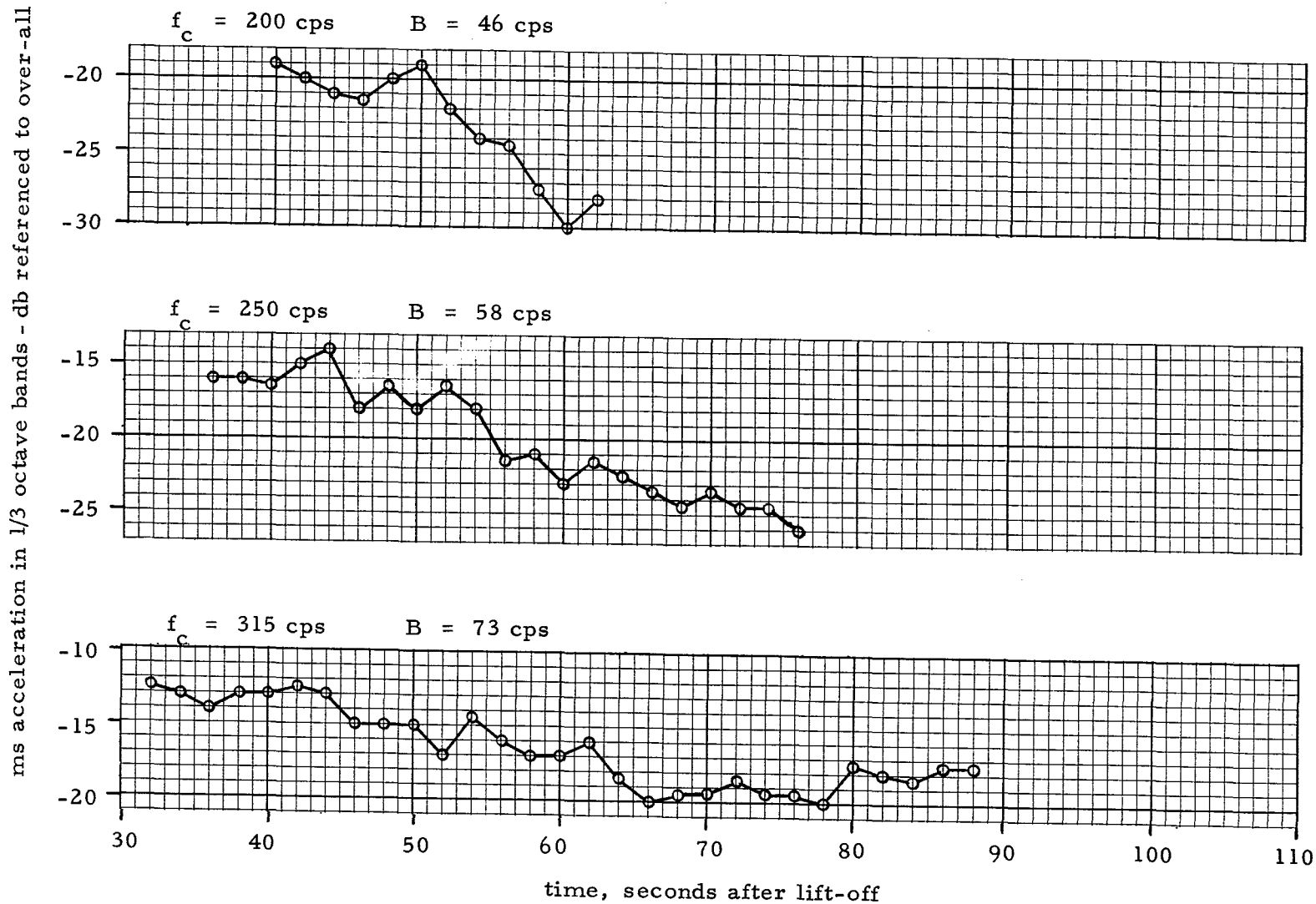

Figure C-10a. Relative Mean Square Values in 1/3 Octave Bands for NIMBUS, Location 1, Flight Vibration

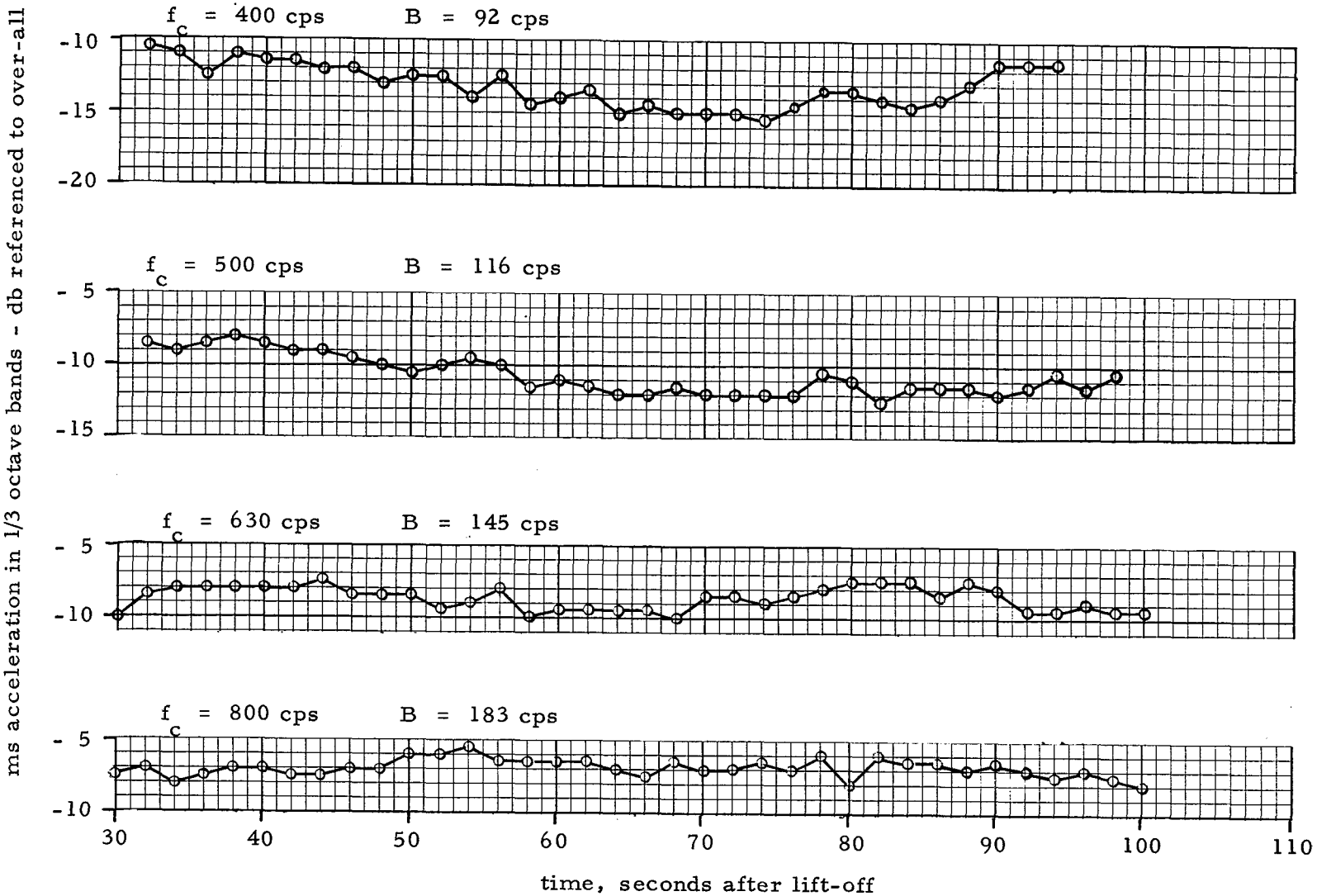

Figure C-10b. Relative Mean Square Values in 1/3 Octave Bands for NIMBUS, Location 1, Flight Vibration

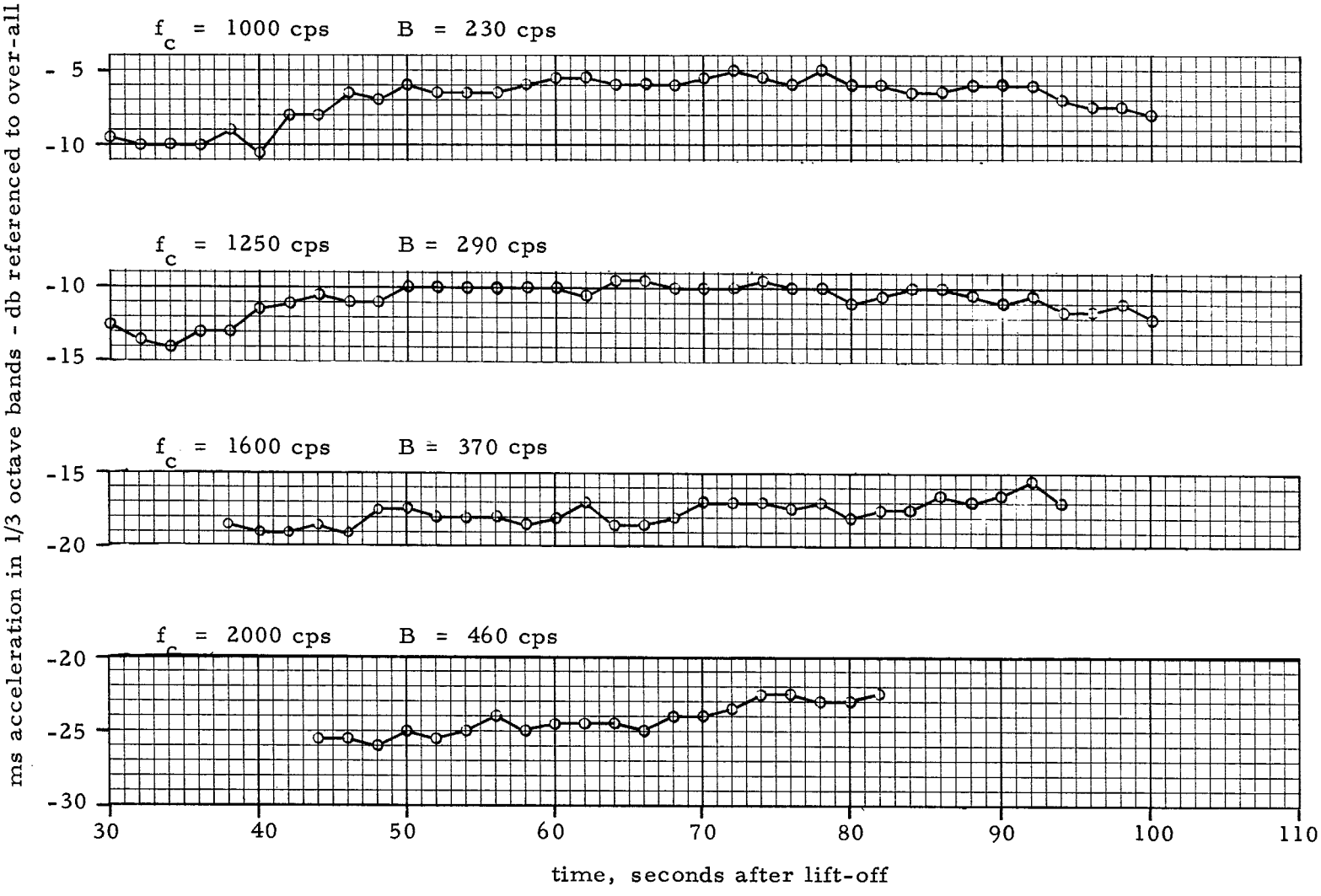

Figure C-10c. Relative Mean Square Values in 1/3 Octave Bands for NIMBUS, Location 1, Flight Vibration

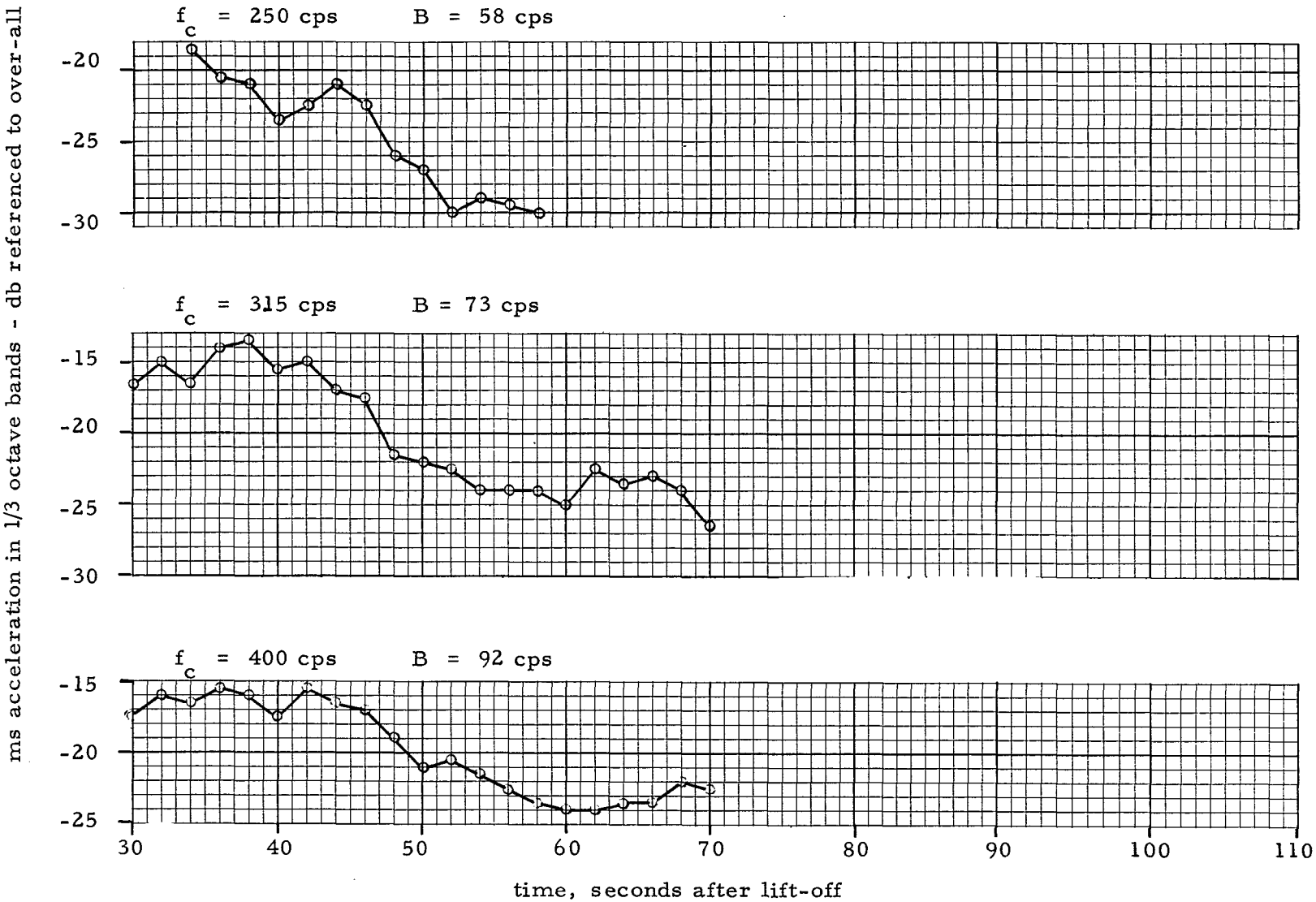

Figure C-11a. Relative Mean Square Values in 1/3 Octave Bands for NIMBUS, Location 2, Flight Vibration

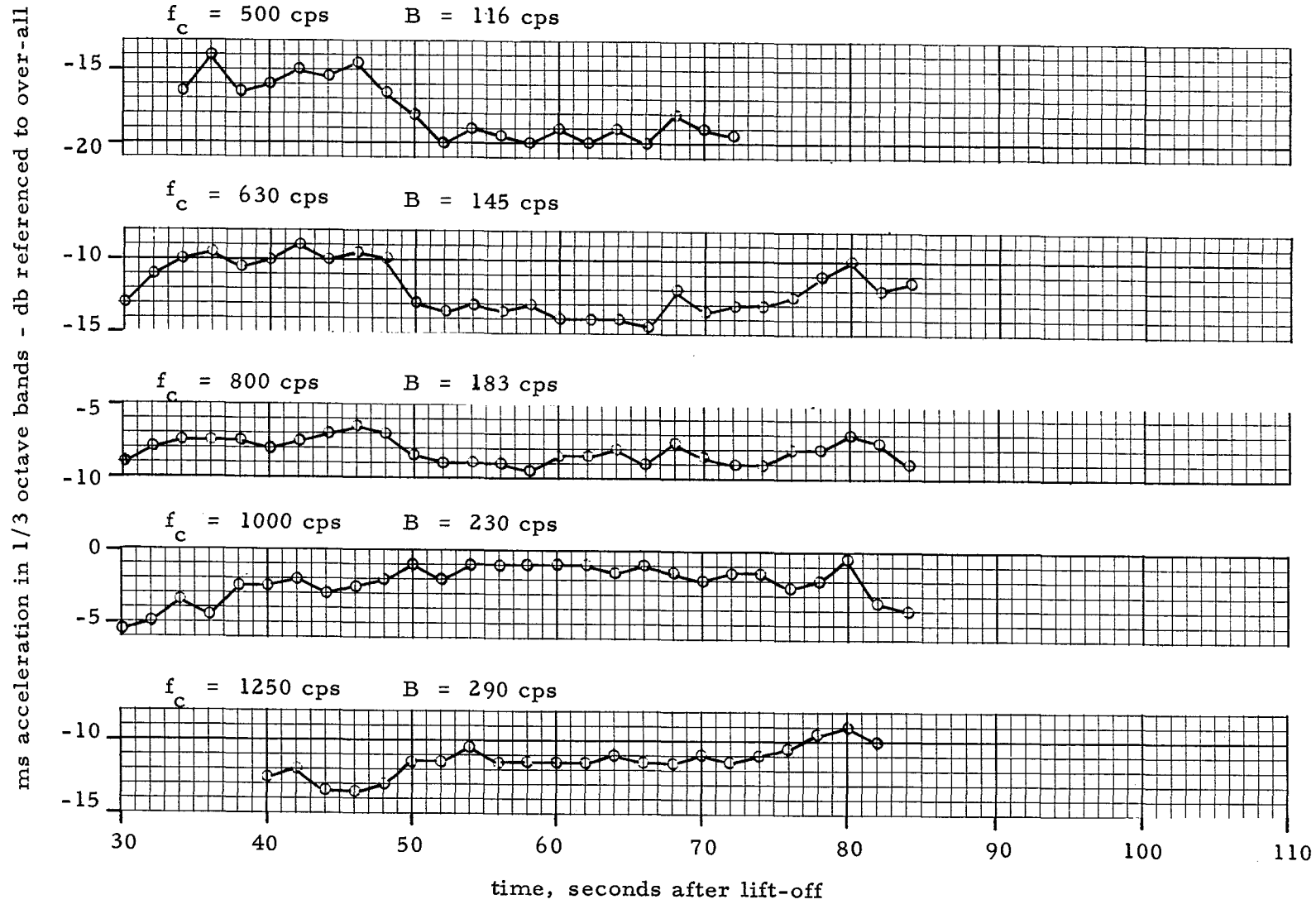

Figure C-11b. Relative Mean Square Values in 1/3 Octave Bands for NIMBUS, Location 2, Flight Vibration

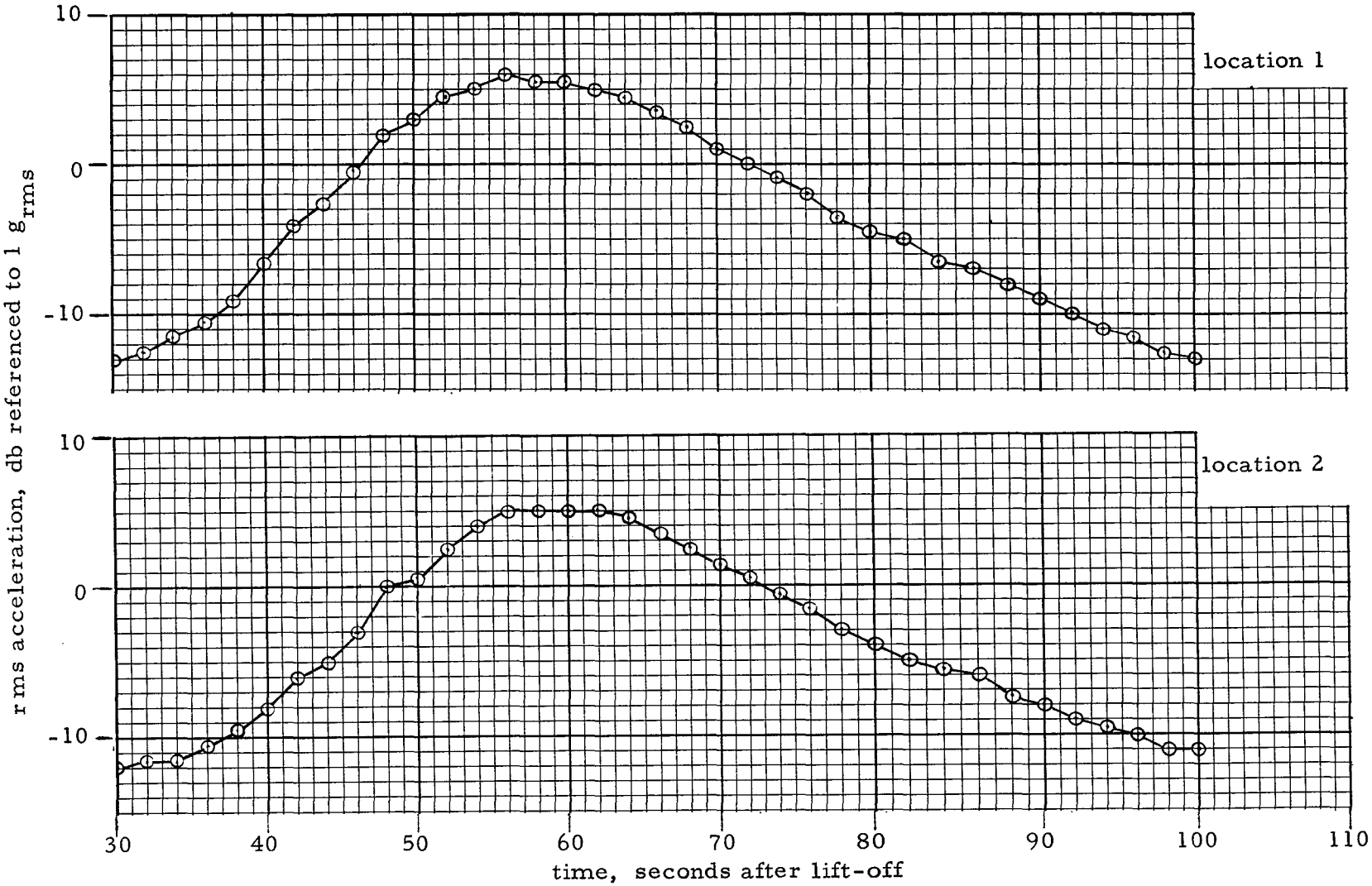

Figure C-12. Over-all RMS Time History for OGO Flight Vibration

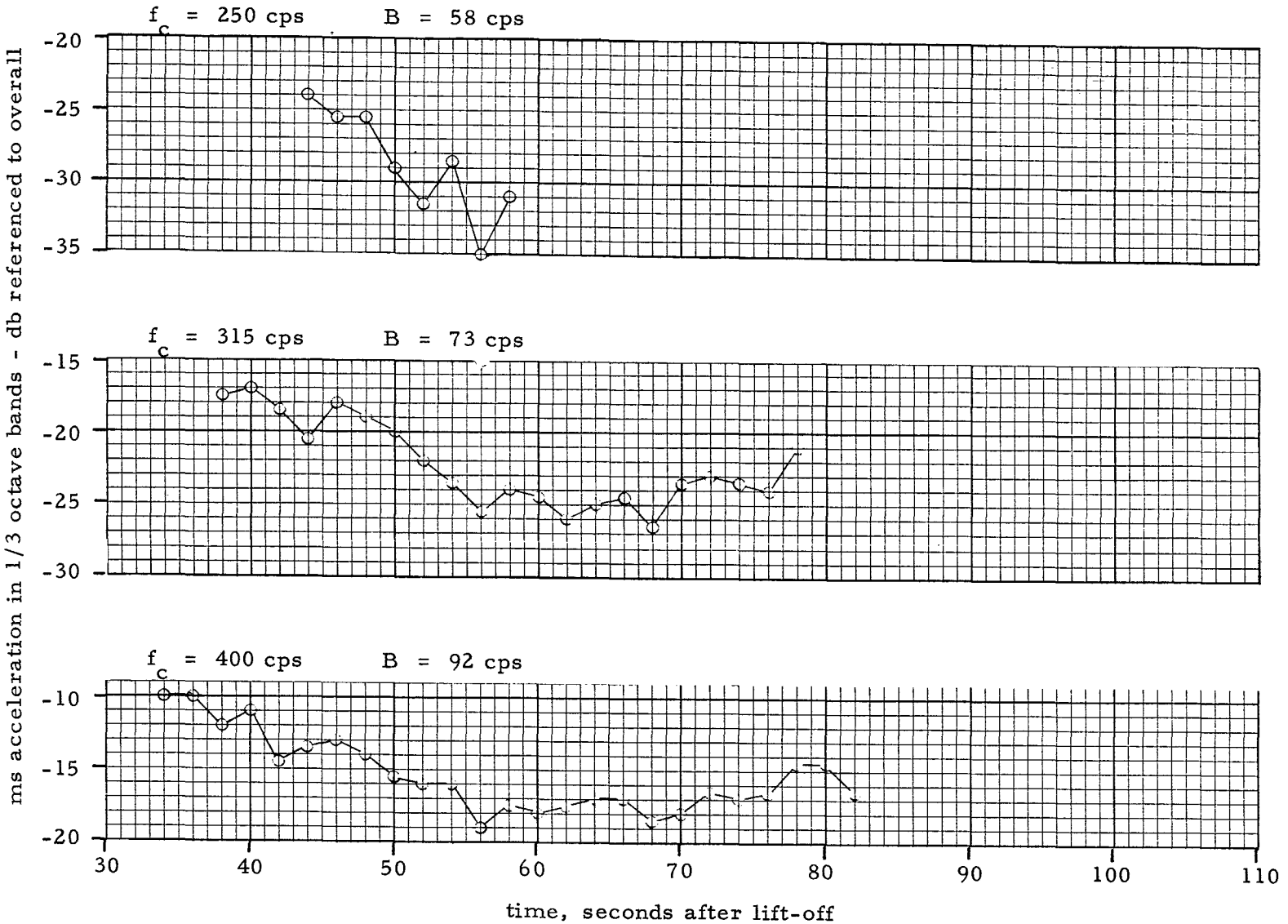

Figure C-13a. Relative Mean Square Values in 1/3 Octave Bands for OGO, Location 1, Flight Vibration

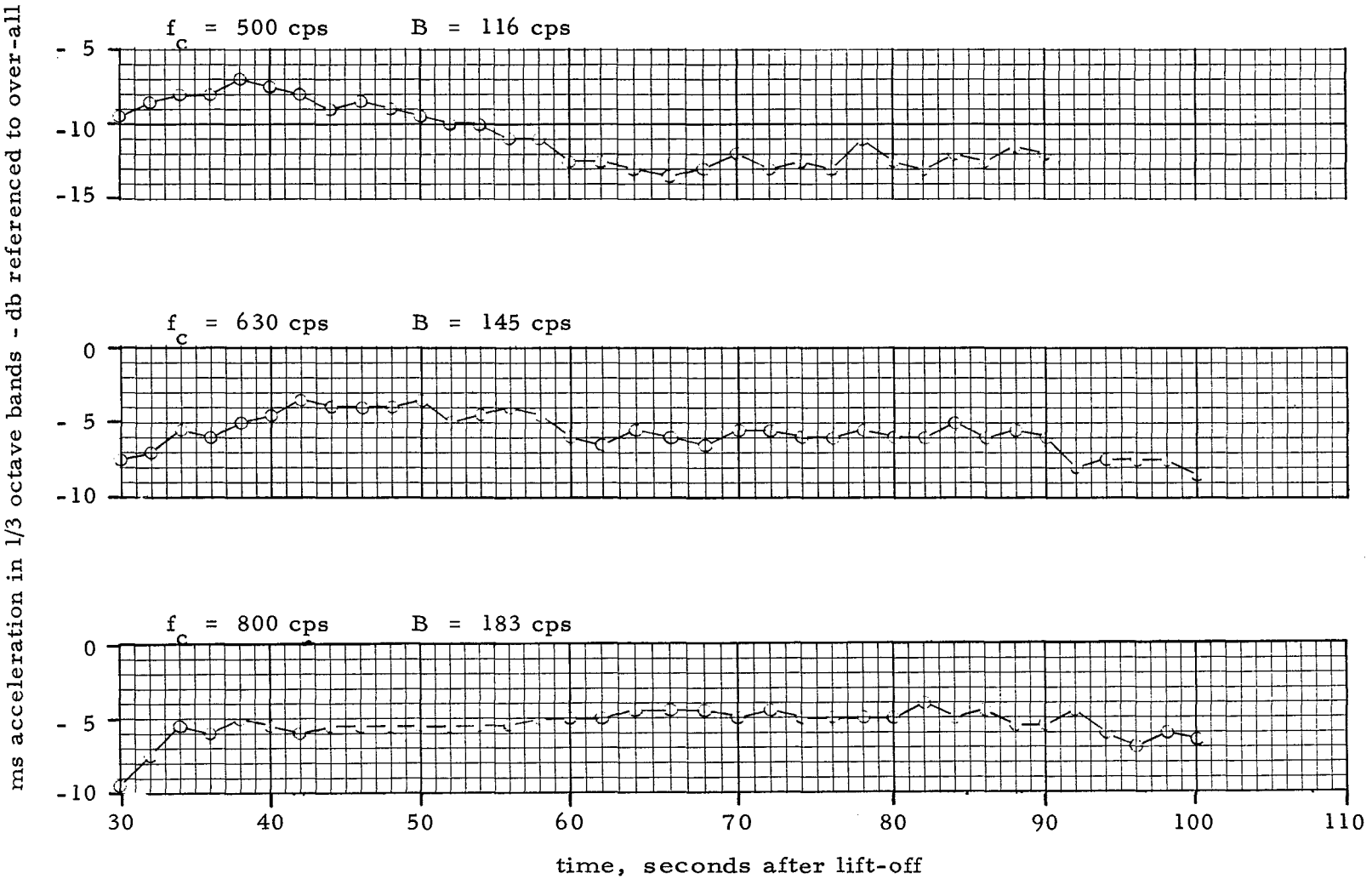

Figure C-13b. Relative Mean Square Values in 1/3 Octave Bands for OGO, Location 1, Flight Vibration

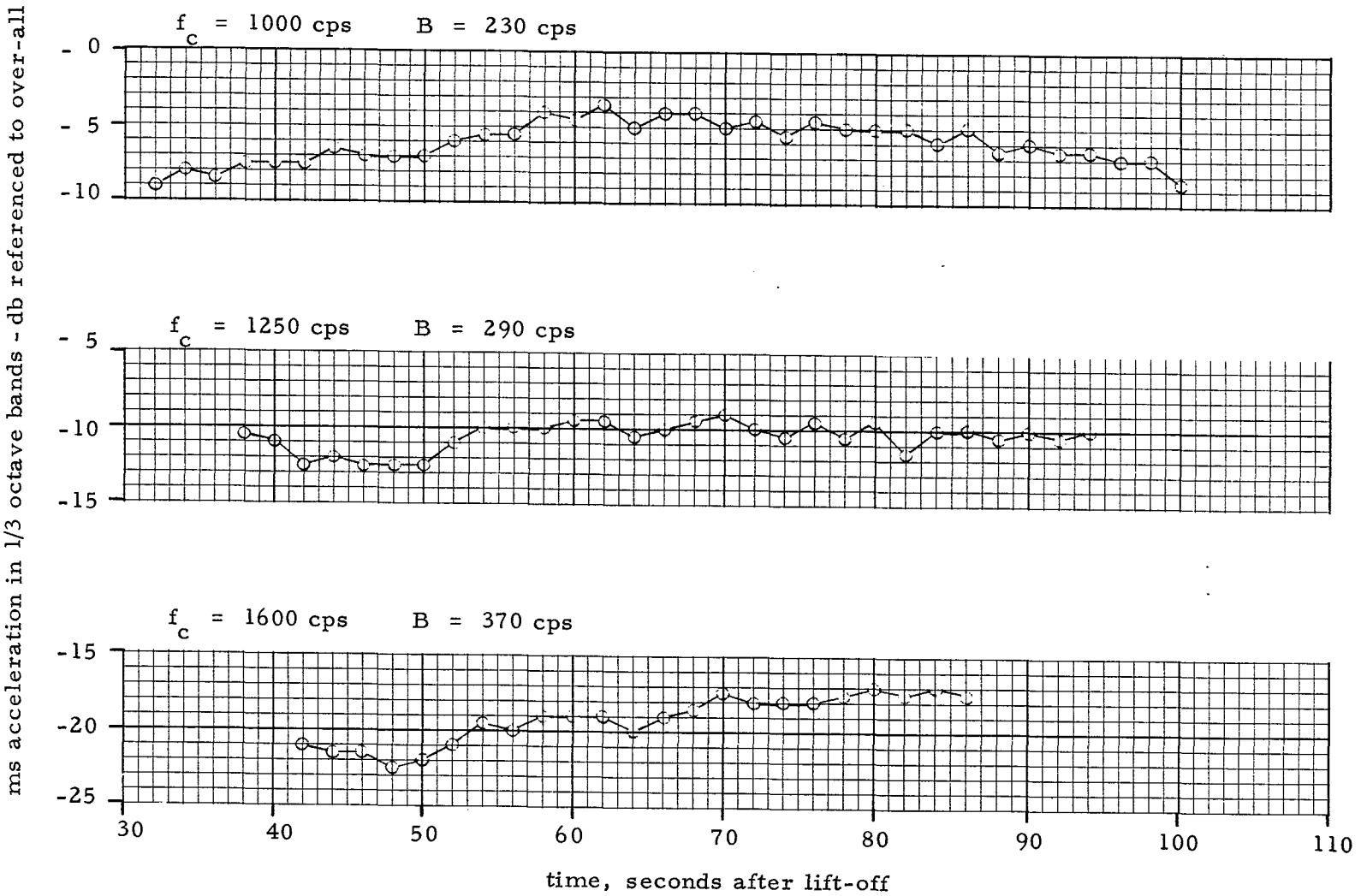

Figure C-13c. Relative Mean Square Values in 1/3 Octave Bands for OGO, Location 1, Flight Vibration

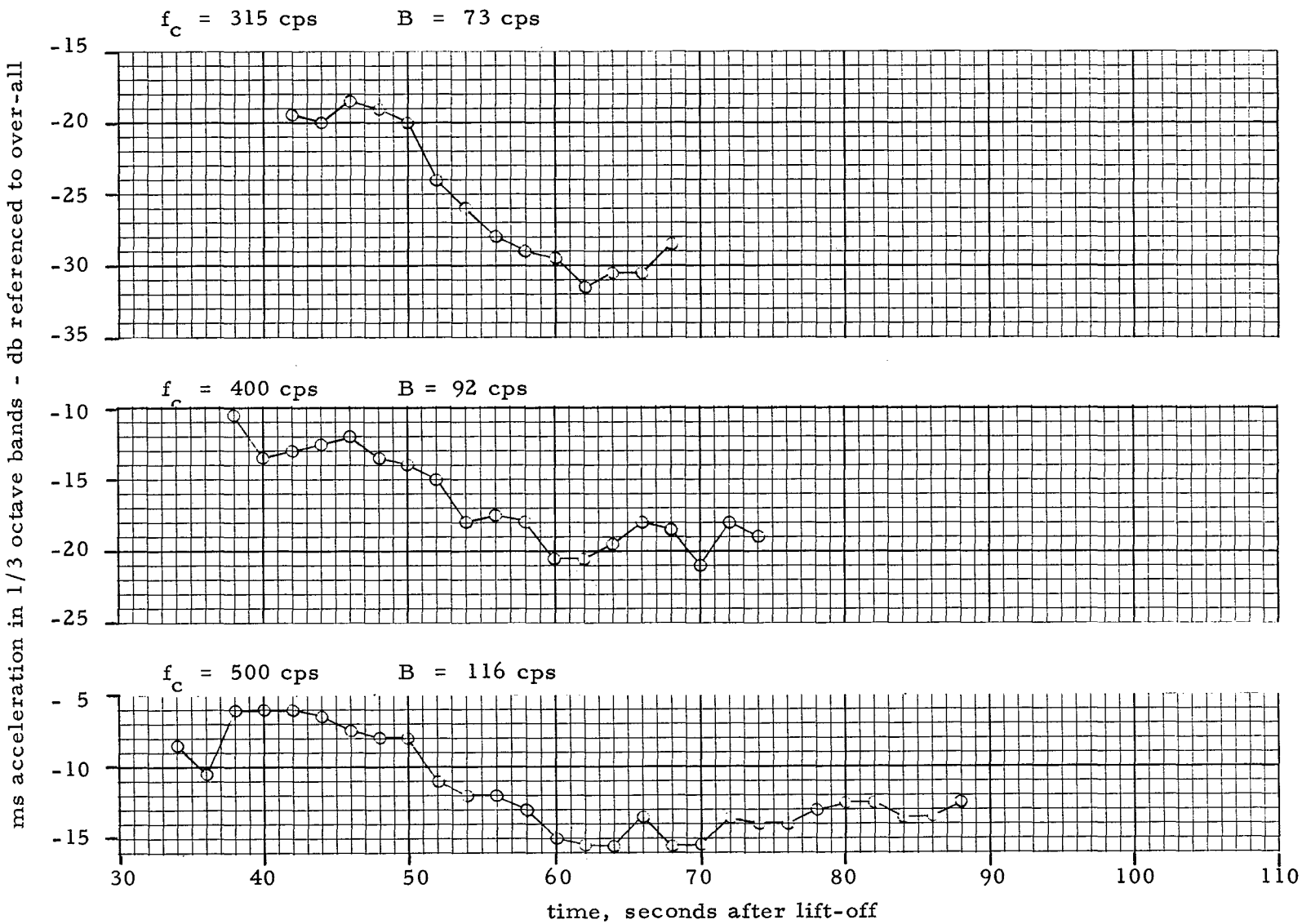

Figure C-14a. Relative Mean Square Values in 1/3 Octave Bands for OGO, Location 2, Flight Vibration

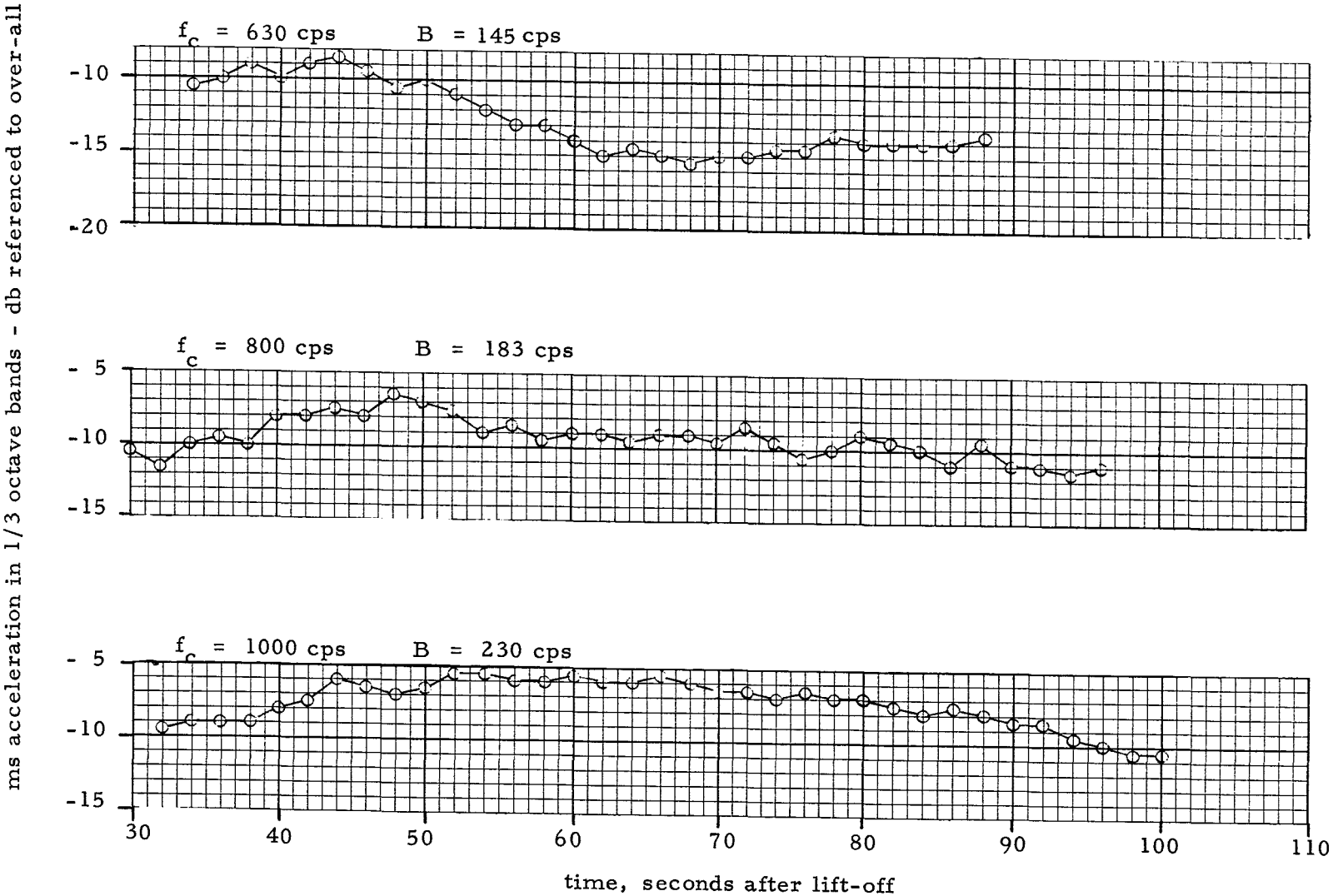

Figure C-14b. Relative Mean Square Values in 1/3 Octave Bands for OGO, Location 2, Flight Vibration

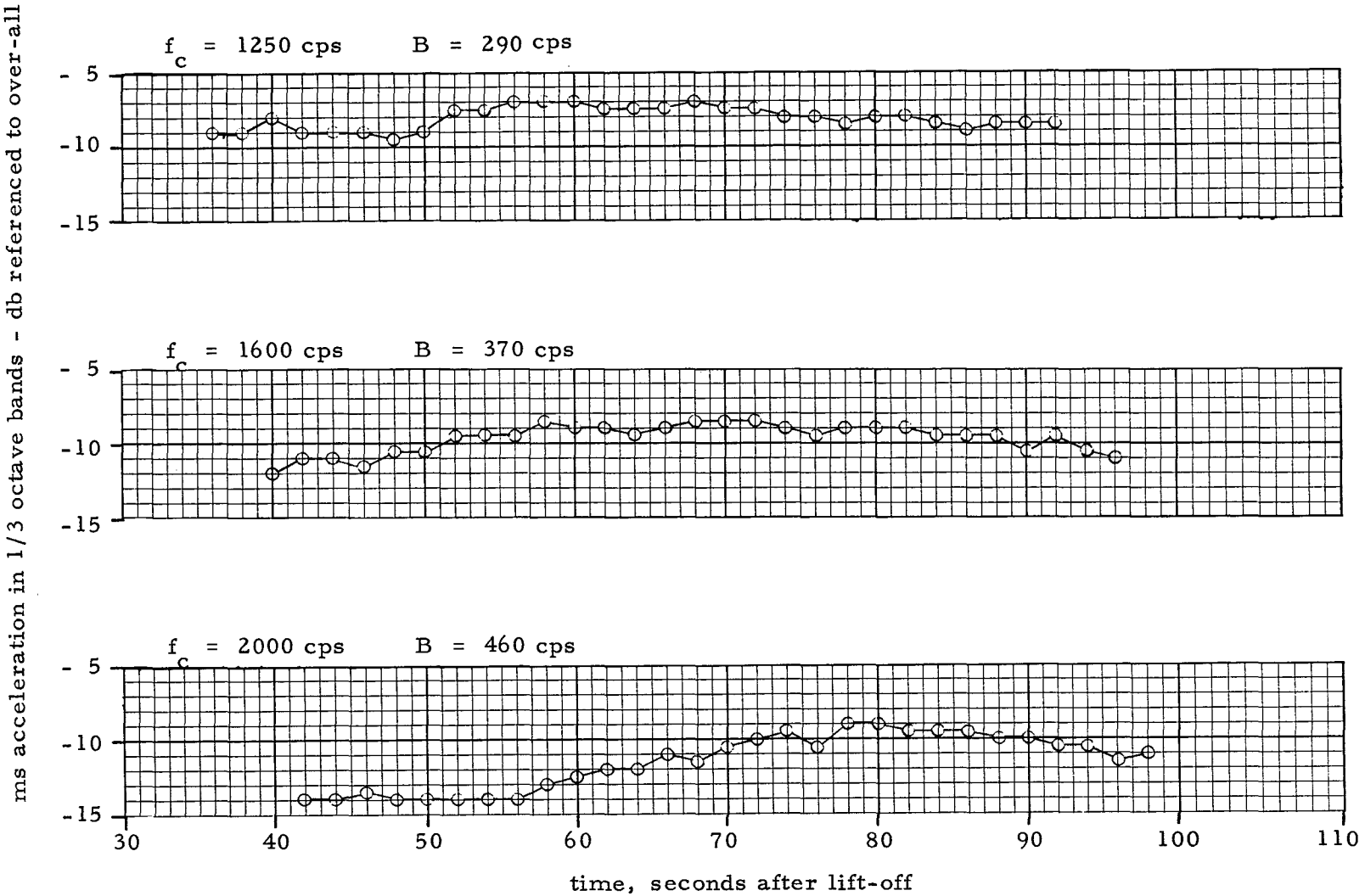

Figure C-14c. Relative Mean Square Values in 1/3 Octave Bands for OGO, Location 2, Flight Vibration

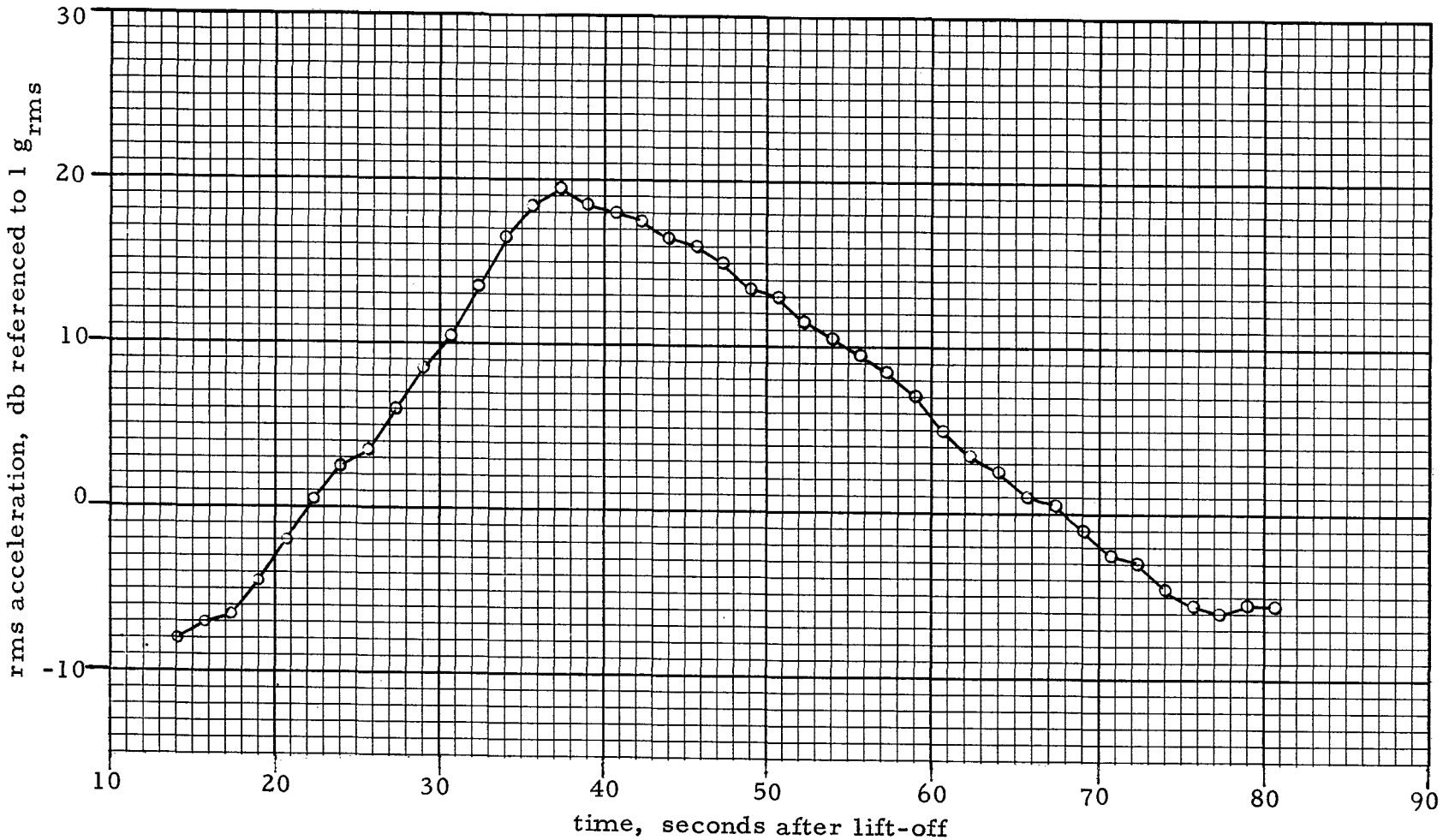

Figure C-15. Over-all RMS Time History for AVT Flight Vibration

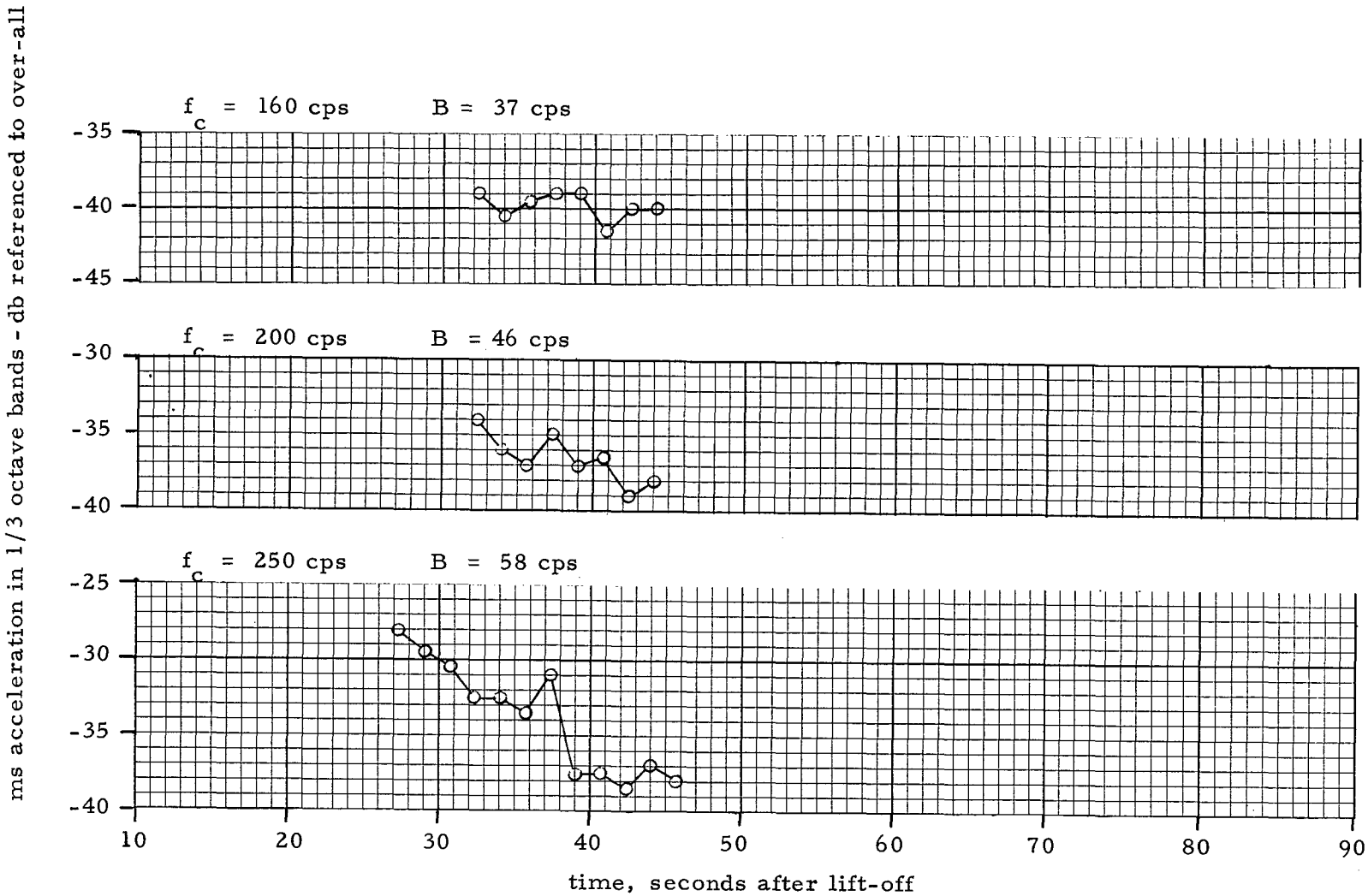

Figure C-16a. Relative Mean Square Values in 1/3 Octave Bands for AVT Flight Vibration

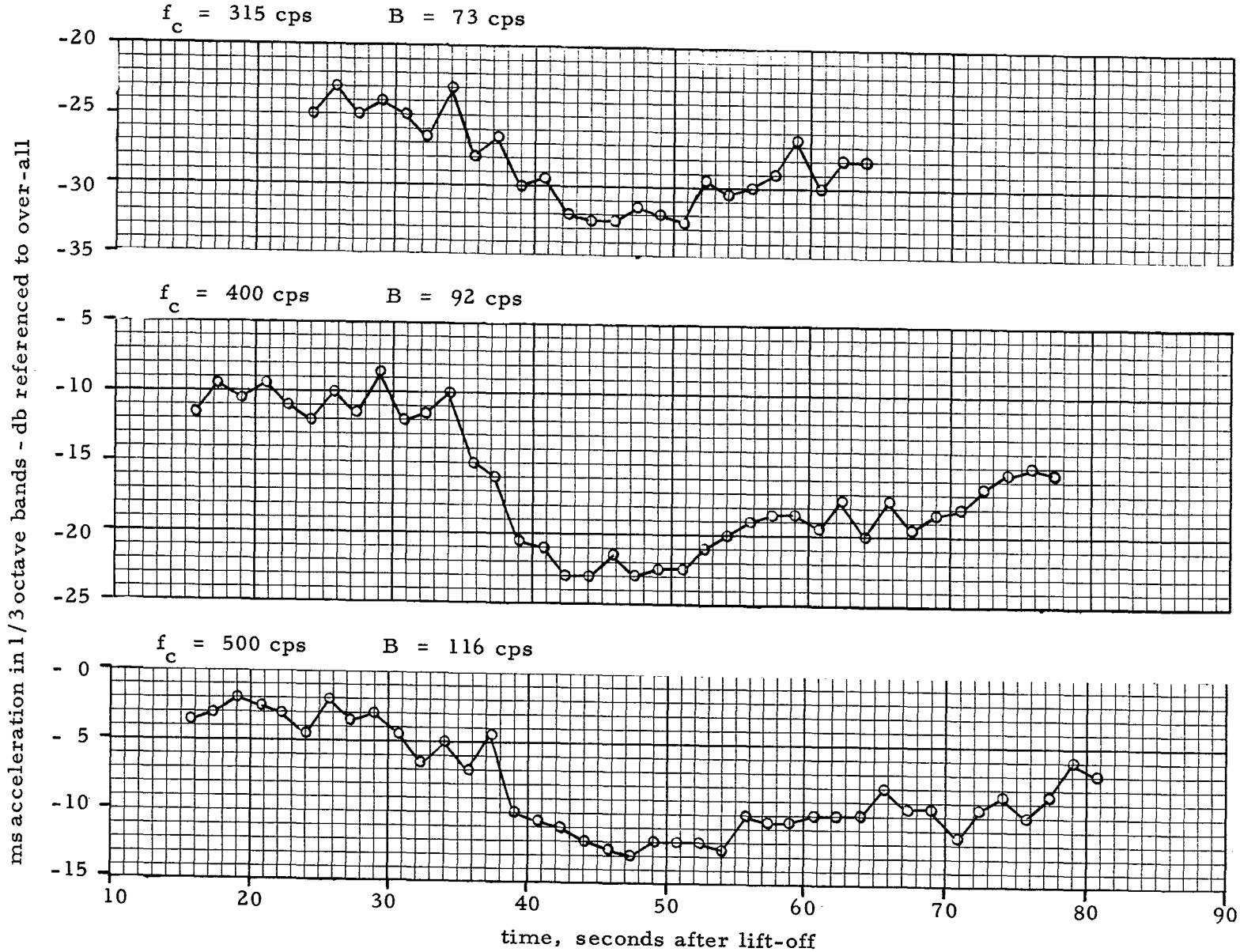

Figure C-16b. Relative Mean Square Values in 1/3 Octave Bands for AVT Flight Vibration

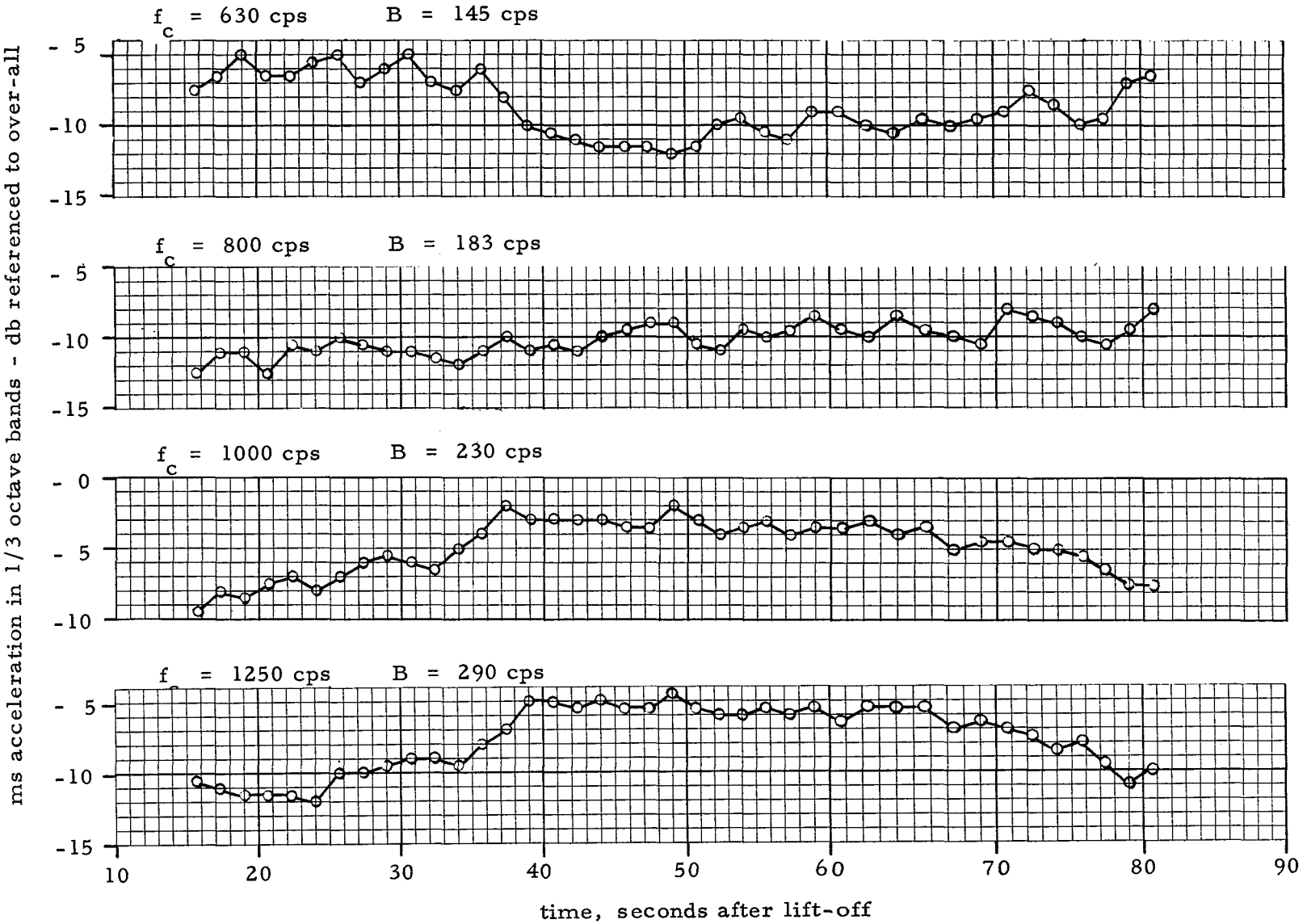

Figure C-16c. Relative Mean Square Values in 1/3 Octave Bands for AVT Flight Vibration

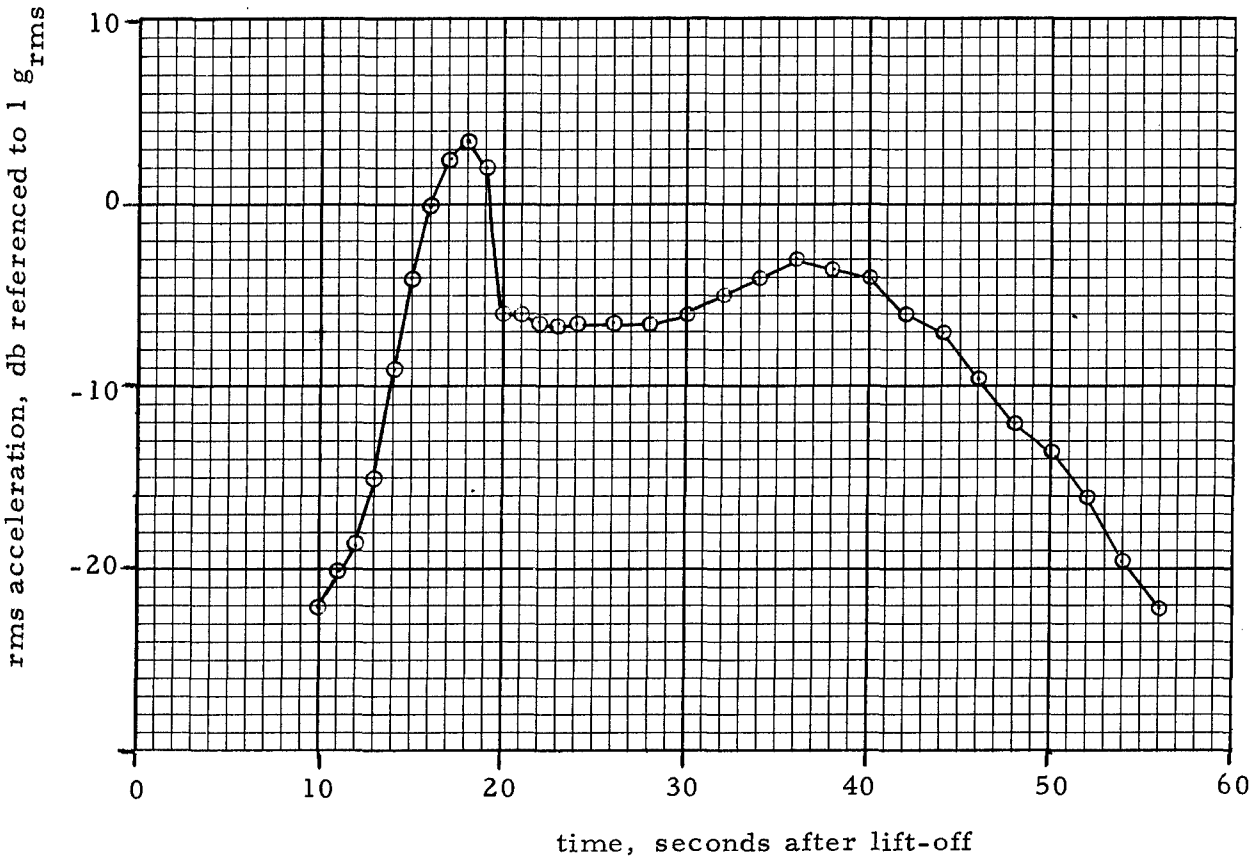

Figure C-17. Over-all rms Time History for MINUTEMAN Flight Vibration

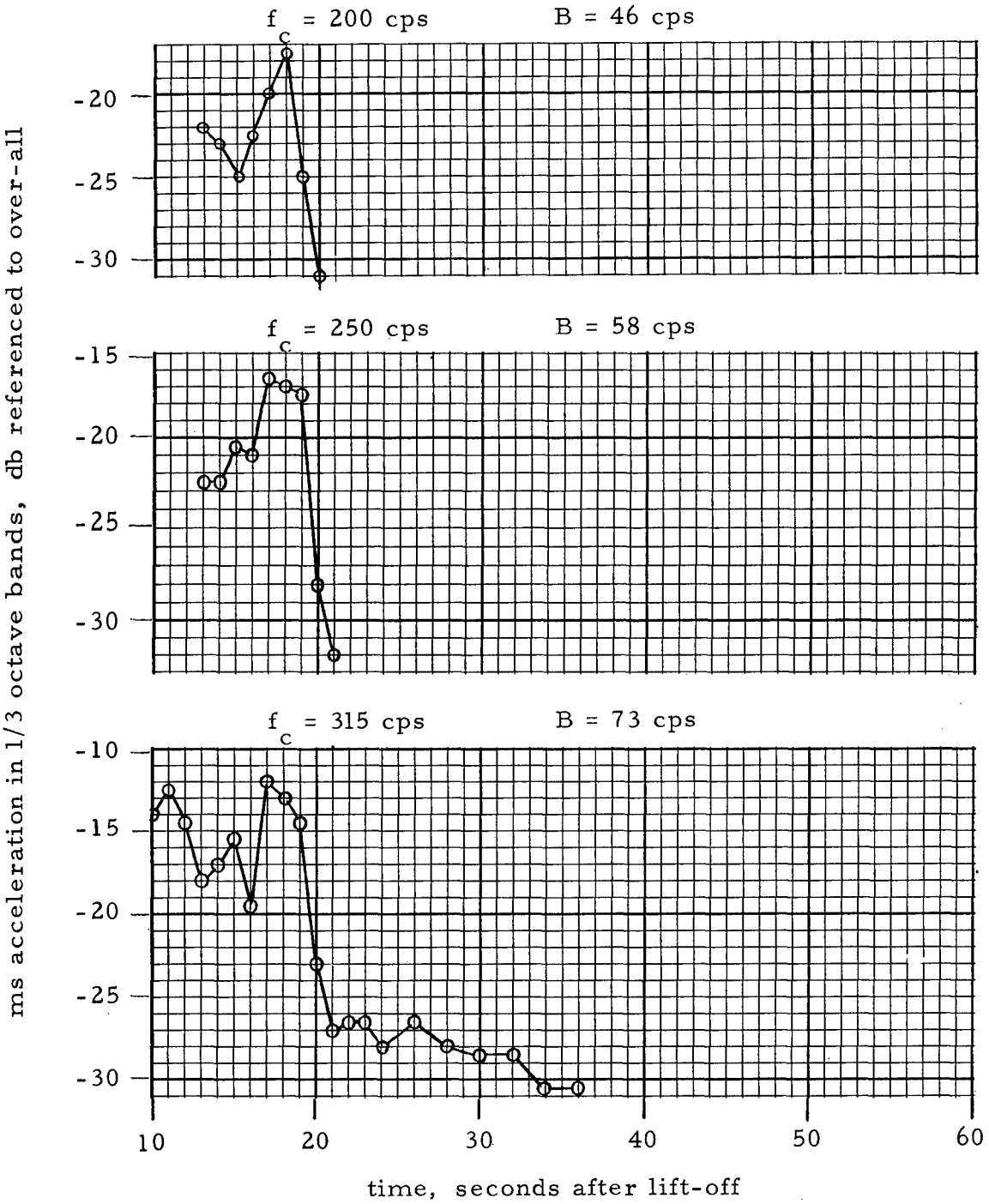

Figure C-18a. Relative Mean Square Values in 1/3 Octave Bands for MINUTEMAN Flight Vibration

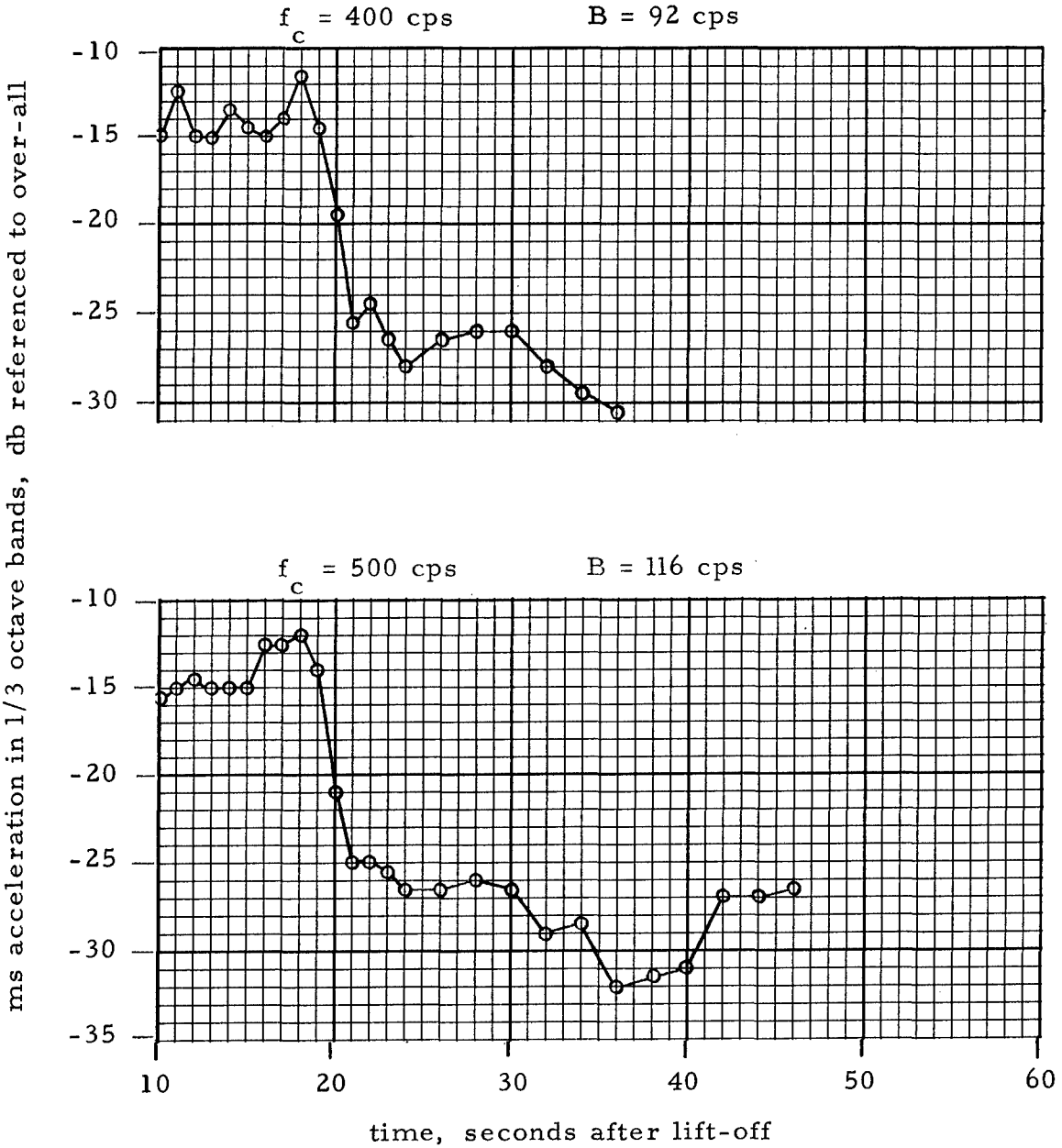

Figure C-18b. Relative Mean Square Values in 1/3 Octave Bands for MINUTEMAN Flight Vibration

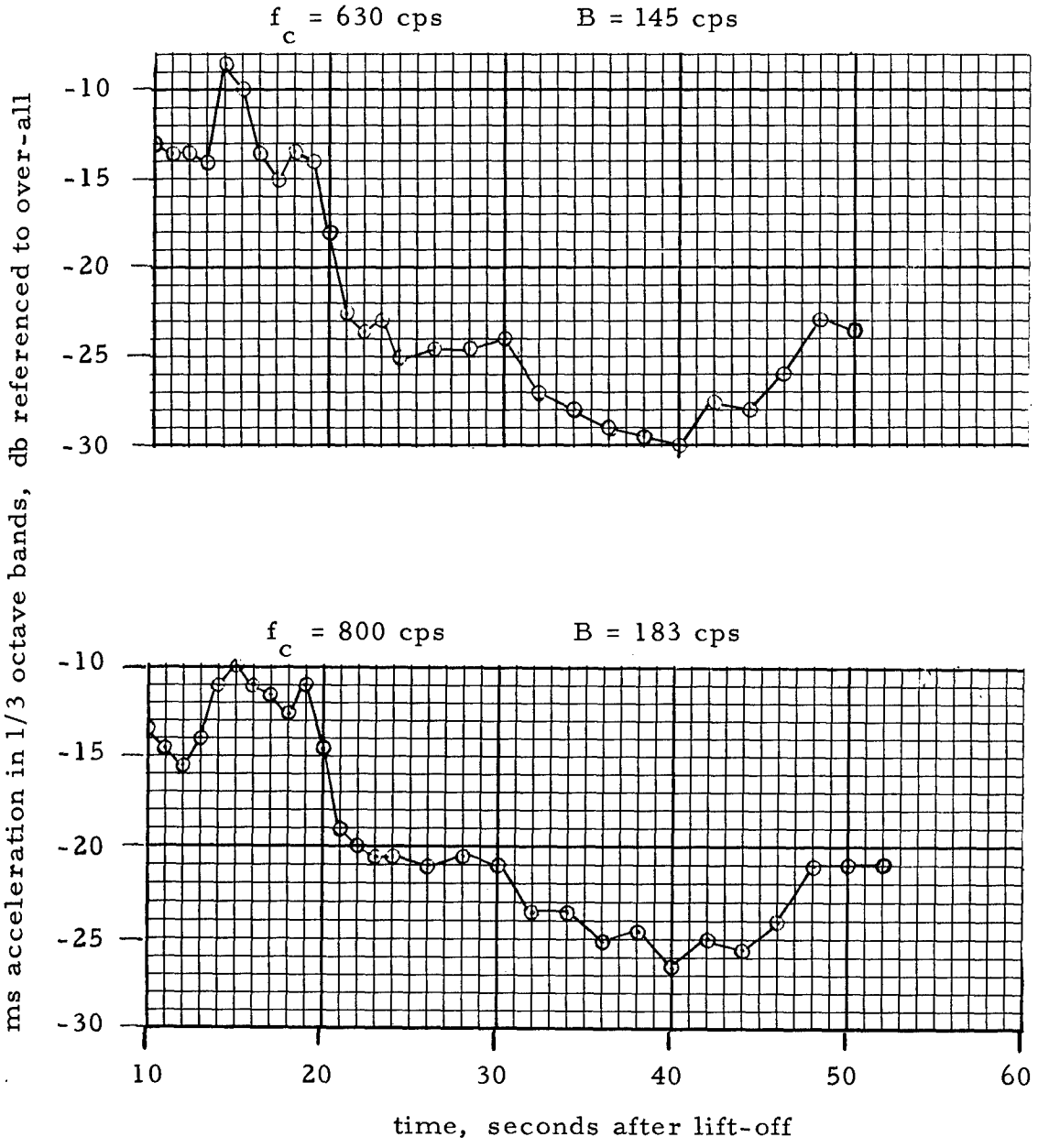

Figure C-18c. Relative Mean Square Values in 1/3 Octave Bands for MINUTEMAN Flight Vibration

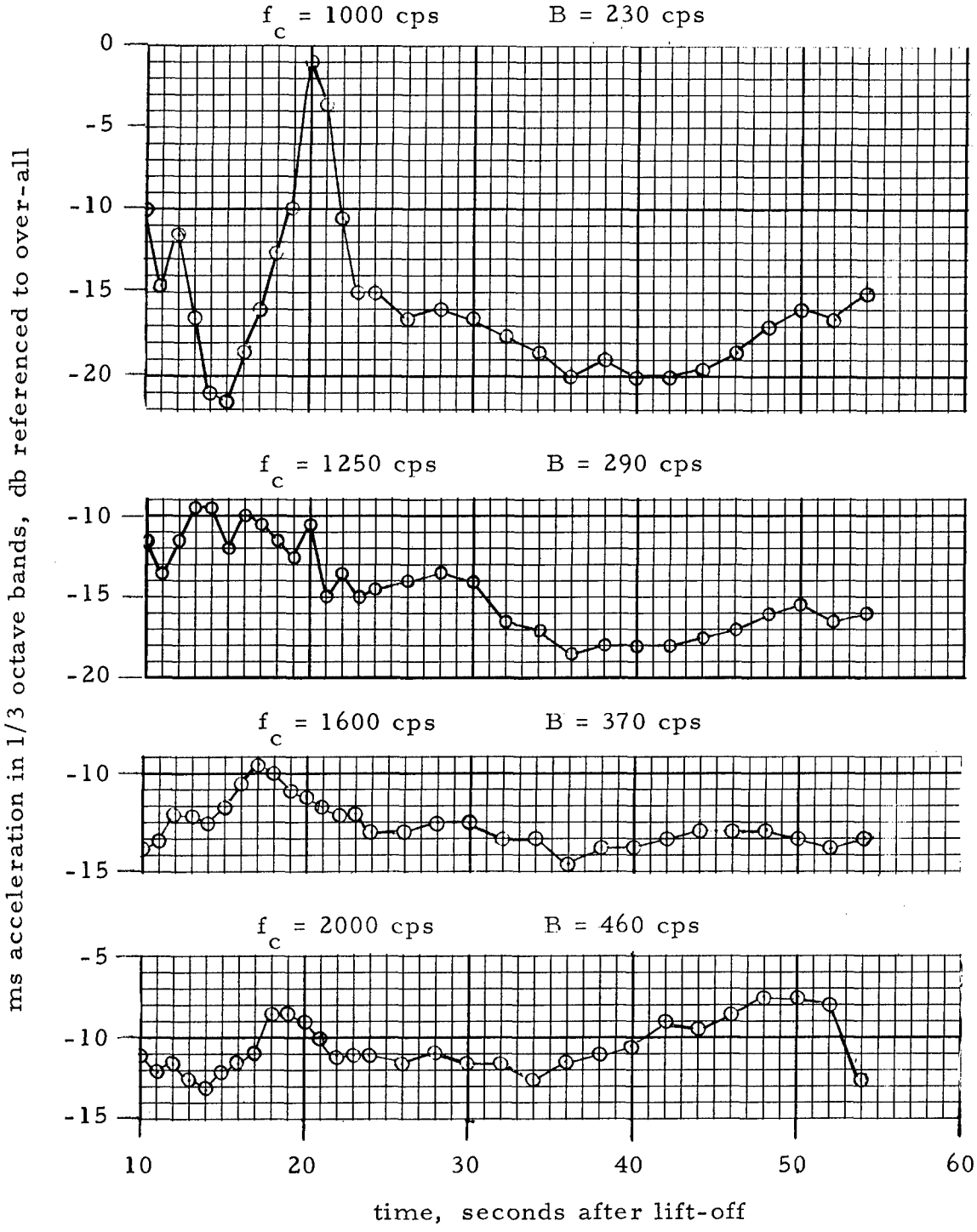

Figure C-18d. Relative Mean Square Values in 1/3 Octave Bands for MINUTEMAN Flight Vibration

NASA-Langley, 1965 CR-341